UNIVERSITA' VITA-SALUTE SAN RAFFAELE

CORSO DI DOTTORATO DI RICERCA INTERNAZIONALE IN MEDICINA MOLECOLARE

CURRICULUM IN EXPERIMENTAL AND CLINICAL MEDICINE

MOLECULAR CHARACTERIZATION OF SARS-CoV-2 VIRAL VARIANTS CELL INFECTION KINETIC AND EVALUATION OF THEIR INFECTIVITY FROM FOMITES

DoS: Prof. Nicola Clementi

Second Supervisor: Prof. Mauro Pistello

Tesi di DOTTORATO di RICERCA di Sofia Sisti

matr. 020169

Ciclo di dottorato XXXVII

SSD MED07

Anno Accademico 2023/2024

CONSULTAZIONE TESI DI DOTTORATO DI RICERCA

La sottoscritta/ I	Sofia Sisti
Matricola / *registration number*	020169
Nata a / *born at*	Sora
il/*on*	12/10/1995

autore della tesi di Dottorato di ricerca dal titolo / *author of the PhD Thesis titled*

Molecular characterization of SARS-CoV-2 viral variants cell infection kinetic and evaluation of their infectivity from fomites

☐ AUTORIZZA la Consultazione della tesi / AUTHORIZES *the public release of the thesis*

☒ NON AUTORIZZA la Consultazione della tesi per 6 mesi /DOES NOT AUTHORIZE *the public release of the thesis for* 6 *months*

a partire dalla data di conseguimento del titolo e precisamente */ from the PhD thesis date, specifically*

Dal / *from* …25…/…02…/…25… Al / *to* …25…/…08…/…25…

Poiché /*because*:

□ l'intera ricerca o parti di essa sono potenzialmente soggette a brevettabilità/ *The whole project or part of it might be subject to patentability;*

□ ci sono parti di tesi che sono già state sottoposte a un editore o sono in attesa di pubblicazione/ *Parts of the thesis have been or are being submitted to a publisher or are in press;*

□ la tesi è finanziata da enti esterni che vantano dei diritti su di esse e sulla loro pubblicazione/ *the thesis project is financed by external bodies that have rights over it and on its publication.*

E' fatto divieto di riprodurre, in tutto o in parte, quanto in essa contenuto / *Copyright the contents of the thesis in whole or in part is forbidden*

Data /Date .....05/03/25..... Firma /Signature Sofia Sisti

DECLARATION

This thesis has been:

- composed by myself and has not been used in any previous application for a degree. Throughout the text I use both 'I' and 'We' interchangeably.
- has been written according to the editing guidelines approved by the University.

Permission to use images and other material covered by copyright has been sought and obtained. For the following images (from Figure 1 to 19), it was not possible to obtain permission and is/are therefore included in thesis under the "fair use" exception (Italian legislative Decree no. 68/2003).

All the results presented here were obtained by myself.

ABSTRACT

The emergence of Severe Acute Respiratory Syndrome Coronavirus 2 (SARS-CoV-2) resulted in an unprecedented global pandemic, heavily impacting economic and social aspects of our society. As a member of the *Coronaviridae* family, SARS-CoV-2 shared similarities with other highly pathogenic coronaviruses but possessed unique characteristics that contributed to its widespread transmission and pathogenicity.

This study focused on the molecular characterization and infection kinetics of emerging SARS-CoV-2 variants, aiming to elucidate four key virological aspects: their entry mechanisms, replication dynamics, immune evasion strategies, and persistence on surfaces. The results obtained using environmentally friendly disinfectants, addressed critical knowledge gaps by investigating one of the less-characterized transmission mechanisms.

To achieve our goals, we firstly isolated 11 different SARS-CoV-2 variants of concern from clinical samples. *In vitro* studies of viral replication and immune evasion were conducted using Calu-3 cell lines, in combination with pseudovirus systems, to gain a deeper understanding of the viral entry mechanism. Whole-genome sequencing allowed to characterize the genetic mutations among the variants, while quantitative RT-PCR assays provided detailed profiles of replication dynamics and host immune responses. To explore indirect transmission mechanisms, we set up an experimental workflow using environmental surfaces (copper, aluminum, and polystyrene-plastic), common materials found in both hospital and everyday environments. Additionally, we performed disinfection studies on these surfaces to assess the efficacy of environmentally friendly 'green' disinfectants, such as tea tree oil (TTO) and quercetin-based compounds.

Our results revealed that mutations in the spike protein were directly associated with increased replication rates and more efficient entry mechanisms, alongside enhanced immune evasion through the inhibition of interferon responses. Together, these features contributed to increased infectivity, transmission, and pathogenicity. Notably, persistence studies also revealed that specific mutations, such as G446S, contributed to enhanced viral stability on surfaces, suggesting alternative transmission routes beyond direct person-to-person contact.
The G446S mutation, present in the most recent variants, appeared to confer a selective advantage in terms of environmental persistence, thereby promoting indirect transmission dynamics. Furthermore, our investigation into 'green' disinfectants revealed that compounds such as TTO and quercetin achieved a viral

load reduction exceeding 95% within minutes, outperforming conventional alcohol- and UV-based disinfection methods. These findings emphasized the distinct strategies SARS-CoV-2 employed to ensure survival and transmission, including its ability to adapt under selective pressure and evade host defenses. This work underscored the complex interplay between viral genetic evolution and its phenotypic manifestations, highlighting the importance of ongoing surveillance of emerging variants. Additionally, the efficacy of environmentally sustainable disinfectants presented a promising avenue for reducing transmission in both clinical and community settings.

TABLE OF CONTENT

ABSTRACT *7*

ACRONYMS AND ABBREVIATIONS *4*

LIST OF FIGURES AND TABLES *6*

INTRODUCTION *12*

SARS-COV-2 ..... *13*

Structure **14**

Non-structural proteins **15**

Structural proteins **17**

S protein 17

E protein 20

M protein 21

N protein 22

Accessory proteins 22

Replicative cycle **24**

Attachment 25

Entry 28

Replication 32

Assembly and release 34

IMMUNE RESPONSE TO PATHOGEN *35*

Innate immune response **35**

Innate immunity 35

Adaptive immune response **38**

Immune evasion mechanisms of SARS-CoV-2 ..... **41**

Viral evasion: structural viral protein 41

Viral evasion: non-structural and accessory viral proteins 42

Viral evasion: adaptive immune escape 44

CLINICAL RELEVANCE *45*

Epidemiology and Evolution **45**

Transmission mechanisms **54**

Pathogenesis **56**
Clinic manifestations 56
Immune mediate injury 57
Comorbidities 59
Long COVID condition 60
Diagnosis **62**
Therapeutic and prophylactic strategies **64**
AIM OF THE WORK ***70***
RESULTS ***72***
Insights into the replication kinetics of 11 SARS-CoV-2 variants **72**
Replication kinetics may be driven by distinct entry efficacy **74**
Immuno-escape: how the antiviral response impact on the replication kinetic. **78**
Study the persistence mechanisms of SARS-CoV-2 variants **83**
Implication of different mutations in the persistence mechanism **85**
Evaluating the efficacy of "green" disinfectants **89**
DISCUSSION ***92***
CONCLUSION ***100***
MATERIALS AND METHODS ***101***
Cell lines **101**
Virus isolation **101**
Virus sequencing **102**
Virus titration **103**
Kinetic profiles **103**
Immune-response **103**
Pseudovirus generation and titration **104**
Pseudovirus mutation **105**
Quantification of spike protein in pseudoviruses assay **106**

XTT Assay for determination of cell viability and cytotoxicity 107

Inhibition of pseudovirus entry process 107

Immunofluorescence 108

Persistence experiment 108

Disinfectant analysis 110

In silico characterization..... 110

Data analysis and statistics 111

REFERENCES* *113

ACRONYMS AND ABBREVIATIONS

ACE2	Angiotensin-Converting Enzyme 2
ADCC	Antibody-Dependent Cell-mediated Cytotoxicity
APCs	Antigen Presenting Cells
Ang	Angiotensin
ARDS	Acute Respiratory Distress Syndrome
AUC	Area Under the Curve
BCA	Bicinchoninic Acid Solution
BFLA-1	Baflomycin A1
CAM	Camostat mesylate
CD	Cytoplasm domain
CLRs	C-type lectin receptors
CRS	Cytokine Release Syndrome
COVID-19	Coronavirus disease 2019
Cryo-EM	Cryo-electron microscopy
DAMPs	Damage-Associated Molecular Patterns
DCs	Dendritic cells
DMV	Double-membrane vesicles
DMVs	Double-Membrane Vesicles
dsRNA	Double-strand RNA
E	Envelope
ELISA	Enzyme-Linked Immunosorbent Assay
ERGIC	ER-Golgi intermediate compartment
FP	Fusion Peptide
HR	Heptad-repeat domains
hpi	Hours post infection
IFN	Interferon
IL	Interleukin
ICUs	Intensive Care Units
M	Membrane
MALT	Mucosa-Associated Lymphoid Tissue
MDA5	Melanoma Differentiation-Associated gene 5
Mpro	Main protease
NAB	Nucleic Acid-Binding domain

N	Nucleocapsid
NRP1	Neuropilin 1
NTD	N-terminal domain
ORFs	Open Reading Frames
PAMPs	Pathogen-Associated Molecular Patterns
PLpro	Papain-Like protease
PRRs	Pattern Recognition Receptors
QRE	Quercetin
RBD	Receptor-binding domain
RLRs	RIG-I-like receptors
RLU	Relative Luminescence Units
RdRp	RNA-dependent RNA polymerase
RTC	Replication-Transcription Complexes
RNP	Ribonucleoprotein
RT-PCR	Reverse Transcription Polymerase Chain Reaction
SARS-CoV-2	Severe Acute Respiratory Syndrome Coronavirus 2
sgRNA	Subgenomic RNA
S	Spike
TLRs	Toll-like receptors
TMD	Transmembrane domain
TMPRSS2	Transmembrane serine protease 2
TSP	Transmembrane serine protease
TM	Transmembrane domain
TNF-α	Tumor Necrosis Factor alpha
TTO	Tea Tree Oil
TRS	Transcriptional Regulatory Sequence
TRS	Transcription Regulatory Sequence
VOI	Variant of Interest
VOC	Variant of Concern
WB	Western Blot
WGS	Whole Genome Sequencing

LIST OF FIGURES AND TABLES

Figure 1 SARS-CoV-2 virion structure. *Three representative tomography slices of the virions of SARS-CoV-2 collected from the supernatant of infected Calu-3 cells. Virions appear as almost spherical, with granular density corresponding to RNP. S trimers protrude from viral envelope, giving the crown-shape morphology. Scale bar, 10 nm. Open access (Ke et al., 2020)* *13*

Figure 2 The genome of SARS-CoV-2: a schematic representation. *(A) SARS-CoV-2 genome is between the longest RNA viral genome known with about 30 kb and is organized in different ORF (B) Several ORFs have been identified which encode for three different groups of proteins: non-structural (blu) structural (red) and accessory (grey) proteins. Two- thirds of the total length of the genome encode for two long polyproteins (PP1a and PP1ab) cleaved by either PLpro (black triangle) or Mpro (grey triangle) to generate sixteen Nsps. The functional domains in the Nsps are also indicated Open access (Romano et al., 2020).* *14*

Figure 3 Spike Protein Structure. (A) *Schematic diagram of the S protein of SARS-CoV-2, with its distinct domains color-coded for clarity. Arrows indicate the cleavage sites recognized by host proteases, including the furin cleavage site, which is characterized by a specific motif.* ***(B)*** *Cryo-EM structural images of the S protein, showing the two conformational states of the receptor-binding domain (RBD): the "closed" conformation (left) and the "open" conformation (right), with the latter corresponding to the RBD being prepared for binding to the host cell receptor, ACE2. Open access (Santopolo, Riccio and Santoro, 2021) (Y. Huang et al., 2020).* *18*

Figure 4 Domain structure of E protein. (A) *Schematic representation of the E protein, with the N-terminal domain (NTD), transmembrane domain (TM), and C-terminal domain (CTD) labeled.* ***(B)*** *A pentameric model of E proteins, illustrating the channel structure. Open access (Mou et al., 2021).* *20*

Figure 5 Domain structure of M protein. (A) *Schematic representation of M protein domain in different color.* ***(B)*** *Schematic view of the M protein protomer. Secondary structure elements and hinge regions are indicated. The unstructured N-terminal and C-terminal regions are marked with dashed lines. Open access (Zhang et al., 2022).* *22*

Figure 6 Spike-ACE2 binding process. *On the top there is the representation of close conformation of spike glycoprotein. Clockwise, spike structure with one RBD in "up" conformation, that subsequentially could be bound to ACE2 molecule. This interaction induces a conformational change in one of the other two RBDs, leading to open state (bottom of the circle). Erected RBD could bind another ACE2 receptor, reaching the full-open conformation. At the end, all the three RBDs interact with ACE2. Open access (Benton et al., 2020).* *26*

Figure 7 Entry mechanisms of SARS-CoV-2 infection. *Upon binding of the receptor-binding domain (RBD) of the S glycoprotein to the ACE2 receptor on the host cell, several host cell proteases can cleave the S protein in different subcellular locations.* ***(A)*** *At the plasma membrane, the protease TMPRSS2 cleaves the S protein, exposing the fusion peptide (FP) domain, which enables the direct fusion of the viral and host cell membranes.* ***(B)*** *Alternatively, SARS-CoV-2 may enter host cells via endocytosis, where cathepsin L activates the spike glycoprotein, leading to membrane fusion and the subsequent release of the viral RNA into the cytoplasm. Open access (Cesar-Silva et al., 2022) (Jackson et al., 2021)* *29*

Figure 8 SARS-CoV-2 replicative cycle. *Step 1 of SARS-CoV-2 lifecycle occurs with RBD-ACE2 interaction and entry mechanism. Regardless of the mechanism, the viral RNA is released into the cytosol, where ORF1 is translated into two polyproteins, pp1a and pp1ab (step 2). Two viral proteases, PLpro and Mpro, cleave the two polyproteins, generating 16 Nsps (step 3). Replication begins in double membrane vesicles (DMV), where Nsps assembly together with gRNAs to form replication transcription complex (RTC). DMVs create a microenvironment for genomic replication and the transcription of subgenomic RNAs (step 4). Cellular machinery translates these subgenomic RNAs into structural and accessory proteins (step 6), which are*

essential for the virion formation and for the escape from immune response, respectively. Structural proteins M, E and S translocate into ER membrane and ERGIC compartment (step 7), while N protein interacts with newly produced genomic RNA to form nucleoprotein complex. The release of mature virions occurs via exocytosis: nucleoprotein complex assemblies with structural proteins budding into the lumen of secretory vesicular compartments (step 8), and then virions are secreted from plasma membrane to extracellular space to infect adjacent cells (step 9). Open access (V'kovski et al., 2020) (Katiyar et al., 2024). *32*

Figure 9 A schematic illustration of discontinuous transcription*. The full-length positive-strand genomic RNA uses as a template for the synthesis of both full-length negative-strand RNA and subgenomic RNAs. Specifically, when the viral polymerase encounters TRS-B (yellow), it may either proceed with transcription or translocate to TRS-L, as indicated by the arrow. The resulting subgenomic RNA (sgRNA) then acts as a template for the production of positive-sense sgRNAs, which are recognized by the host cell machinery initiating the translation of structural and accessory proteins. Open access (V'kovski et al., 2020).* *33*

Figure 10 Viral Assembly and Budding Process. *SARS-Cov-2 infection induces the formation of perinuclear membranous structures derived from the ER and surrounded by double membranes protecting the viral replication machinery from host immune responses. The novel synthesized viral proteins and RNA are transported to ERGIC compartment for assembly. The mature virion is then shipped to the plasma membrane and released into the extracellular. Open access (Jackson et al., 2021).* *34*

Figure 11 Innate immune response upon SARS-CoV-2 infection. *SARS-CoV-2 is detected by various PRRs that recognize foreign RNA, including endosomal TLR3 and TLR7, as well as cytoplasmic RIG-I and MDA5. Based on genetic, functional, clinical, and interaction mapping studies, downstream signaling events triggered by these interactions are depicted. Direct interactions between viral proteins and host cellular mechanisms are shown, with key pathways highlighted. Open access (Schultze and Aschenbrenner, 2021).* *36*

Figure 12 Immune response activation upon SARS-CoV-2 infection. *Starting from the left side of the image, we can observe the early stages of the cellular response following SARS-CoV-2 infection and how these events trigger a cascade that leads to the activation of immune cells, culminating in the initiation of an adaptive immune response. Intracellular TLRs can detect single-stranded RNA (ssRNA) in endosomes (via TLR7/8) or double-stranded RNA (dsRNA) (via TLR3), while RIG-I and MDA5 sense viral RNA in the cytoplasm. Upon detection of viral RNA, these sensors recruit adaptor proteins that initiate signaling pathways, resulting in the activation of NF-κB and interferon regulatory factor (IRF) transcription factors. This leads to the production of pro-inflammatory cytokines. Viral antigens are then processed and presented on major histocompatibility complexes (MHCs) to T cells, accompanied by co-stimulatory molecules. This process enhances the immune response by activating CD8+ T cells for direct cytotoxic activity and CD4+ T cells, which help stimulate B cells to produce antibodies. Open access (Manfrini et al., 2024).* *39*

Figure 13 Dynamics of host humoral response to SARS-CoV-2 infection. *Studies on antibody response to SARS- CoV-2 revealed that level of specific IgM starts rise during the first week of infection, followed closely by the increase in IgA levels. Finally, IgGs become detectable, remaining detectable for months after the symptoms. More studies need to be performed to examine the presence of SARS-CoV-2 specific IgGs during time and to address their protective role from re-infection. Open access (Galipeau et al., 2020).* *40*

Figure 14 SARS-CoV-2 evasion of the innate immune response through multiple mechanisms. *The M protein inhibits IRF3 activation, blocking type I interferon (IFN) production. The N protein further suppresses IRF3 and RIG-I activation. Non-structural proteins like PLpro, Nsp1, and Nsp13-16 disrupt RNA sensing and prevent IFN production. Accessory proteins such as ORF6 and ORF3a interfere with IFN signaling and the cGAS-STING pathway, enhancing viral survival and immune evasion. Open access (Latifi-Pupovci, 2022).* *43*

Figure 15 Temporal distribution of SARS-CoV variants. *The graph depicts the emergence and relative prevalence of various SARS-CoV-2 variants over time, from the early 2020 to January 2025. Curves represent the frequency of each variant, illustrating their temporal dynamics and shifts in dominance. This graph clary illustrates the ongoing evolution of SARS-CoV-2 in response to selective pressures and public health interventions. Open access Update on Omicron --- who.int, no date* *50*

Figure 16 Mutations in the SARS-CoV-2 spike protein and identification of Variants of Concern (VOCs). *This figure highlights key mutations in the S protein that have facilitated the identification of the different SARS-CoV-2 VOCs over time. The mutations are annotated on the S1 and S2 subunits, including the RBD, and the FP. Open access (Sars-CoV-2 circulating variants, no date)* *53*

Figure 17 Transmission Routes of SARS-CoV-2*. The ongoing COVID-19 pandemic has highlighted several transmission routes for SARS-CoV-2. Droplet transmission (particles >5 μm) is the most widely recognized and significant mode of spread. Direct contact between infected and uninfected individuals, particularly in close settings like households, is another major route. Although less frequent, transmission via fomites (e.g., door handles) is also being investigated as a contributing factor. Airborne and fecal-oral transmissions, observed in past coronaviruses (like SARS-CoV), have not been confirmed for SARS-CoV-2. Open access (Harrison, Lin and Wang, 2020).* *55*

Figure 18 COVID-19-Associated ARDS Development Model *SARS-CoV-2 infects the upper airways and spreads to the alveoli, triggering a disrupted immune response. This leads to alveolar damage, fluid leakage, platelet activation, and microthrombi formation. Dysfunctional immune cells, including neutrophils and macrophages, exacerbate inflammation and coagulation. The resulting lung injury impairs oxygen exchange, causing hypoxemia and acute respiratory distress syndrome (ARDS). Open access (Lamers and Haagmans, 2022).* *59*

Figure 19 COVID-19 vaccines and immune activation*. This schematic figure depicts the mechanisms of action of the three SARS-CoV-2 vaccine platforms:* ***(1)*** *mRNA vaccines, where mRNA encoding the S protein* ***(2)*** *adenovirus (AdV) vector vaccines, where the S protein is encoded by a DNA sequence; and* ***(3)*** *recombinant protein-based vaccines, where SARS-CoV-2 S proteins are assembled on nanoparticles design to mimic structure of the virus. All three vaccine types are processed by dendritic cells in a similar manner; after internalization, the S protein is degraded by dendritic cells and presented by MHC class I and II. The main difference lies in how the S protein is produced. Open access (Manfrini et al., 2024).* *69*

Figure 20. Replication kinetics of 11 SARS-CoV-2 VOCs in Calu-3 cells. *Viral genomes copy numbers in the supernatant were measured at six time points post-infection (0.001 MOI). (A) Pre-Omicron VOCs: G614D, Alpha, Beta Gamma and Delta replication kinetics. Statistically significant differences were observed between Beta/Gamma and G614D/Alpha (**p < 0.01). (B) Omicron family variants: BA.1, BA.2, BA.4, BQ.1.1, XBB.1, and XBB.1.5 were assessed for viral replication. Significant differences were observed between BA.2, BQ.1.1, and XBB.1.5 (***p < 0.001), with no significant differences among BA.1, BA.4, and XBB.1 (p > 0.1). The viral RNA levels were quantified by Real-Time PCR and expressed as ΔCt values, with mean ± SD for each variant. Statistically significant differences in replication kinetics were determined, with **p < 0.01, ***p < 0.001, and ****p < 0.0001. Ct: threshold cycle.* *73*

Figure 21 Validation of Pseudovirus System Production. *To investigate the entry mechanisms of SARS-CoV-2 VOCs, we employed a lentiviral-based pseudovirus system expressing full-length S protein and ZsGreen or luciferase for trasduction monitoring. We validated the system trasducting susceptible cell lines.* ***(A)*** *G614D pseudovirus production was assessed by examining mCherry-positive cells under 20x magnification detecting the GFP (green) signal. Nuclei were counterstained with Hoechst 33342 (blue). Scale bar: 100 μm.* ***(B)*** *VOCs pseudovirus production was valitaed trasducting the VeroE6/TMPRSS2 cells using 10 different dilutions, followed by measurement of luminescence signal units (RLU) at 37°C for 72 h. Data*

*from six replicates are shown as the mean ± SD, Two-way ANOVA ** p<0.01 ****, p < 0.0001. The luminescence signal confirmed successful production of the various spike proteins*..... 74

Figure 22 BCA Protein Assay for Quantification of Total Protein in Different Pseudovirus Batches. *(A)The total protein concentration (ug/ml) of pseudovirus stocks was determined using a BCA protein assay. The results highlight variability in the protein content across different batches, with the Beta variant stock showing a significantly higher total protein concentration compared to the other variants. (B) The spike protein levels in various pseudovirus variants were quantified using an ELISA assay with an anti-S antibody. The S- detection was reported as mean values ± SD, One-way ANOVA ** p<0.01 ****, p < 0.0001.*..... 75

Figure 23 Entry mechanisms of different VOCs on Calu-3 models. *Entry experiments were performed using the pseudovirus carrying different S-proteins to infect Calu-3 cells at equal doses, and luciferase activity (Relative luminescence units, RLU) was detected after incubation at 37°C for 72 h. Data from six replicates are shown as the mean ± SD, **** p < 0.0001.* 76

Figure 24 Characterization of the two different entry mechanisms in Calu-3 models. *Mechanisms used by the virus to infect Calu-3 thought endocytosis and direct fusion with plasma membrane were selectively hampered by chemical compounds. Targeting only one of the two entry mechanism resulted in different degree of infection inhibition. The infection inhibition percentages were reported as mean values ± SD, ** p<0.01 ****, p < 0.0001.* 77

Figure 25 Different immune-escape mechanisms for VOCs. *Heatmap showing the activation of the interferon signaling pathway following infection with 0.1 MOI. The activation (value > 1) or downregulation (value < 1) of IFN-related genes was calculated by subtracting the Ct values of specific genes from the Ct values of the housekeeping gene (GAPDH), yielding the ΔCt. Gene expression is presented as log2 fold change relative to uninfected cells (ΔΔCt). Monitoring the immune response at different time points provided insights into how specific VOCs may mediate distinct activation or suppression path.* 78

Figure 26 Statistical analysis of immune response. *Study of gene expression levels in the Calu-3 model at 1 hours post-infection (hpi) with six SARS-CoV-2 variants.*..... 79

Figure 27 Statistical analysis of immune response. *Study of gene expression levels in the Calu-3 model at 3 hours post-infection (hpi) with six SARS-CoV-2 variants.*..... 80

Figure 28 Statistical analysis of immune response*. Study of gene expression levels in the Calu-3 model at 6 hours post-infection (hpi) with six SARS-CoV-2 variants.*..... 80

Figure 29 Statistical analysis of immune response*. Study of gene expression levels in the Calu-3 model at 24 hours post-infection (hpi) with six SARS-CoV-2 variants*..... 81

Figure 30 Correlation analysis of entry, replication and immune escape mechanisms. *Correlation analysis was performed on 11 VOCs, considering entry values (x-axis), replication kinetics (y-axis), and immune response (size). Entry values are indicated by the RLU signal, replication kinetics are represented by the AUC value, and immune escape is reflected by the upregulation of IFNB levels at 24 hpi. Pearson correlation analysis is shown in the heatmap, highlighting a strong correlation between entry and replication mechanisms (0.95).*..... 82

Figure 31 Persistence mechanism as an alternative transmission route of SARS-CoV-2 variants. *Fomite transmission was studied on copper, polystyrene-plastic and aluminum surfaces at different time points. The persistence percentage was calculated based on the detected viral load ($TCID_{50}$/ml) at each time point, relative to the titer of viral stock ($TCID_{50}$/ml). The decrease in viral load was estimated by fitting a logistic growth curve. Data are shown as the mean ± SD, **** p < 0.0001.*..... 84

Figure 32 Correlation between persistence values and stability conformation. *The graph shows persistence value (x-asses) expressed as 100-fold and the DDG obtained from MAESTRO analysis (y-asses) and expressed as 2^DDG considering the value from 0-1 spike conformation*

with higher stability while value from 1-2 spike conformation with lowest stability. The Spearman's correlation analysis (dotted line, r =- 0.03, p = 0.9) is shown. *86*

Figure 33 Characterization of the G446S mutation in the persistence mechanism. (A) *Pseudovirus particles carrying XBB.1.5 or XBB.1.5_wt S proteins were used to infect Calu-3 cells, and luciferase activity (RLU) was measured after 72 hours of incubation at 37°C. Data from six replicates are presented as mean ± SD and are not statistically different (p = ns).* ***(B)*** *An equal amount of pseudoviruses was used in persistence experiments, where the recovered pseudoparticles was used to infect Calu-3 cells, and RLU signals were measured after 72 hours of incubation at 37°C. The data are presented as mean and ± SD and T-test analysis was performed ** p < 0.01 **** p < 0.0001.* *87*

Figure 34 3D modeling of G446S mutation. *Representative structure of the G614D spike protein in the 1-up state to map the location of the G446S mutation within the RBD domain and assess its potential role in increased persistence.* *88*

Figure 35 Persistence mechanisms of influenza strains on aluminum and polystyrene-plastic. *Persistence assays was calculated by infecting MDCK cells with recovered viral particles, and viral load was expressed as the fold change in TCD_{50}/ml relative to the starting stock titer. The decrease in viral load was estimated by fitting a logistic growth curve. Data are shown as the mean ± SD.* *89*

Figure 36 Assessment of disinfectant efficacy against persistent SARS-CoV-2 variants and influenza strains. *The efficacy of disinfectants, including TTO, QRE, DAP, and two positive controls (alcohol and UV-C), was tested on polystyrene-plastic and aluminum surfaces at 1, 5, and 10-minute time points. All disinfectants reduced viral load by up to 80% after 1 minute. TTO, DAP, and QRE achieved >95% reduction in viral load for SARS-CoV-2 variants, with TTO being the most effective on aluminum (1.88 ± 0.36%) and polystyrene-plastic (8.4 ± 2.08%) at 1 minute. Alcohol and UV-C achive complete disinfection within 1 minute.* *90*

Table 1 Neutralization activites of monoclonal antibodies (mAbs) against VOCs Open access *(Cox et al., 2023).* *66*

Table 2 Variant calling and mutation analysis across the Genome of 11 VOCs. *85*

Table 3 List of primers used for RNA identification, immune response and pseudovirus G446S mutation *104*

INTRODUCTION

On March 11, 2020, the Director-General of the World Health Organization (WHO) declared the novel coronavirus outbreak a global pandemic, stating: "Over the past two weeks, the global number of COVID-19 (COronaVIrus Disease 19) cases has surged by 13 times, and the number of affected countries has increased threefold. Currently, there are more than 118,000 confirmed cases across 114 countries, with 4,291 deaths reported. Based on this data, we have concluded that COVID-19 can be classified as a pandemic" (*WHO Director-General's opening remarks at the media briefing on COVID-19 - 11 March 2020*, no date).

The causative agent of COVID-19 was identified on January 7, 2020, in China as a novel coronavirus (2019-nCoV), and shortly thereafter, Chinese authorities released the first genome sequence of the virus. Given its genetic similarity to the SARS coronavirus (SARS-CoV), the virus was subsequently renamed SARS-CoV-2 (Severe Acute Respiratory Syndrome Coronavirus 2). The identification of SARS-CoV-2 enabled the development of diagnostic tests, but containment of the virus proved challenging, and its global spread continued unabated.

COVID-19, caused by SARS-CoV-2, has had a profound impact on public health, economies, and societies worldwide. By December 29, 2024, there had been over 777 million confirmed infections, and more than 7.03 million deaths attributed to the disease (Zhu, Zhang, Wang, Li, Yang, Song, Zhao, Huang, Shi, Lu, Niu, Zhan, Ma, Wang, Xu, Wu, George F Gao, *et al.*, 2020) (*COVID-19 deaths | WHO COVID-19 dashboard --- data.who.int*, no date). SARS-CoV-2 belongs to the *Coronaviridae* family and is genetically related to other highly pathogenic coronaviruses, such as SARS-CoV and Middle East Respiratory Syndrome Coronavirus (MERS-CoV). The latter two viruses were responsible for over 8,000 and 2,500 confirmed cases, respectively, with fatality rates of approximately 10% and 35% (*COVID-19 Map - Johns Hopkins Coronavirus Resource Center --- coronavirus.jhu.edu.*, no date)[-](Zhu, Zhang, Wang, Li, Yang, Song, Zhao, Huang, Shi, Lu, Niu, Zhan, Ma, Wang, Xu, Wu, George F. Gao, *et al.*, 2020).

In response to the pandemic, extensive efforts have been dedicated to understanding the structure of the virus and the molecular mechanisms underlying its pathogenicity (Zhu, Zhang, Wang, Li, Yang, Song, Zhao, Huang, Shi, Lu, Niu, Zhan, Ma, Wang, Xu, Wu, George F. Gao, *et al.*, 2020).

SARS-COV-2

Cryo-electron microscopy (Cryo-EM) analysis revealed that the SARS-CoV-2 virion adopts an approximately spherical shape, with a diameter ranging from 80 to 120 nm (Ke *et al.*, 2020). The virion is encased by a lipid bilayer envelope, which embeds three key structural proteins: the spike (S), membrane (M), and envelope (E) proteins. Among these, the S protein is particularly evident, as it forms club-like projections that extend from the viral surface, giving the virion its characteristic crown-like "corona" appearance, which is the hallmark of coronaviruses (Figure 1).

Inside the viral envelope, the nucleocapsid (N) protein tightly associates with the RNA genome, forming a helical ribonucleoprotein (RNP) complex essential for viral replication and packaging (Bai *et al.*, 2021) (Arya *et al.*, 2021).

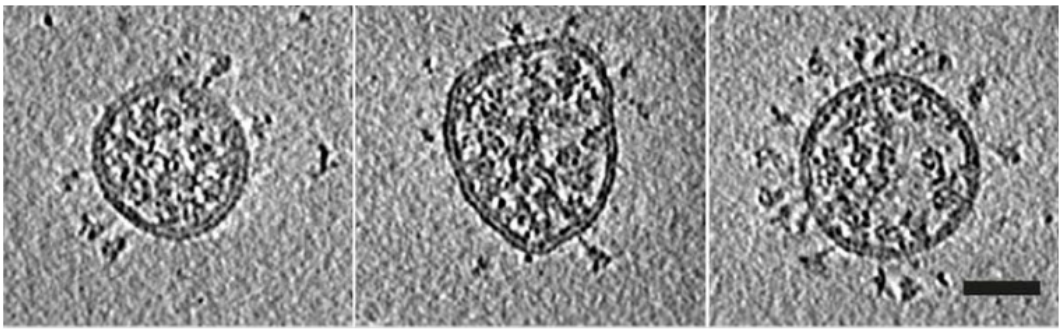


Figure 1 SARS-CoV-2 virion structure. Three representative tomography slices of the virions of SARS-CoV-2 collected from the supernatant of infected Calu-3 cells. Virions appear as almost spherical, with granular density corresponding to RNP. S trimers protrude from viral envelope, giving the crown-shape morphology. Scale bar, 10 nm. Open access (Ke *et al.*, 2020)

Structure

SARS-CoV-2 is an enveloped, non-segmented RNA virus with a positive-sense single-stranded genome approximately 30 kilobases in length. The genome contains a 5' cap structure, 14 open reading frames (ORFs), each preceded by a Transcriptional Regulatory Sequence (TRS), and a 3' polyadenylated tail (Arya *et al.*, 2021).

The viral genome encodes a total of 29 proteins, comprising 25 putative non-structural and accessory proteins, along with four structural proteins. Upon viral entry, two large ORFs (ORF1a and ORF1b) are translated into two polyproteins, pp1a and pp1ab, due to a -1 ribosome frameshift site (Figure 2)(Thomas, 2021) (Pišlar *et al.*, 2020) (Romano *et al.*, 2020). The two polyproteins are cleaved by two different viral proteases, papain-like protease (PLpro) and main-protease (Mpro), to generate 16 non-structural proteins (Nsps), which play crucial role involved both directly and indirectly in the SARS-CoV-2 lifecycle. The remaining viral genome contains ORFs that encode for four structural proteins: S, M, E, and N.

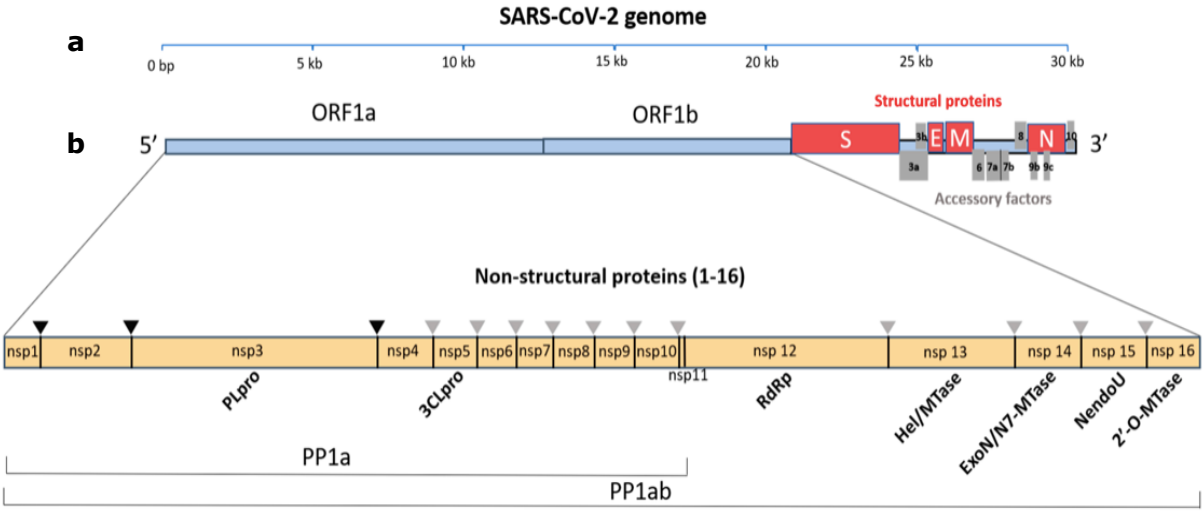


Figure 2 The genome of SARS-CoV-2: a schematic representation. (A) SARS-CoV-2 genome is between the longest RNA viral genome known with about 30 kb and is organized in different ORF (B) Several ORFs have been identified which encode for three different groups of proteins: non-structural (blu) structural (red) and accessory (grey) proteins. Two- thirds of the total length of the genome encode for two long polyproteins (PP1a and PP1ab) cleaved by either PLpro (black triangle) or Mpro (grey triangle) to generate sixteen Nsps. The functional domains in the Nsps are also indicated Open access (Romano *et al.*, 2020).

Non-structural proteins

Alone, ORF1 constitutes two-thirds of the total length of the SARS-CoV-2 genome. It is composed ORF1a and ORF1b, which are directly translated in cell cytoplasm into pp1a and pp1ab. Two viral proteases cleave pp1a and pp1ab to obtain 16 Nsps, which have a role in viral replication, pathogenesis, and evasion from host immune response, but the precise function of some of them needs to be elucidated (Romano *et al.*, 2020).

The N-terminal cleavage product of polyprotein precursors is Nps1, which is cleaved by viral PLpro (Nsp3). This protein has a role in the control of viral proteins expression through the inhibition of cell protein synthesis (Arya *et al.*, 2021). Nps1 binds to the 40S ribosomal subunit, preventing the adequate expression of host factors (Arya *et al.*, 2021). The role of Nsp1 is direct only against cellular protein synthesis because viral RNAs have a 5'-UTR stem-loop region which seems to interact with Nsp1, preventing its inhibitory mechanisms (Arya *et al.*, 2021). Anyway, the precise molecular process is still unclear.

Indeed, Nsp2 is involved in the interaction between viral transcription and translation coupling ribosome and replication-transcription complexes (RTC) (Korneeva *et al.*, 2023).

Nsp3 is the largest protein encoded by the SARS-CoV-2 genome and it is a multi-domain membrane-bound protein (Arya *et al.*, 2021). It has multiple roles in SARS-CoV-2 biology due to the presence of different domains that composed the protein. The main role of Nsp3 is performed by PLpro domain: it cleaves viral polyproteins precursors at three different sites, generating three Nsps (Nsp1, Nsp2, Nsp3) (Arya *et al.*, 2021). In addition to the PLpro domain, Nsp3 contains numerous other functional regions, including a nucleic acid-binding domain (NAB), a ubiquitin-like domain, a SARS-CoV-unique domain, and a transmembrane domain (Lei, Kusov and Hilgenfeld, 2018). The final domain of Nsp3, in combination with Nsp4 and Nsp6, is essential for the reorganization of endoplasmic reticulum (ER) membranes, facilitating membrane curvature. This curvature is critical for the formation of double-membrane vesicles (DMVs), which are required for efficient viral replication (Oostra *et al.*, 2008).

The second protease involved in polyprotein precursors cleavage is Nsp5. It is a cysteine protease, also called the Mpro due to its central role in gene expression and replication process. Dimerization is fundamental for the correct activity of Nsp5, which performs its catalytic activity only in dimer form (Pišlar *et al.*, 2020). Once

dimerized, this non- structural protein is responsible for the cleavage of pp1a and pp1ab in 11 sites to generate 12 Nsps (Roe *et al.*, 2021).

Coronaviruses employ multi-subunit machinery for replication and transcription. The key factor is the RNA-dependent RNA polymerase (RdRp), which is known also as Nsp12, responsible for viral RNA replication and gene transcription. To have the correct activity, Nsp12 forms the RTC together with Nsp7 and Nsp8, two proteins that stabilize the polymerase domain, enabling higher affinity with template RNA and regulating the replication and transcription of SARS-CoV-2 (Peng *et al.*, 2020).

Nsp13 is another non-structural protein involved in the replication and transcription of the viral genome. Indeed, it has helicase activity that can unwind the double-strand RNA (dsRNA) resulting from RNA replication (Robson *et al.*, 2020). Analysis of protein structure showed that Nsp13 can interact with Nsp12 and Nsp8, and these protein-protein interactions lead to an increase of helicase function (Q. Wang *et al.*, 2020).

To maintain such a large genome, coronaviruses need to have a protein that controls the correct replication of viral RNA. Nsp14 has an N-terminal exonuclease (ExoN) domain involved in the proof-reading activity. The peculiar presence of an exonuclease in RNA genome viruses could be the crucial factor for the maintenance of the large genome that characterized all *Coronaviridae* family members (Robson *et al.*, 2020).

Moreover, Nsp14 has a dual role in SARS-CoV-2 biology: it has a C-terminal guanin-N7 methyl transferase domain implicated in the methylation of viral RNA cap (Ma *et al.*, 2015). It performs this second activity together with Nsp10, which is important for the prevention of viral RNA degradation in host cytoplasm (Robson *et al.*, 2020). Capped RNA molecules could be directed recognized by cellular initiating factor 4E, which recruits translation machinery to synthesize proteins.

Nsp15 is a uridine-specific endoribonuclease, conserved among coronaviruses, which cleaved RNA at 3'-end (Pillon *et al.*, 2021). Through this activity, Nsp15 degrades dsRNAs, which otherwise could be recognized by the host immune system. The important role of Nsp15 is supported by animal experiments: it has been shown that mutation in Nsp15 leads to an attenuated disease in mice (Deng *et al.*, 2017).

Structural proteins

Four structural proteins compose the architecture of mature SARS-CoV-2 virions: S, E, M, and N protein. They play a crucial role in the viral life cycle and are essential for viral assembly, infectivity, and immune evasion; in particular, the S protein mediates host cell entry by binding host receptor, the envelope and membrane proteins are involved in viral assembly and budding, while the nucleocapsid protein is critical for RNA packaging and viral replication. Understanding the structural characteristics and functional roles of these proteins is fundamental for the development of therapeutic strategies aimed at inhibiting viral propagation and mitigating the effects of COVID-19.

S protein

S protein has become the most investigated protein from SARS-CoV-2 spread due to its pivotal role in viral lifecycle together with its highly immunogenicity and it is also the main target of host humoral response (Duan *et al.*, 2020).

The S protein is a fusion glycoprotein composed of 1273 amino acids, forming a class I homotrimer, and is responsible for the characteristic 'crown' morphology of SARS-CoV-2. With a size of 180-200 kDa, S is composed of a signal peptide and two main domains, S1 and S2, which remain noncovalently bound in a pre-fusion metastable conformation (Figure 3) (Lan *et al.*, 2020). The S protein is a structural component essential for viral entry, with the S1 subunit responsible for mediating viral attachment and the S2 subunit facilitating the fusion of the viral and host cell membranes (Lan *et al.*, 2020).

In detail, the distal S1 subunit plays a central role in viral attachment, and especially the receptor- binding domain (RBD) is responsible for the high-affinity binding to host receptor, Angiotensin-Converting Enzyme 2 (ACE2) (Wan *et al.*, 2020). RBD undergoes hinge motions, and it could be found in two different conformations: up and down, reflecting RBD accessibility (Figure 3B). It has a consequence not only for its capability to bind ACE2 but also for the possibility of the immune system to target this key region. The RBD has been indicated as the immunodominant site of S protein and the target of the 90% of neutralizing antibodies in SARS-CoV-2 infected subjects (Piccoli *et al.*, 2020). This novel evidence is useful also for diagnostic purposes. Indeed, the detection of antibodies against RBD could also give information about protection, because they seem to better correlate with neutralization activity (Wagner *et al.*, 2021).

The membrane-anchored subunit, S2, mediates the fusion of the viral envelope with the host cell membrane. It involves the Fusion Peptide (FP) domain, two heptad repeat regions (HR1/HR2), a transmembrane domain (TM), and a cytoplasmic domain (CD) (Wrapp *et al.*, 2020). Cryo-EM studies of the prefusion conformation reveal that the HR1 region forms four helices, composing the main helical stalk of S2 together with HR2, while the FP domain is arranged in a loop buried inside due to its high hydrophobicity (Y. Huang *et al.*, 2020) (Wrapp *et al.*, 2020). TM is responsible for the anchor of spike protein to the viral membrane, for spike trimerization and membrane fusion due to the interaction with FP during the fusion process (Zhu *et al.*, 2021). Moreover, structural studies highlighted that around 97% of spike trimers are in the prefusion conformation, while only 3% adopt the post-fusion state, crucial for viral entry (Ke *et al.*, 2020).

The last portion of the S2 subunit is composed of a CD tail, which is involved in viral assembly and intracellular transport (Petit *et al.*, 2005).

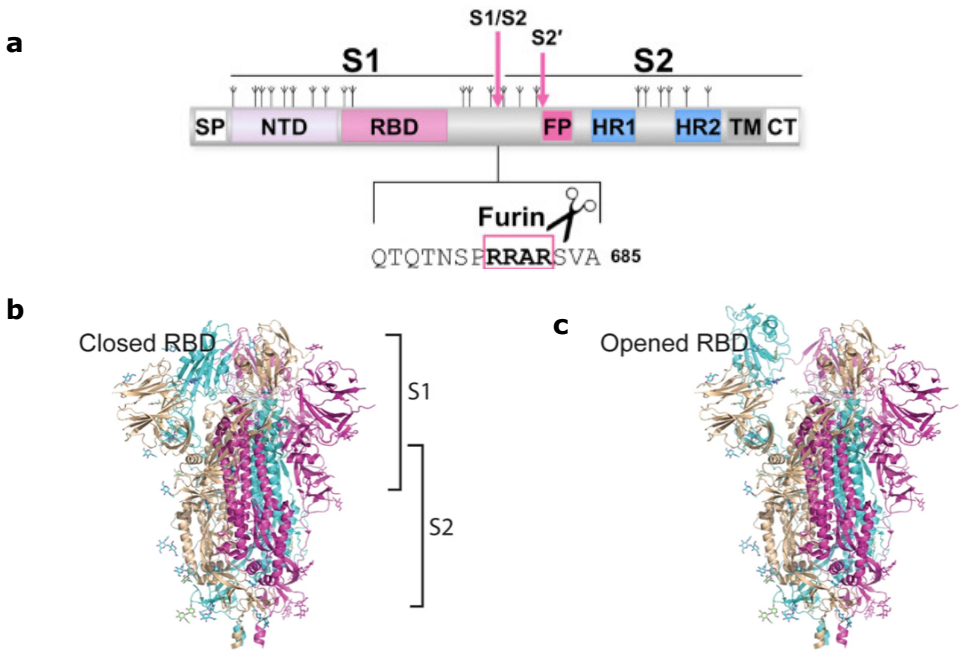


Figure 3 Spike Protein Structure. (A) Schematic diagram of the S protein of SARS-CoV-2, with its distinct domains color-coded for clarity. Arrows indicate the cleavage sites recognized by host proteases, including the furin cleavage site, which is characterized by a specific motif. **(B)** Cryo-EM structural images of the S protein, showing the two conformational states of the receptor-binding domain (RBD): the "closed" conformation (left) and the "open" conformation (right), with the latter corresponding to the RBD being prepared for binding to the host cell receptor, ACE2. Open access (Santopolo, Riccio and Santoro, 2021) (Y. Huang *et al.*, 2020).

Knowing the biogenesis of S protein is extremely important because it is processed by cell proteases in host compartments (Jaimes *et al.*, 2020). In detail, S glycoprotein is synthesized from cellular machinery on rough endoplasmic reticulum (rER) (Duan *et al.*, 2020). The precursor protein possesses an N-terminal signal sequence, which is cleaved by signal peptidases within the ER lumen upon proper protein synthesis (Duan *et al.*, 2020). Shortly after its synthesis, three S protein monomers spontaneously assemble into a homotrimeric structure, a process that likely facilitates the transport of the protein from the endoplasmic reticulum (ER) to the Golgi apparatus. Within the Golgi, the high-mannose oligosaccharide side chains undergo modifications, and O-linked glycosylation is also introduced. These post-translational modifications are critical for masking the spike protein from immune surveillance, thereby contributing to its ability to circumvent the host's antiviral immune response(Walls *et al.*, 2016).

Sequence analyses highlight the presence of polybasic cleavage motif (PRRAR), which is the consensus sequence for furin and furin- like proteases, at S1/S2 junction (Figure 3A) (Jaimes *et al.*, 2020). In ER-Golgi intermediate compartment (ERGIC), host furin protease cleaves S protein into two subunits, which remain non-covalently associated. It has been demonstrated that the furin cleavage leads to a pre-activation form of S glycoprotein, with dramatic consequences for viral entry kinetics (Peacock *et al.*, 2021). The deletion of PRRAR consensus sequence site leads to a decrease in SARS-CoV-2 capability to infect pulmonary cells, which underlines the important role of furin cleavage for the entry process (Johnson *et al.*, 2021). Interestingly, the furin cleavage site is absent in closely related coronaviruses, a difference that may account for the rapid global spread of SARS-CoV-2 (Hoffmann, Kleine-Weber and Pöhlmann, 2020).

Spike protein also has a second cleavage site, S2', which is essential for fusion activation. Indeed, as shown in Figure 3A, S2' is immediately before FP domain: proteolytic cleavage triggers the exposure of FP and the consequent fusion between viral and host cell membranes (Zhu *et al.*, 2021). Multiple cellular proteases are implied in the second proteolytic process, and between them, transmembrane serine protease 2 (TMPRSS2) and cathepsin L play a pivotal role. Indeed, different studies highlighted the importance of host cell protease cleavage for entry in pulmonary cells, using inhibitors and knock-down experiments (Bestle *et al.*, 2020).

The cleavage and processing of the S protein remain areas of ongoing research; however, their importance for viral entry is unequivocal.

E protein

The E protein is a small highly conserved integral membrane protein composed of 76 amino acids and weighing 8–12 kDa (Liu, Yuan and Liao, 2007) (Fung and Liu, 2018).

It consists of three domains: a hydrophilic N-terminal domain (NTD), a hydrophobic transmembrane domain (TMD), and a hydrophilic C-terminal domain (CTD) (Arya *et al.*, 2021). The E protein is involved in various stages of the virus life cycle, including the assembly, budding, and release of the virion (Figure 4A).

Structurally, the E protein contains seven alpha helices and eight loop regions forming a pentameric configuration with 35 alpha-helical regions and 40 looped ring regions (Figure 4B) (Surya, Li and Torres, 2018).

The E protein plays a structural role in mediating the assembly and trafficking of the mature virion, ultimately contributing to its budding and the formation of the characteristic spherical morphology of the virus (Zhou *et al.*, 2023).

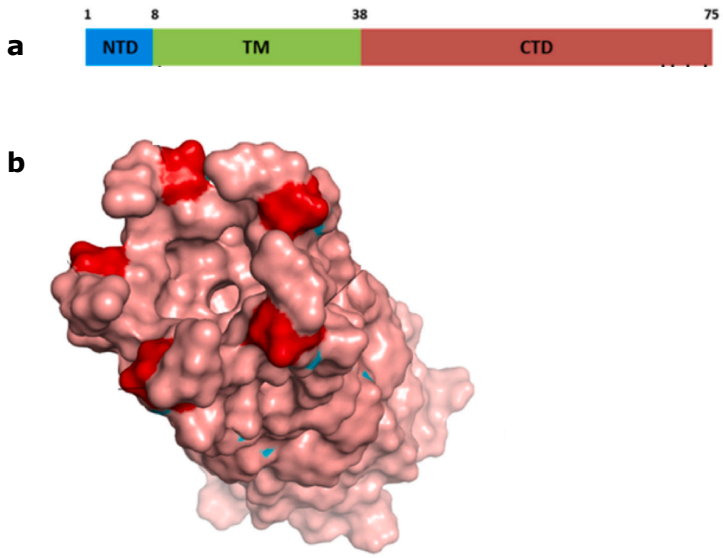


Figure 4 Domain structure of E protein. (A) Schematic representation of the E protein, with the N-terminal domain (NTD), transmembrane domain (TM), and C-terminal domain (CTD) labeled. **(B)** A pentameric model of E proteins, illustrating the channel structure. Open access (Mou *et al.*, 2021).

Furthermore, this protein functions as a viroporin, forming ion channels that disrupt cellular ion homeostasis, particularly calcium, sodium, and magnesium, which contributes to cellular damage and viral release altering the electrochemical gradients of host cells and triggering inflammatory responses and cytokine release. This function is crucial for the pathogenesis of COVID-19, as it modulates immune responses, including activation of the immunity response and enhancing the release

of pro-inflammatory cytokines, a key feature of severe COVID-19 cases, resulting in tissue damage, organ failure, and death (Zhou *et al.*, 2023).

The E protein also interacts with host proteins like PALS1, ZO-1, and syntenin, disrupting epithelial cell polarity and promoting viral dissemination and immune cell infiltration into lung tissues. This interaction may contribute to the increased virulence of SARS-CoV-2 compared to other coronaviruses (Zhou *et al.*, 2023).

Overall, the E protein is a multifunctional protein that plays critical roles in viral replication, assembly, immune modulation, and host cell disruption. Its small size relative to other structural proteins belies its significance in the viral life cycle and pathogenesis, making it a crucial target for therapeutic interventions aimed at limiting SARS-CoV-2 infection.

M protein

M protein is one of the most conserved and abundant structural protein in SARS-CoV-2 virion, and it is composed of 223 amino acids and is organized in one the N-terminal ecto-domain, three transmembrane helices (TMH1, TMH2, and TMH3), and one C-terminal endo-domain (Arya *et al.*, 2021) (Zhang *et al.*, 2022) (Figure 5). It has a low mutation rate and shares structural and functional similarities with the M proteins of other coronaviruses. This protein could have homotypic interaction (M-M interaction), or it could bind to other structural proteins in a heterotypic interaction (Arya *et al.*, 2021).

Both are essential for the correct formation and budding of mature virions. Briefly, M-N protein interaction stabilize the viral RNA genome, M-E interactions induce membrane curvature, aiding in the assembly and release of virus-like particles, while M-S interactions are critical for S protein retention and integration into virions (Marques-Pereira *et al.*, 2022). Additionally, M protein modulates host immune responses, enhancing viral replication through the inhibition of cellular factors involved in the activation of innate immune response to pathogens (Satarker and Nampoothiri, 2020).

Despite its central role in viral biology, the structure of the M protein remains elusive, as it has been difficult to stabilize and crystallize, preventing the use of techniques like NMR, X-ray crystallography, and cryo-EM. Understanding the structure-function relationship of M protein is critical for developing targeted therapeutics, given its importance in viral life cycle and immune evasion.

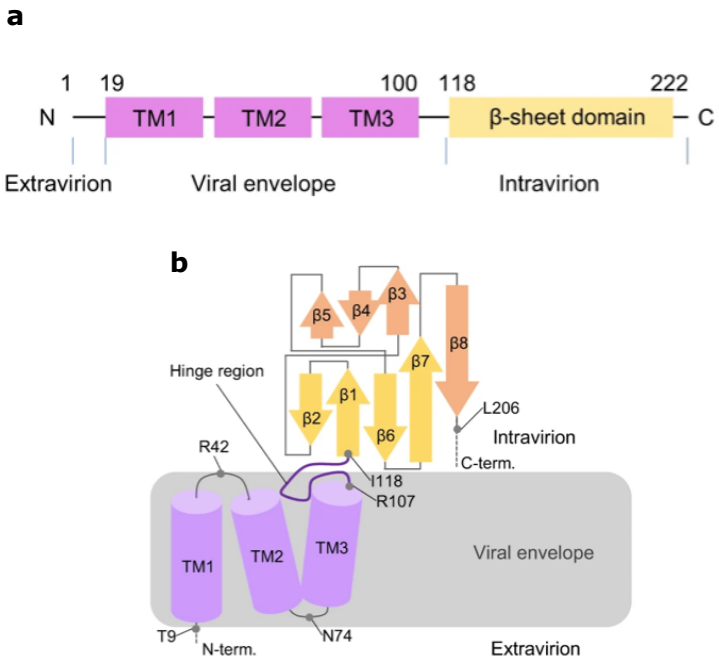


Figure 5 Domain structure of M protein. (A) Schematic representation of M protein domain in different color. **(B)** Schematic view of the M protein protomer. Secondary structure elements and hinge regions are indicated. The unstructured N-terminal and C-terminal regions are marked with dashed lines. Open access (Zhang *et al.*, 2022).

N protein

Nucleocapsid protein is encoded by ORF9 and it is composed of two highly structured domains, divided by disorder linker region: N-term RNA binding domain and a C-terminal domain responsible for dimerization (Bai *et al.*, 2021). N protein is a structural protein involved in RNA packaging. The N-terminal domain of the protein is responsible for both binding to viral RNA and the self-association process, which lead to the formation of helical RNP (Arya *et al.*, 2021) (Bai *et al.*, 2021).

The interaction between N and the other structural proteins is essential for the correct genome encapsidation during the virion assembly process (Bai *et al.*, 2021).

Accessory proteins

Interspersed among the structural genes, there are also nine putative ORFs for accessory factors. There are still unanswered questions about their role in SARS-CoV-2 biology, but they seem to participate in mechanisms that the virus used to escape from immune response (Redondo *et al.*, 2021).

For example, ORF3b, together with ORF6, ORF8, and ORF9b, suppress IFN response (Redondo *et al.*, 2021). To support, studies show that deletion of ORF8 result in milder pathology and more robust production of type I IFN during the early phases of the infection (Young *et al.*, 2020). Additionally, accessory proteins could also hamper cellular functions. For example, ORF3a alters autophagy and apoptosis, while ORF3d impact mitochondrial homeostasis (Redondo *et al.*, 2021).

Accessory proteins are not directly involved in viral replication, but they are implicated in different pathogenic mechanisms of SARS-CoV-2 infection. For these reasons, further elucidations about their role are required.

Replicative cycle

Viruses are obligate intracellular parasites that lack the genetic encoding necessary for the synthesis of all proteins required for their replication.

To propagate, they subvert the host cell's molecular machinery, to facilitate their replication and assembly. The highly regulated and stepwise sequence of molecular interactions that underpins viral replication and progeny formation is referred to as the viral life cycle. This process unfolds in a series of specific and well-defined steps, beginning with the ability of the virus to attach and enter the host cell, thereby propagating its genome and generating infectious viral particles capable of infecting neighboring cells.

The first crucial step in this cycle is viral attachment, where the virus binds to host cell receptors, a process that determines the tissue tropism of the virus. The subsequent step involves viral entry, which occurs via distinct mechanisms depending on the viral characteristics. Once inside the cytoplasm, the virus takes control of the host cell metabolic processes to replicate its genome and synthesize viral proteins. Finally, these viral proteins and genomes assemble into new virions, which are then released from the host cell to infect new cells.

This paragraph will focus on the mechanisms SARS-CoV-2 employs to infect host cells. Understanding the SARS-CoV-2 life cycle has been a major area of research, as deciphering the virus strategies for cellular entry and replication could provide valuable insights for the development of targeted therapeutic interventions.

Attachment

The first stage of the viral replication mechanism is viral attachment: the viral receptor binds cellular protein to penetrate the host cells. For the SARS-CoV-2, receptor involved is the S protein. Due to its sequence similarity with the S glycoprotein of SARS- CoV-1, scientists predicted that also the novel coronavirus used Angiotensin-converting enzyme 2 (ACE2) as primary cellular receptor for entry into host cells (Shang *et al.*, 2020).

To date, *in silico* and *in vitro* studies supported this thesis, as the work of Hoffman and colleagues in which demonstrated anti-ACE2 antibody blocks SARS-CoV-2 infection in susceptible cells (Hoffmann *et al.*, 2020).

ACE2 is a type I transmembrane protein composed of 805-amino acid. Functional domains include the C-terminal membrane anchor portion and the N-terminal region which contains the catalytic site (Scialo *et al.*, 2020). Its enzymatic activity on angiotensin (Ang) I leads to the formation of Ang 1–9, a peptide that plays a role in vasoconstriction and regulation of blood pressure within the renin-angiotensin-aldosterone system. Literature data shows that ACE2 is ubiquitously expressed, with a relatively high level in the gastrointestinal tract, kidney, testes (*The Human Protein Atlas --- proteinatlas.org*, no date). Nevertheless, it is also present in other districts of the body, such as the heart, thyroid, and pulmonary tissue. ACE2 expression in the lung is mainly limited to type II alveolar epithelial cells (Y. Wang *et al.*, 2020). The comprehension of the distribution of the SARS-CoV-2 receptor is important to better investigate the mechanisms involved in infection and spread. The broad expression of ACE2 in human tissues explains the wide spectrum of symptoms caused by SARS-CoV- 2 infection.

The interaction between the virus and host cells occurs through the molecular recognition between the RBD portion of the spike glycoprotein and the N-terminal peptidase domain of ACE2. Cryo-EM studies examined the binding between spike and its cellular receptor (Benton *et al.*, 2020).

Spike glycoprotein on mature virions is in trimeric conformation and all the three RBDs could be in "down", representing an inaccessible state, or "up" conformation. Only in this last conformation, RBD is accessible, and an ACE2-binding event could occur (Yan *et al.*, 2021).

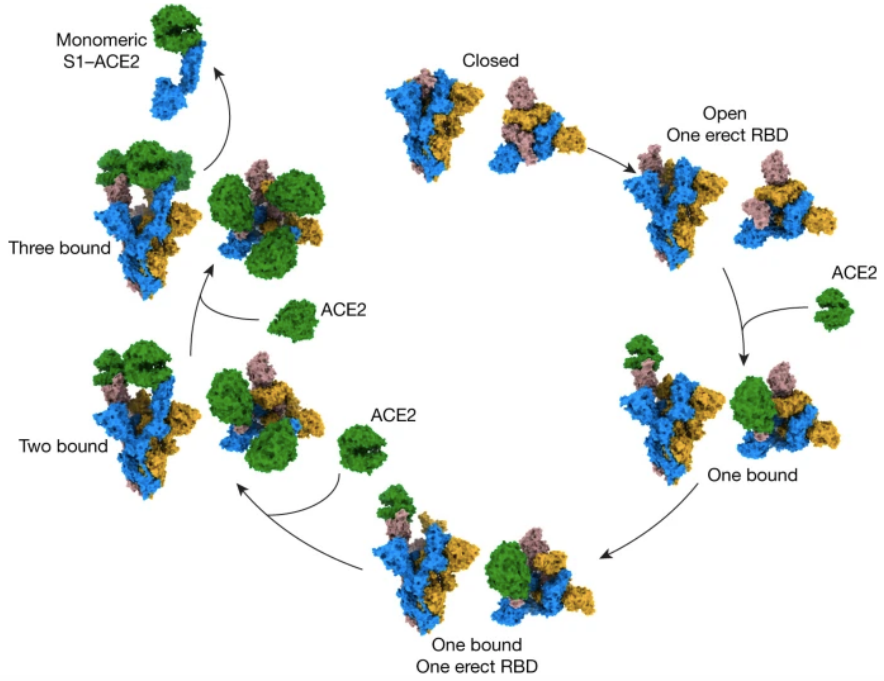


Figure 6 Spike-ACE2 binding process. On the top there is the representation of close conformation of spike glycoprotein. Clockwise, spike structure with one RBD in "up" conformation, that subsequentially could be bound to ACE2 molecule. This interaction induces a conformational change in one of the other two RBDs, leading to open state (bottom of the circle). Erected RBD could bind another ACE2 receptor, reaching the full-open conformation. At the end, all the three RBDs interact with ACE2. Open access (Benton *et al.*, 2020).

In detail, as represented in Figure 6 in its initial state, the S protein is in a closed conformation, where the RBDs are buried, making them inaccessible to ACE2; when the spike encounters the host cell, the protein undergoes a conformational change that opens one of the RBDs, exposing the ACE2 binding site. Upon binding, ACE2 induces a rigid-body rotation of the RBD, shifting its position and destabilizing the closed state of the spike protein. This binding event leads to an increasingly open conformation, which facilitates the binding of additional ACE2 molecules. As more ACE2 receptors bind, the spike protein progressively adopts a more open structure. This transition reduces the interactions between the S1 subunits and the S2 core and creates the conditions necessary for the are essential for SARS-CoV-2 infectivity (Benton *et al.*, 2020).

To date several alternative receptors for SARS-CoV-2 have been proposed in addition to ACE2. These include C-type lectins, such as DC-SIGN and L-SIGN, which bind to glycans on the viral surface and facilitate viral entry by promoting attachment to host cells (Jeffers *et al.*, 2004) (Amraei *et al.*, 2021). Other potential receptors include TIM1 and AXL, members of the phosphatidylserine receptor family, which enhance viral entry by binding phosphatidylserine present on the membrane of the virus (Wang *et al.*, 2021) (Richard *et al.*, 2017). However, these molecules are considered "attachment factors" rather than specific receptors, as they do not efficiently support infection in the absence of ACE2.

CD147, a widely expressed transmembrane glycoprotein, has been proposed as an alternative receptor for SARS-CoV-2, although its exact role in viral entry is uncertain due to its inability to directly interact with the spike protein (Chen *et al.*, 2005) (K. Wang *et al.*, 2020). Furthermore, neuropilin 1 (NRP1) has been implicated in facilitating viral entry by enhancing TMPRSS2-mediated S1 shedding and exposing the S2’ cleavage site, particularly in wild-type SARS-CoV-2 (Cantuti-Castelvetri *et al.*, 2020) (Li and Buck, 2021). However, NRP1 is primarily expressed in olfactory and respiratory epithelial cells, with lower expression in ciliated airway cells, which are the main target for the virus.

Additionally, B0AT1, an amino acid transporter involved in ACE2 expression in the small intestine, may also play a role in SARS-CoV-2 infection in non-lung tissues, though further research is needed to confirm the significance of these factors (Camargo *et al.*, 2009) (Yan *et al.*, 2020).

Entry

Upon spike-ACE2 interaction, S glycoprotein requires activation. Like other respiratory viruses, host cell proteases cleave the S protein, leading to the exposure of FP and the consequent initiation of the fusion process between viral and cellular membranes (Hoffmann *et al.*, 2020) (Hoffmann, Kleine-Weber and Pöhlmann, 2020).

The first cellular protease involved in spike cleavage is furin, a ubiquitous endoprotease that cleaves at RX(K/R)R consensus motif. S glycoprotein harbors a multibasic cleavage site at S1/S2 junction (PRRAR) which is recognized by furin during spike maturation in ERGIC compartment (Hoffmann, Kleine-Weber and Pöhlmann, 2020). Several studies underline the importance of the furin cleavage site in pre-activation of spike: it seems that it promotes replication in the respiratory tract but also it increases transmission in the ferret model (Peacock *et al.*, 2021). Indeed, comparative studies among coronaviruses have highlighted that the absence of a furin cleavage site in the S proteins of SARS-CoV and MERS-CoV likely contributes to their comparatively lower infectivity and more restricted transmission efficiency (Peacock *et al.*, 2021) (Hoffmann, Kleine-Weber and Pöhlmann, 2020). Moreover, among the *Paramyxoviridae* family, such as Human Respiratory Syncytial Virus (RSV) and Influenza A viruses also possess furin recognition motifs in their surface glycoproteins, necessary for optimal fusion and infection (Lubinski and Whittaker, 2024). Indeed, the hemagglutinin (HA) protein, which is responsible for viral attachment and fusion, also undergoes cleavage by host proteases like furin necessary for the activation and the fusion of the viral envelope with the host cell membrane (Russell, 2021).

Activation of S protein is a complex multistep process mainly driven by host proteases in different cellular compartments. Viral receptor requires another proteolytic cleavage at S2' site to unmask FP domain and to enable viral-host membrane fusion. This event occurs either at the plasma membrane or at the endosomal level, distinguishing the two mechanisms that SARS-CoV-2 exploits to enter the host cells: plasma membrane/ph independent (early) and endosomal membrane/ph dependent (late) pathways, respectively (

Figure **7**).

plasma membrane/ph independent

Transmembrane serine protease 2 (TMPRSS2) is a type II transmembrane serine protease (TSP) that is expressed in the respiratory, gastrointestinal, and urogenital tract. Among TSP, previous works identified TMPRSS2 as a virus-activating protease, initiating the fusion proteins of respiratory viruses such as influenza viruses, human parainfluenza viruses, and coronaviruses (Bestle *et al.*, 2020) .

Upon RBD-ACE2 interaction, TMPRSS2 cleaves at monobasic S2' site of spike glycoprotein. This event leads to the exposure of the FP and the consequent direct fusion between viral and cellular membranes (

Figure **7**A) (Hoffmann *et al.*, 2020). Recent data prove the pivotal role of TMPRSS2 protein in the SARS-CoV-2 entry process. *In vitro* administration of camostat mesylate, an inhibitor of TMPRSS2 activity, supports the importance of the early pathway in human airway cells (Hoffmann *et al.*, 2020).

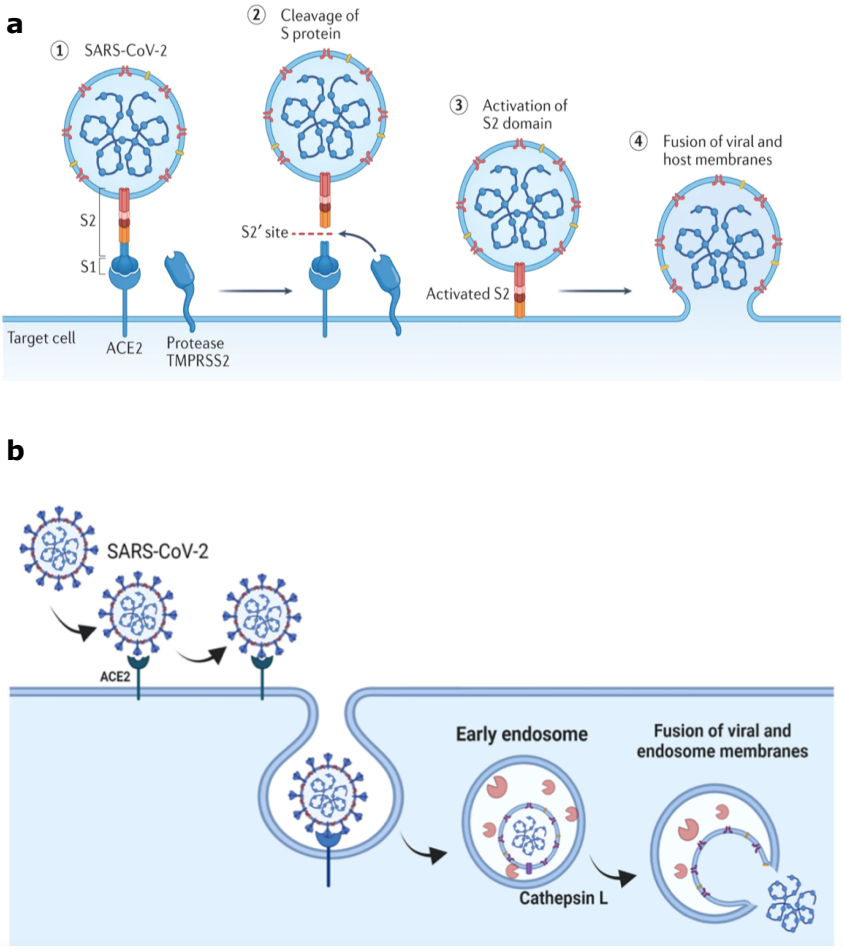


Figure 7 Entry mechanisms of SARS-CoV-2 infection. Upon binding of the receptor-binding domain (RBD) of the S glycoprotein to the ACE2 receptor on the host cell, several host cell proteases can cleave the S protein in different subcellular locations. **(A)** At the plasma membrane, the protease TMPRSS2 cleaves the S protein, exposing the fusion peptide (FP) domain, which enables the direct fusion of the viral and host cell membranes. **(B)** Alternatively, SARS-CoV-2 may enter host cells via endocytosis, where cathepsin L activates the spike glycoprotein, leading to membrane fusion and the subsequent release of the viral RNA into the cytoplasm. Open access (Cesar-Silva *et al.*, 2022) (Jackson *et al.*, 2021)·

Indeed, the inhibition of TMPSS2 dramatically reduces the capability of SARS-CoV-2 to infect susceptible cells (Hoffmann *et al.*, 2020). Interestingly, neither TMPRSS2 nor furin could compensate each other: to activate the early pathway, both proteolytic cleavages are required (Bestle *et al.*, 2020).

endosomal membrane/ph dependent

SARS-CoV-2 can use an alternative mechanism to enter the host cells, which is called the late pathway. If TMPRSS2 does not cleave the S glycoprotein, the binding between viral and host receptors induces the internalization of the virion (

Figure **7**B). The endocytic pathway was well characterized in a recent study, in which, following the binding of the RBD to ACE2, clathrin-coated capsid proteins began to assemble on the inner leaflet of the plasma membrane. The authors concluded that the endocytosis pathway is mediated by clathrin-coated pits, suggesting a possible mechanism for viral internalization (Miao *et al.*, 2023).

The central molecular host players in the late pathway of SARS-CoV-2 infection are cathepsins, which play a crucial role in the activation of the spike (S) protein. In the context of SARS-CoV-2, the most studied cathepsins are cathepsin B and cathepsin L, both of which are lysosomal endopeptidases involved in intracellular protein catabolism. These enzymes are synthesized as inactive precursors (zymogens), and their enzymatic activity is optimal in an acidic environment, typically between pH 4.5 and 5(Gomes *et al.*, 2020). Cathepsins B and L are present in all tissues, and their main role is the proteolysis of foreign proteins within the endolysosomal compartment (Miao *et al.*, 2023) (Gomes *et al.*, 2020) (Storti *et al.*, 2021). Moreover, other cathepsins, such as cathepsin D, may also play a lesser role in virus processing and entry (Miao *et al.*, 2023).

Several *in vitro* works emphasized the importance of the proteolysis of S from lysosomal enzymes. In TMPRSS2 cells, the administration of E-64d, a cathepsin inhibitor, efficiently hampers the entry of SARS-CoV-2, demonstrating that cathepsins are involved in priming S protein (Hoffmann *et al.*, 2020). Notably, the expression of TMPRSS2 could partially rescue the capability of SARS-CoV-2 to penetrate host cells even in the presence of E-64d, emphasizing the importance of this surface protease (Hoffmann *et al.*, 2020).

To dissect the role of different lysosomal proteases, several studies have treated specific cell lines with cathepsin inhibitors. One study demonstrated that the use of a cathepsin L inhibitor prevented the entry of SARS-CoV-2 pseudoviruses,

highlighting the important function of cathepsin L in SARS-CoV-2 biology(Ou *et al.*, 2020). In contrast, other studies using the entire virus revealed that the application of Cathepsin B inhibitors significantly decreased SARS-CoV-2 infection rates in cell culture models, further underscoring the crucial role of this protease in the viral life cycle(Milan Bonotto *et al.*, 2023).

Replication

Regardless of the entry pathway used by SARS-CoV-2 to infect susceptible cells, fusion of the viral and host cell membranes results in the release of the viral genomic RNA (gRNA) into the cytoplasm. As an RNA virus, SARS-CoV-2 replication occurs in the cytoplasm of the infected cells, exploiting its replication machinery (Figure 8) (V'kovski *et al.*, 2020).

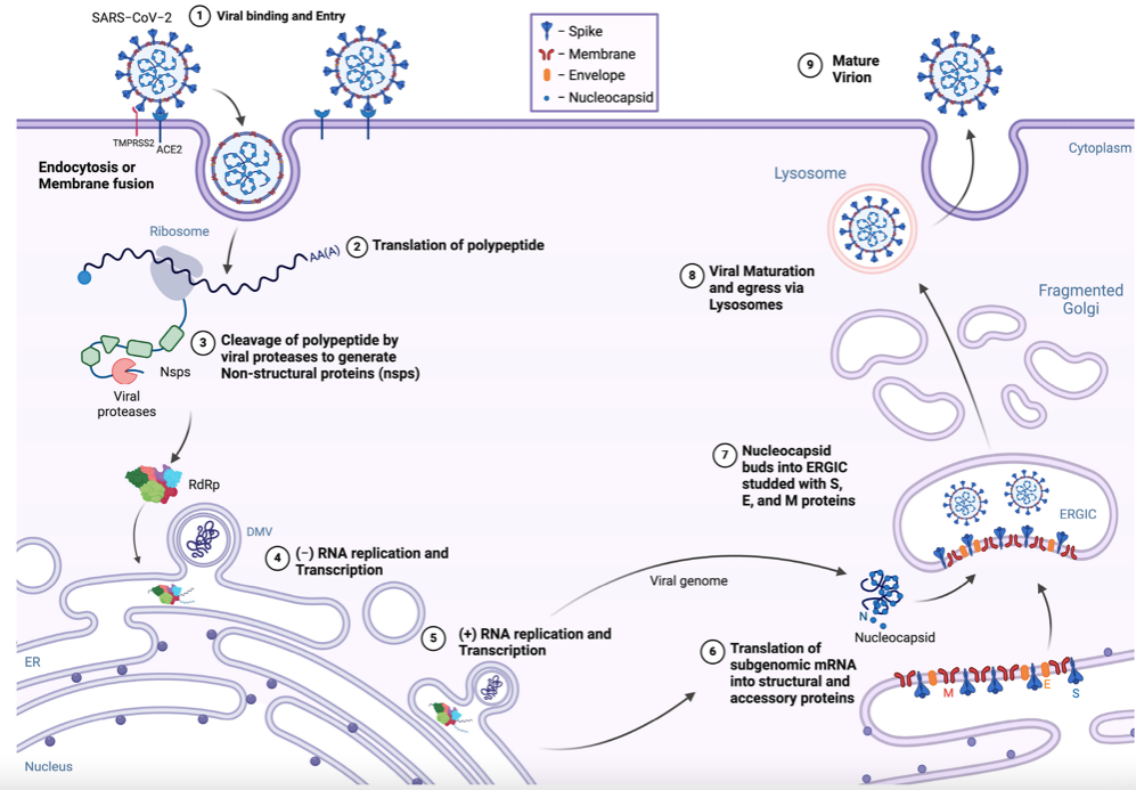


Figure 8 SARS-CoV-2 replicative cycle. Step 1 of SARS-CoV-2 lifecycle occurs with RBD-ACE2 interaction and entry mechanism. Regardless of the mechanism, the viral RNA is released into the cytosol, where ORF1 is translated into two polyproteins, pp1a and pp1ab (step 2). Two viral proteases, PLpro and Mpro, cleave the two polyproteins, generating 16 Nsps (step 3). Replication begins in double membrane vesicles (DMV), where Nsps assembly together with gRNAs to form replication transcription complex (RTC). DMVs create a microenvironment for genomic replication and the transcription of subgenomic RNAs (step 4). Cellular machinery translates these subgenomic RNAs into structural and accessory proteins (step 6), which are essential for the virion formation and for the escape from immune response, respectively. Structural proteins M, E and S translocate into ER membrane and ERGIC compartment (step 7), while N protein interacts with newly produced genomic RNA to form nucleoprotein complex. The release of mature virions occurs via exocytosis: nucleoprotein complex assemblies with structural proteins budding into the lumen of secretory vesicular compartments (step 8), and then virions are secreted from plasma membrane to extracellular space to infect adjacent cells (step 9). Open access (V'kovski et al., 2020) (Katiyar *et al.*, 2024).

Due to its structure, ribosomes recognize the viral genome as an mRNA, and ORF1a and ORF1b are directly translated in pp1a and pp1ab, which are cleaved by Mpro and PLpro, to produce 16 Nsps (1-16) (V'kovski *et al.*, 2020) (Brant *et al.*, 2021) . The study of the virus replication mechanisms shows that Nsps are an essential factor for the correct replication of the viral genome. Nsps2-11 modulate intracellular membranes, host evasion and provide essential functions for the correct formation of the RTC (V'kovski *et al.*, 2020).

Nsps12-16 are the enzymatic core of RNA synthesis, RNA proofreading, and RNA modification (V'kovski *et al.*, 2020).

SARS-CoV-2, like other RNA viruses, replicates in structures called double-membrane vesicles (DMV), which are ER-derived and interconnected perinuclear double-membrane structures (Knoops *et al.*, 2008) .

These vesicles create a controlled microenvironment in which SARS-CoV-2 could replicate without being recognized by the host immune system (V'kovski *et al.*, 2020).

The replication of the gRNA starts with the synthesis of negative-sense genomic copies, which could be continuous o discontinuous, generating either the template for gRNA or subgenomic RNA (sgRNA). A body Transcription Regulatory Sequence (TRS-B) precedes every structural and accessory ORFs and a leader TRS (TRS-L) is present at the 5' untranslated region of the viral genome (Figure 9) (Kim *et al.*, 2020).

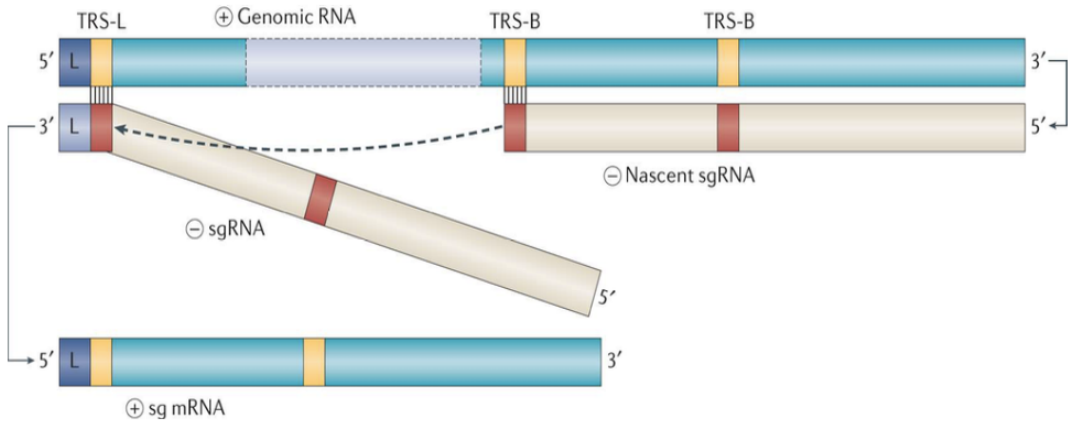


Figure 9 A schematic illustration of discontinuous transcription. The full-length positive-strand genomic RNA uses as a template for the synthesis of both full-length negative-strand RNA and subgenomic RNAs. Specifically, when the viral polymerase encounters TRS-B (yellow), it may either proceed with transcription or translocate to TRS-L, as indicated by the arrow. The resulting subgenomic RNA (sgRNA) then acts as a template for the production of positive-sense sgRNAs, which are recognized by the host cell machinery initiating the translation of structural and accessory proteins. Open access (V'kovski *et al.*, 2020).

When RdRp encounters TRS-B, the synthesis of negative RNA could either proceed or translocate to TRS-L: the outcome is the production of negative-strand sgRNAs with different lengths. They act as a template to generate positive sgRNA that are translated into structural and accessory proteins by cellular ribosomes (Kim *et al.*, 2020). S, M, and E proteins enter the ER where they undergo maturation, while N protein interacts with gRNAs to produce nucleoprotein complex.

Assembly and release

The genomic RNA and structural proteins synthesized at the replication site, are subsequently transported to the ER-Golgi intermediate compartment (ERGIC) through where viral assembly and budding take place (Figure 10). Only the four structural proteins are included into the virion. The N protein binds the viral genome and is then encapsulated, while the structural proteins S, E, and M are incorporated into the viral membrane (Jackson *et al.*, 2021). The S protein is cleaved in the Golgi apparatus by furin or furin-like proteases, resulting in the split-up into the S1 and S2 subunits, which remain associated. The proteins M and E facilitate viral assembly and budding through interactions with other viral components. Once assembled, the mature virions bud into the ER-Golgi intermediate compartment (ERGIC) lumen and via the secretory exocytosis pathway are transported to the plasma membrane where are released to the extracellular space (V'kovski *et al.*, 2020).

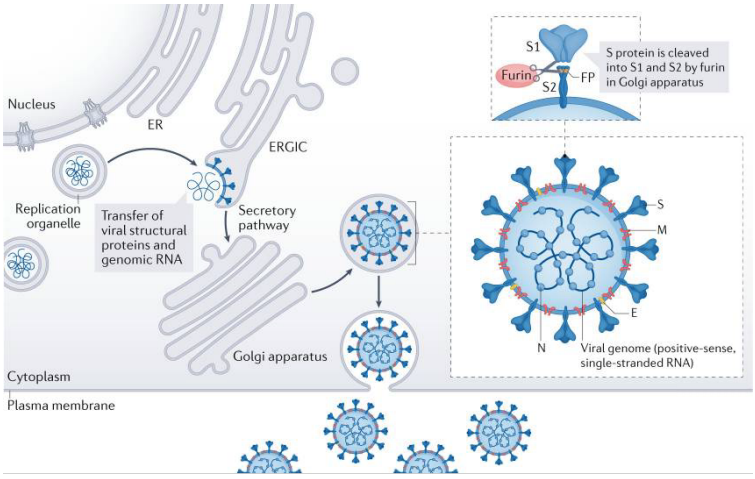


Figure 10 Viral Assembly and Budding Process. SARS-Cov-2 infection induces the formation of perinuclear membranous structures derived from the ER and surrounded by double membranes protecting the viral replication machinery from host immune responses. The novel synthesized viral proteins and RNA are transported to ERGIC compartment for assembly. The mature virion is then shipped to the plasma membrane and released into the extracellular. Open access (Jackson *et al.*, 2021).

IMMUNE RESPONSE TO PATHOGEN

Innate immune response

Innate immunity

Upon cellular entry, SARS-CoV-2 triggers host immune responses, activating both humoral and cell-mediated adaptive immunity. The first line of antiviral defense involves the activation of the innate immune system via pattern recognition receptors (PRRs), which detect pathogen-associated molecular patterns (PAMPs) in the form of viral single-stranded RNA (ssRNA) and double-stranded RNA (dsRNA) (Züst *et al.*, 2011).

PPRs are essential elements, playing a crucial role in the detection of viral infections, activation of inflammatory responses, and ultimately promoting viral clearance.

These receptors, distributed across cellular membranes, cytosol, and nucleus, recognize both PAMPs from infectious agents and damage-associated molecular patterns (DAMPs) released by compromised cells. Within the pattern recognition receptor (PRR) families, several key receptors are involved in the detection of viral pathogens, including Toll-like receptors (TLRs), RIG-I-like receptors (RLRs), and melanoma differentiation-associated gene 5 (MDA5) (Kanneganti, 2020). However, it has been demonstrated that only a subset of PRRs, including TLRs, RLRs, NLRs, MDA5, and the inflammasome, activate their signaling pathways in response to SARS-CoV-2. Downstream of PRR sensing of PAMPs and damage-associated molecular patterns (DAMPs), several signaling cascades are initiated leading to proinflammatory cytokine and chemokine secretion and cell death, among other outcomes (Züst *et al.*, 2011).

Initial innate immune activation against SARS-CoV-2 (Figure 11) occurs through viral ssRNA detection by cytosolic PRR (specifically RIG-I and MDA5) and endosomal TLRs (primarily TLR3 and TLR7). This recognition triggers interferon (IFN) production, a critical antiviral defense mechanism. The downstream signaling cascade following PRR activation induces Type I/III interferons and proinflammatory cytokines tumor necrosis factor alpha (TNF-α), interleukin (IL)-1, IL-6, and IL-18, which enhance an adaptive immune response(C. Wang *et al.*, 2020). Specifically, RIG-I and MDA5 activate the mitochondrial antiviral signaling protein (MAVS), a downstream adaptor located on the mitochondria, which subsequently triggers the activation of tumor

necrosis factor receptor-associated factor 3 (TRAF3), TBK1 (TANK-binding kinase 1), a key activator of NF-kB, and IKKε (inhibitor of NF-kB kinase-ε). This cascade leads to the phosphorylation of the interferon-regulator genes (IRF)-3 and IRF7 leading to the activation of type I interferons (IFNs) and numerous interferon-stimulated genes (ISGs) (Loo and Gale, 2011). A comparable signaling cascade occurs downstream of TLR3 and TLR7 (Figure 11). Secreted type I IFN bind to interferon receptors (IFNAR), leading to the activation of JAK/STAT Tyrosine kinase 2 (Tyk2) cascade, where the activation of STAT1, STAT2, and IRF9, translocates to the nucleus. There, the complex binds to interferon-stimulated response elements (ISREs) in the genomic DNA, triggering the expression of different ISGs with antiviral functions. This cascade can further amplify the immune response through positive feedback loops(Loo and Gale, 2011).

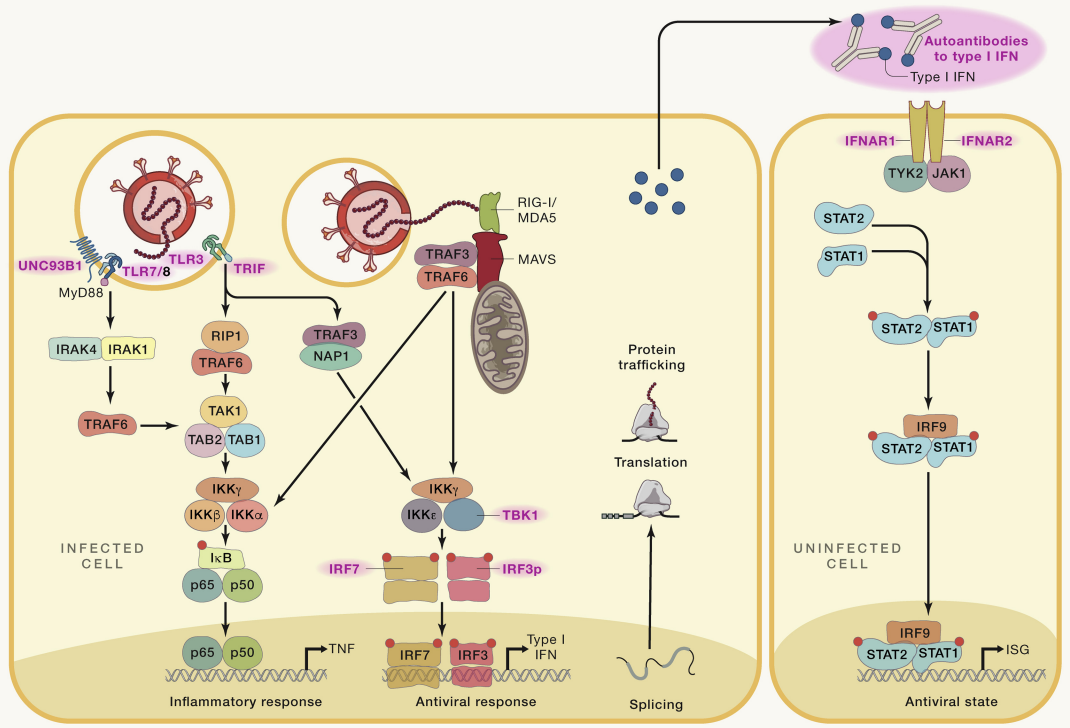


Figure 11 Innate immune response upon SARS-CoV-2 infection. SARS-CoV-2 is detected by various PRRs that recognize foreign RNA, including endosomal TLR3 and TLR7, as well as cytoplasmic RIG-I and MDA5. Based on genetic, functional, clinical, and interaction mapping studies, downstream signaling events triggered by these interactions are depicted. Direct interactions between viral proteins and host cellular mechanisms are shown, with key pathways highlighted. Open access (Schultze and Aschenbrenner, 2021).

Upon detection of PAMPs innate immune cells secrete a range of proinflammatory cytokines. These cells then migrate to the site of infection to mount a response (Schultze and Aschenbrenner, 2021) (Hosseini *et al.*, 2020). In addition, innate

lymphoid cells, including natural killer (NK) cells, are activated, playing a critical role in the direct elimination of infected cells through processes such as degranulation or apoptosis (Bao *et al.*, 2021).

The dysfunction of these first-line defense cells is a key factor in the onset of severe COVID-19 cases, often referred to as cytokine release syndrome (CRS) (Taefehshokr *et al.*, 2020). One significant consequence is the excessive activation macrophages, which leads to an overproduction of IL-6. This contributes to macrophage activation syndrome, further impairing recovery in severe COVID-19 patients (Park, 2020) (McGonagle *et al.*, 2020). Certain immunological markers, as the elevated neutrophil-to-lymphocyte ratio, may act as predictors of disease progression and outcomes (Liu *et al.*, 2020) (Zheng *et al.*, 2020). IFN-I are effective in limiting coronavirus infections, and SARS-CoV-2 appears more susceptible to pre-treatment with IFN-I/III *in vitro* compared to SARS-CoV-1 (Channappanavar *et al.*, 2016) (Channappanavar *et al.*, 2019) (Mantlo *et al.*, 2020).

Interferon secretion activates the expression of ISGs, which serve to inhibit SARS-CoV-2 entry by blocking spike protein-mediated membrane fusion and by inducing interferon-induced transmembrane proteins (IFITMs). Among these, IFITM3 is particularly important for its localization in lysosomes and endosomes, where it prevents the release of viral particles into the cytoplasm, thereby inhibiting viral replication (Huang *et al.*, 2011). A reduced expression of IFITM3 in immune cells within the circulation and lungs, compared to other organs, is thought to contribute to the severity of COVID-19 and the development of CRS (Dai *et al.*, 2020).

In response to SARS-CoV-2 infection, another PRRs the NOD-like receptors (NLRs) are activated, promoting the production IFN-I and pro-inflammatory cytokines (Hu *et al.*, 2017). Additionally, the activation of inflammasome sensors, particularly NLRP3, leads to the activation of caspase-1, the release of IL-1β and IL-18, and the cleavage of gasdermin D, which triggers pyroptotic cell death (Christgen and Kanneganti, 2020). Furthermore, the cytoplasmic DNA released from damaged mitochondria trigger the interferon genes (STING) pathway important in inhibiting the replication of both DNA and RNA viruses after infection (Singh *et al.*, 2020) (Briard, Place and Kanneganti, 2020).

Adaptive immune response

Once the primary defense against SARS-CoV-2 is overwhelmed, the secondary immune response is stimulated to essentially eliminate infected cells (Figure 12).

After viral exposure and recognition, the adaptive immune response occurs triggering multiple transcription factors, which finlly stimulate the production of pro-inflammatory cytokines and chemokines, including tumor necrosis factor-α (TNF-α), interleukin-1 (IL-1), interleukin-6 (IL-6)(Park, 2020). Moreover, the downstream activation of IFN-I response stimulates maturation of immunity cells into antigen presenting cells (APCs), exhibiting with the class II major histocompatibility complex (HLA-Class II) the viral antigenic peptides(Tarke *et al.*, 2021)$^{-}$(Kalfaoglu *et al.*, 2021).

The presentation of antigens on antigen-presenting cells (APCs) triggers the differentiation of $CD4^{+}$ and $CD8^{+}$ T lymphocytes, along with regulatory T cells (T-regs)(O'Connell and Aldhamen, 2020) (Kalfaoglu *et al.*, 2021). $CD4^{+}$ follicular helper T cells promote the activation and proliferation of naive B lymphocytes, enhancing their antibody affinity within the specialized lymphoid structures called germinal centers (Crotty, 2014) (Pioli, 2019). S and N viral antigens elicit immunoglobulin production, as the IgM first immunoglobulin isotype secreted in serum (Burbelo *et al.*, 2020). They are present in blood and in mucosal tissues, but in the last one they represent a small percentage (Suthar *et al.*, 2020). They represent the first line of the humoral response, and even if they don't have a high affinity for viral antigens, they are able to robustly activate antibody-dependent cell-mediated cytotoxicity (ADCC) response. This is an immune mechanism where antibodies bind to infected cells, marking them for destruction by immune cells (e.g., NK cells) that recognize the antibody's Fc-receptor (CD16). This interaction triggers the release of cytotoxic molecules, killing the infected cell (Figure 12) (Bao *et al.*, 2021).

Indeed, the most abundant antibodies are IgAs which represent the main defense actors against pathogens that enter through the mucosa. IgA is mainly produced by mucosa-associated lymphoid tissue (MALT) in the respiratory tract, where it serves a crucial function in blocking viral attachment to the epithelial surface (Cesta, 2006).

A deficiency in IgA may worsen COVID-19 infection highlighting its effector function in defending physical barriers against viral invasion (Quinti *et al.*, 2021).

The specific IgA response to viral infection is both stronger and more sustained compared to the IgM response, with IgA being detectable in 75% of patients within the first week of infection (Padoan *et al.*, 2020).

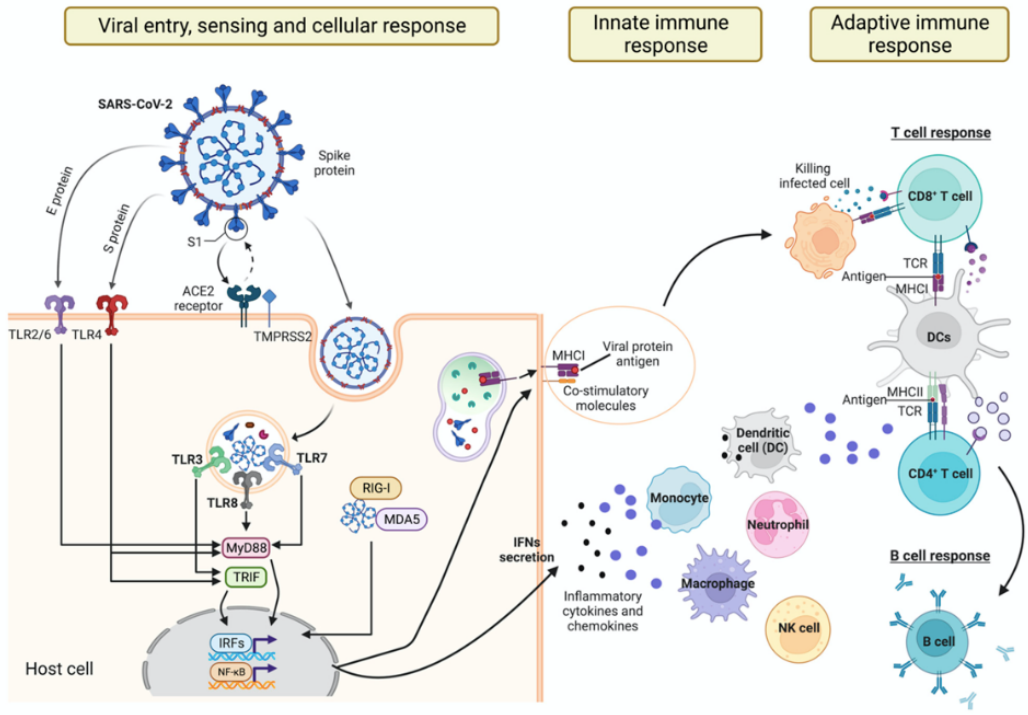


Figure 12 Immune response activation upon SARS-CoV-2 infection. Starting from the left side of the image, we can observe the early stages of the cellular response following SARS-CoV-2 infection and how these events trigger a cascade that leads to the activation of immune cells, culminating in the initiation of an adaptive immune response. Intracellular TLRs can detect single-stranded RNA (ssRNA) in endosomes (via TLR7/8) or double-stranded RNA (dsRNA) (via TLR3), while RIG-I and MDA5 sense viral RNA in the cytoplasm. Upon detection of viral RNA, these sensors recruit adaptor proteins that initiate signaling pathways, resulting in the activation of NF-κB and interferon regulatory factor (IRF) transcription factors. This leads to the production of pro-inflammatory cytokines. Viral antigens are then processed and presented on major histocompatibility complexes (MHCs) to T cells, accompanied by co-stimulatory molecules. This process enhances the immune response by activating CD8+ T cells for direct cytotoxic activity and CD4+ T cells, which help stimulate B cells to produce antibodies. Open access (Manfrini *et al.*, 2024).

The production of IgGs, resulting from isotype switching in B cells expressing IgM and IgD, has a pivotal role in antibody response, allowing a tailored action against pathogens. Due to this mechanism, the IgGs require time to be present in serum and are detected after 14 while IgM and IgA antibodies are detected 5 days after the onset of symptoms (Figure 13) (Meyer, Drosten and Müller, 2014).

IgGs are implied in complement activation, neutralization, and the protection from further infections by the same pathogen and the intensity of the IgG response is related to both viral load and COVID-19 severity (Guo *et al.*, 2020).

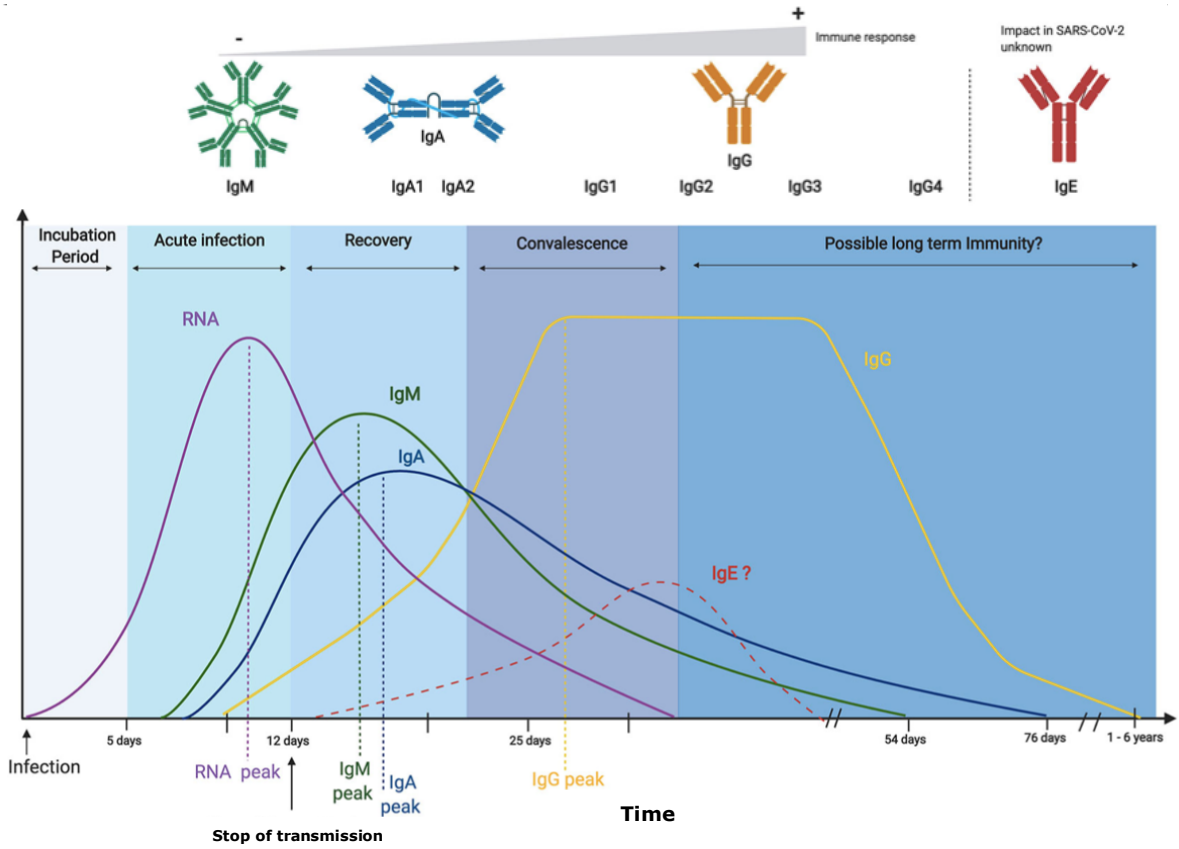


Figure 13 Dynamics of host humoral response to SARS-CoV-2 infection. Studies on antibody response to SARS- CoV-2 revealed that level of specific IgM starts rise during the first week of infection, followed closely by the increase in IgA levels. Finally, IgGs become detectable, remaining detectable for months after the symptoms. More studies need to be performed to examine the presence of SARS-CoV-2 specific IgGs during time and to address their protective role from re-infection. Open access (Galipeau *et al.*, 2020).

Immune evasion mechanisms of SARS-CoV-2

As previously discussed, the cellular machinery detects PAMPs through PRRs, initiating an immune response. However, SARS-CoV-2 utilizes a range of mechanisms to evade this defense, particularly through the deployment of both structural and non-structural proteins that inhibit the activation of the interferon signaling pathway, a critical early step in viral recognition (Blanco-Melo *et al.*, 2020) (Sa Ribero *et al.*, 2020).

Viral evasion: structural viral protein

To escape the immune activation response, SARS-CoV-2 employed the structural proteins (Figure 14). As described, the M protein counteracts the antiviral defense by inhibiting the activation of IRF3 blocking its phosphorylation. IRF3 is a member of a family of nine IRF proteins in mammals, which regulate various cellular functions, including immune responses and apoptosis mechanisms(Jefferies, 2019). Among these, IRF3 and IRF7 are particularly important in the activation of antiviral immunity, as they induce the production of type I interferons, such as IFN-β (Ning, Pagano and Barber, 2011). Once secreted, IFN-β binds to its receptor, IFNAR (IFN-α/β receptor), which is expressed on both infected and uninfected cells (Fensterl, Chattopadhyay and Sen, 2015) (Cohen *et al.*, 1995). This binding activates downstream signaling via the JAK/STAT pathway, triggering the formation of ISGF3. This complex in turn stimulates the expression of interferon-stimulated genes (ISGs), which contribute to creating an antiviral environment by blocking viral replication at various stages (Subramanian *et al.*, 2018). Notably, many ISGs can be directly induced by IRF3 itself. In addition, IRF3 can directly induced different ISGs and can also plays a part in inducing apoptosis of infected cells Known as RIG-I-like receptor-induced IRF3-mediated apoptosis (RIPA)(Bandyopadhyay *et al.*, 1995)(Chattopadhyay and Sen, 2016).

The N protein further disrupts the innate immune response by inhibiting IRF3 activation early in the pathogen recognition process, as well as suppressing RIG-I ubiquitination and activation (Lu *et al.*, 2010).

Viral evasion: non-structural and accessory viral proteins

SARS-CoV-2 also employs various non-structural and accessory proteins to undermine the antiviral response. PLpro is involved in processing viral polyproteins and promotes viral replication. PLpro prevents the phosphorylation and nuclear translocation of IRF3, thereby hindering its ability to initiate the antiviral response (Devaraj *et al.*, 2007). Additionally, Nsp1 suppresses virus-induced phosphorylation and dimerization of IRF3 (Wathelet *et al.*, 2007); Nsp8 and Nsp9 interfere with protein trafficking to the cell membrane. These three mechanisms modulate the production of IFN-I, leading to a reduction in its synthesis by the infected cells (Banerjee *et al.*, 2020) (Gordon *et al.*, 2020).

The virus also evades detection of its RNA by RIG-I and MDA-5. Specifically, SARS-CoV-2 adds a /−methylguanylate cap to the 5' end of its RNA, preventing recognition by RIG-I and allowing the virus to escape immune detection. This evasion process is mediated by the high conserved Nsp13, Nsp14, and Nsp16 protein (Menachery, Debbink and Baric, 2014) (Viswanathan *et al.*, 2020).

Similarly, Nsp15 evades MDA-5 detection by reducing the accumulation of viral RNA, further suppressing immune activation (Hackbart, Deng and Baker, 2020). In addition, experimental data have shown that Nsp15 can interact with the E3 ubiquitin ligase Nrdp1, which regulates IFN-I production, diminishing IFN-β reporter activity (Gordon *et al.*, 2020).

SARS-CoV-2 also employs ORF6 which interferes with either KPNA2 or nuclear export complex, which are both involved IRF3-induced activation of the IFN-β promoter (Lei *et al.*, 2020). Moreover, accessory proteins ORF3a and 3CLpro are involved in blocking the cGAS-STING pathway, further suppressing the antiviral immune response (Gruner *et al.*, 2023). Interaction mapping further suggested that ORF9b interacts a mitochondrial receptor: TOMM70 (Lei *et al.*, 2020) (Konno *et al.*, 2020). Although these accessory proteins are not essential for the replication of the virus, they contribute to the pathogenesis of COVID-19 by evading innate immunity and enhancing viral survival within the host.

Emerging evidence indicates that SARS-CoV-2 interferes with the IFN-I system at various stages, disrupting the balance between antiviral and proinflammatory innate and adaptive immune responses. Further research, especially longitudinal studies with disease severity stratification, is crucial to understand the dynamics of the early IFN response and its role in shaping the immune response during the initial stages of infection (Lee *et al.*, 2020). This understanding is key to deciphering the delicate balance between immune activation and immune evasion in the early stages of infection. Additionally, identifying biomarkers associated with the severity of disease progression could enable the development of predictive models, aiding in the design of tailored therapeutic strategies based on individual immune responses.

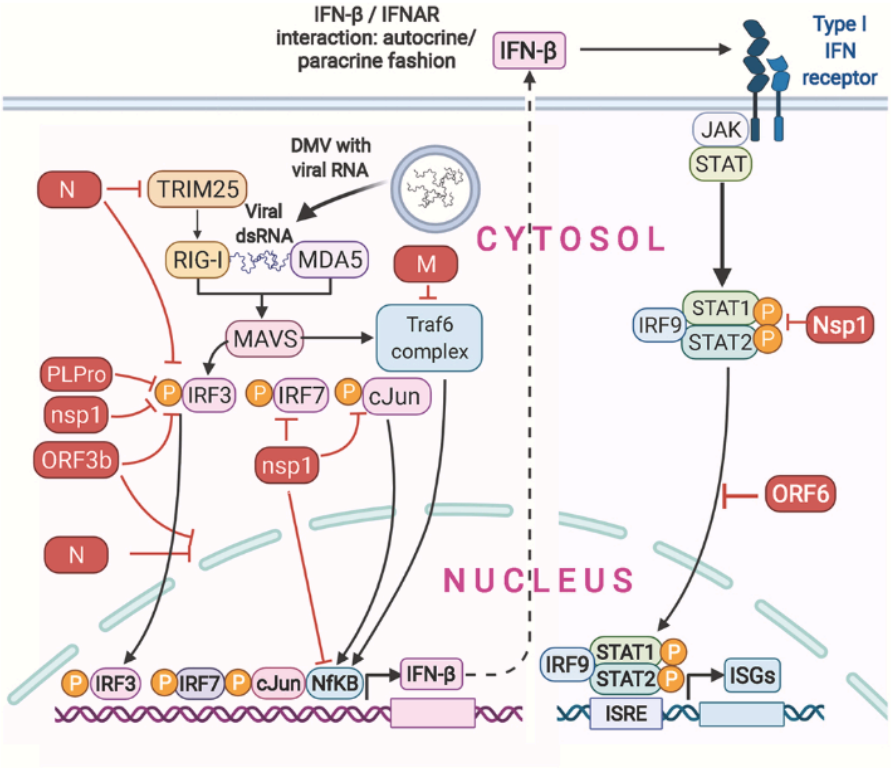


Figure 14 SARS-CoV-2 evasion of the innate immune response through multiple mechanisms. The M protein inhibits IRF3 activation, blocking type I interferon (IFN) production. The N protein further suppresses IRF3 and RIG-I activation. Non-structural proteins like PLpro, Nsp1, and Nsp13-16 disrupt RNA sensing and prevent IFN production. Accessory proteins such as ORF6 and ORF3a interfere with IFN signaling and the cGAS-STING pathway, enhancing viral survival and immune evasion. Open access (Latifi-Pupovci, 2022).

Viral evasion: adaptive immune escape

SARS-CoV-2 can inhibit T-cell mediated immune responses through the downregulation of MHC class I and II molecules, thereby limiting antigen presentation and impeding the activation of T-cells (Zheng *et al.*, 2020).

In patients with mild COVID-19, lymphocyte counts, including both $CD3^+$ T cells and $CD8^+$ T cells ($CD3^+CD8^+$), were significantly higher compared to those with more severe disease. However, despite these differences, $CD8^+$ T cell numbers were lower in mild and severe cases of COVID-19 compared to healthy controls (Cao, 2020). Phenotypic analysis revealed that $CD8^+$ T cells in COVID-19 patients expressed high levels of CD57, a marker indicative of cellular senescence, suggesting a premature aging of these cells during the infection (Mazzoni *et al.*, 2020).

Despite the reduced numbers of T cells, both $CD4^+$ and $CD8^+$ T cells in COVID-19 patients showed increased expression of activation markers, including HLA-DR, CD38, and Ki-67. These changes were closely correlated with disease severity, highlighting a hyperactive immune response (Kuri-Cervantes *et al.*, 2020).

Furthermore, $CD8^+$ T cells from COVID-19 patients exhibited impaired degranulation, with decreased CD107a externalization, and produced lower levels of cytokines such as IL-2, IFN-γ, and granzyme B compared to healthy controls (Zheng *et al.*, 2020).

T cells in bronchoalveolar lavage (BAL) samples from COVID-19 patients showed increased PD-1 expression compared to peripheral blood, indicating functional exhaustion during infection (Saris *et al.*, 2021). Notably, T cells from intensive care units ICU patients expressed significantly higher levels of PD-1 than those from patients with mild disease or healthy controls (Moon, 2020). Additionally, CD^{8+} T cells were found to be significantly reduced in the BAL of patients with severe disease, suggesting that these cells play a critical role in viral clearance (Liao *et al.*, 2020)

In terms of long-term immunity, the generation of SARS-CoV-2-specific memory T cells is essential for durable protective immunity. Despite variability among individuals, studies suggest that the amount of the SARS-CoV-2-specific $CD4^+$ and $CD8^+$ memory T cell responses is generally around 0.5% and 0.2% respectively. These memory T cells target a wide array of viral epitopes: at least 19 for $CD4^+$ T cells and 17 for $CD8^+$ T cells (Cohen *et al.*, 2021). These findings underscore the ability of the virus to effectively suppress adaptive immune responses, which may contribute to both the persistence of the infection and variability in disease outcomes.

CLINICAL RELEVANCE

Epidemiology and Evolution

In December 2019, several cases of pneumonia with unknown etiology were reported in Hubei province, China (Hu *et al.*, 2020). All first patients had a history of exposure to Huanan Seafood Market, a "wet market", in Wuhan city. Because of the co-existence of perishable items with live animals, which are usually slaughtered on-site, wet markets could be linked to the emergence of different zoonotic diseases. The attention of the authorities was focused on the possible appearance of a novel pathogen that may be transmitted from animals to humans.

However, quite soon the number of patients without direct contact to the wet market increased, which rose the concern about the possibility of human-to-human transmission of the new pathogen. This hypothesis was confirmed by the growth of the number of nosocomial infections in healthcare facilities. For about a month and a half from the start of the epidemic, until 20 February 2020, almost all cases remained limited to mainland China, with few infections imported into other countries. Since the second half of February, new outbreaks have erupted, first in South Korea, Iran, and Italy, and then throughout the world. With the above announcement, WHO declared that the local outbreak had become a global threat. In particular, the first case in Italy, referred to as "patient zero," was confirmed on February 21, 2020, in the Lombardy region. By February 27, 2020, Italy had reported over 400 confirmed cases, making it the country with the highest number of infections in Europe at that time (https://data.who.int/dashboards/covid19/about).

SARS-CoV-2 cases have been detected in adults (from 15 to 89 years old), while the incidence in children and infants was very low; the average age of affected adults was 59, with more incidence for males (59%) (Wiersinga *et al.*, 2020). The high-risk group comprehended elderly, immunosuppressed patients, persons with renal, hepatic, and pulmonary dysfunction (Domingo *et al.*, 2020).

The contagiousness of SARS-CoV-2 was measured through the basic reproduction number, R0. This factor, known as the basic reproduction number, is used to quantify the transmissibility or contagiousness of infectious agents as an epidemiological measure. The estimation of R0 was quite difficult considering many undetected infections, but it stood at 2.2, meaning that, statistically, an infected subject could transmit the virus to 2.2 person (Beig Parikhani *et al.*, 2021).

To contain the rapid diffusion of SARS-CoV-2, Chinese authorities mandated a quarantine for Wuhan city: 11 million people were locked down. While reported cases of infection dropped in China, all over the world the virus continued to rush. Europe, USA, Latin America, but also Iran and India faced a rapid increase of confirmed infection (Wu *et al.*, 2020). According to WHO, by April 2020, SARS-CoV-2 has infected 1 million people in 171 countries across six continents, killing at least 51.000 people. Despite the global spread, the SARS-CoV-2 pandemic affected some countries more than others. Between them, USA, UK, and Brazil must face plight due to the quick growth of SARS-CoV-2 positive subjects. Scientists suggested that the delay in control measures, together with an unclear communication with the population, could contribute to the dramatic increase of cases.

States coped with pandemic with different control measures to minimize exposure risk: campaign to increase awareness in hygiene measures, obligation to wear face masks, until the imposition of curfew and lockdown of entire cities or countries. These impositions have challenged SARS-CoV-2 circulation, but they have also impacted the social and economic life of entire populations.

The rapid and unanticipated onset of the SARS-CoV-2 pandemic placed unprecedented strain on healthcare infrastructures and economies globally, profoundly affecting public health. During the initial phase of viral dissemination, prior to the FDA's emergency use authorization of the first vaccine in December 2020, non-pharmaceutical interventions (NPIs), including stringent hygiene measures and social distancing protocols, constituted the primary means of controlling transmission. This early phase emphasized the critical importance of scientific research and international collaboration, which collectively contributed to mitigating viral spread, reducing the severity of clinical manifestations, and minimizing mortality risk, particularly in high-risk and vulnerable populations.

From December 2019, many attempts have been made to improve current knowledge and better characterize SARS-CoV-2. Coronaviruses have the largest known genome between RNA viruses, and they encode for Nsp13, which allows high-fidelity replication. When compared, other RNA viruses, such as influenza and vesicular stomatitis virus (VSV), have smaller genomes (approximately 13-14 kilobases and 11 kilobases, respectively) and lack the robust proofreading mechanisms found in coronaviruses. For example, the influenza virus, which belongs to the *Orthomyxoviridae* family, has a segmented RNA genome and replicates with a lower fidelity due to the absence of a 3' to 5' exonuclease activity (te Velthuis and Fodor, 2016). This higher mutation rate in influenza viruses facilitates rapid evolution and adaptation, particularly in immune evasion.

Despite the presence of Nsp13 protein, SARS-CoV-2 replication during the pandemic has typically exhibited a high error rate (or low viral fidelity), leading to the generation of genome mutants or viral quasispecies. Replication dynamics is one of the key factors influencing SARS-CoV-2 evolution, alongside (1) intra-host diversity, (2) transmission bottlenecks, and (3) genetic drift (Markov *et al.*, 2023).

1. SARS-CoV-2 infections are typically acute and are cleared by the immune system within 10–15 days after the onset of symptoms (Rhee *et al.*, 2020) (Wölfel *et al.*, 2020). Within-host viral diversity is usually measured by the presence of intra-host single nucleotide variants (iSNVs) that exceed a minor allele frequency threshold of 2–5%. During typical acute infections, SARS-CoV-2 shows limited intra-host diversity, with most samples exhibiting few iSNVs at low frequencies (Lythgoe *et al.*, 2021). Tissue compartmentalization of the virus, seen in discordance between viral populations in nasal and oral environments, may further contribute to intra-host diversity (Robinot *et al.*, 2021) (Willett *et al.*, 2022).

2. The concept of a transmission bottleneck refers to the reduction in genetic diversity of the viral population following transmission; infection occurs by one or two viral particles, meaning that most of the variants generated during the prior infection are either lost or rarely transmitted, unless they have a strong selective advantage (Lythgoe *et al.*, 2021). This transmission bottleneck acts as a filter, limiting the genetic diversity of the virus in the new host. The narrow bottleneck, along with the stochastic nature of viral transmission, complicates the estimation of the selective advantages of specific mutations, unless the selection pressure is exceptionally strong (Bruel *et al.*, 2023) (Addetia *et al.*, 2023). Early in the pandemic, it was difficult to determine whether the spread of mutations, such as D614G, was due to natural selection or random genetic drift. However, studies later demonstrated that the D614G mutation conferred a 20% increase in transmissibility over the original B.1 lineage (Moriyama *et al.*, 2023) (Chalkias *et al.*, 2024). This highlighted the role of natural selection in the rise of specific variants, which could have been mistaken for random drift or founder effects.

3. When considering SARS-CoV-2 evolution at the between-host scale, the genetic diversity observed in host populations is often shaped by genetic drift. In most cases, the majority of observed genetic diversity at the population level is neutral

or slightly deleterious. These variants spread mainly through stochastic processes, meaning that they reach higher frequencies by chance, not because of a selective advantage (Bruel *et al.*, 2023). Superspreading events, in which a small fraction of host contributes to transmissions, further increase stochasticity by introducing variability in the number of secondary infections (Saunders *et al.*, 2023) (Cao *et al.*, 2022). This results in a reduction of the effective population size of the virus and further enhances genetic drift (Park *et al.*, 2022).

SARS-CoV-2 genome was sequenced all around the world and sequencing data were shared on Global Initiative on Sharing All Influenza Data (GISAID), allowing near real-time surveillance.

The analysis of deposited sequences showed that over time the SARS-CoV-2 genome undergoes mutations (Kaushal *et al.*, 2020). The first SARS-CoV-2 genome sequence deposited on GISAID derived from Wuhan patient, and it became the reference sequence (hCoV-19/Wuhan/IVDC-HB-01/2019, GISAID ID EPI_ISL_402119).

Mutations could occur in every part of the genome, and most detected mutations were expected to be neutral or mild. Only a small minority could have an impact on viral biology, by altering viral fitness, pathogenicity, and/or antigenicity.

Considering that the S protein plays a key role in viral entry and immunogenicity, it has been closely monitored since the start of the pandemic (Park *et al.*, 2022). For months, several mutations in this region have been identified, with different implications for viral biology. This is the case of the amino acid substitution D614G, caused by an A-to-G nucleotide mutation at position 23,40361. This variant was detected in March 2020 and by that time it represented 10% of the total deposited sequences. Structural studies suggest that this amino acidic substitution leads to a shift of RBD in the "up" conformation, which is required to bind cell receptor (Yurkovetskiy *et al.*, 2020). The crossbreeding of phylogenetic data and clinical patient data showed that the new lineage was associated with higher viral loads and higher human-to-human transmission, but not with an increase in severity of the disease (Korber *et al.*, 2020). The transition from D614 to G614D occurred asynchronously in Europe, followed by North America, Oceania, and then Asia.

The strict surveillance highlighted the presence of new mutations in the SARS-CoV-2 genome, which arose concern for their possible implication in transmissibility and pathogenesis. Center for Disease Control and Prevention defines two categories of variants: Variants of Interest (VOI) and Variants of Concern (VOC). Initially,

scientists identified them with the geographic region of isolation, but WHO established the usage of the Greek Alphabet for tracking SARS-CoV-2 variants. A viral variant with specific genetic markers potentially associated with increased receptor binding capability, decrease in neutralization activity of antibody response, or alteration in disease manifestation is identified as VOI. They require particular attention, enhancing sequence surveillance and epidemiological investigation. On the other hand, VOCs are defined as variants that show increased transmissibility, greater disease severity, or a decrease in the effectiveness of antibody neutralization and treatment efficacy. (Andreano and Rappuoli, 2021).

Since the end of summer 2020, a new variant of SARS-CoV-2, VOC-202012/01 or B.1.1.7 (renamed Alpha) has spread in the United Kingdom, causing alarm, and prompting the British government to take significant containment measures in the area, where this new variant has spread considerably to represent more than 50% of new cases in December. It appears to be more transmissible (40-70%) than the G614D variants due to two additional mutations in spike protein (N501Y, P681H) which enhance the entry process (Tegally *et al.*, 2021).

At the end of 2020, another variant of SARS-CoV-2 has been reported in South Africa, defined as 501Y.V2 or B.1.351 (Beta variant), first observed in samples taken in October, and soon became the dominant lineage in South Africa (Figure 15). Beta variant presents additional mutations to G614D in spike region and first evidence seems to show that this variant could easier interact with ACE2 than spike harbors only G164 mutation. Moreover, the Beta variant arises concern about its ability to escape from the immunity elicited by a previous infection (Figure 16) (Temsah *et al.*, 2022).

A third VOC has been found in Brazil and Japan. This variant, initially identified as B.1.1.28.1 or P.1 and now called Gamma, has D614G substitution, but it shares several mutations with the Beta variant, including K417T, E484K, and N501Y, which were similarly associated with immune evasion. The E484K mutation was crucial for immune evasion and displayed an increase in transmissibility compared to earlier variants (X. Yu *et al.*, 2022).

In April 2021 in India, coinciding with the increase in infections and deaths, a new variant was identified, called B.1.617 (Delta variant), characterized by nine mutations in spike glycoprotein other than D614G64. Two key mutations in the spike protein (L452R and E484Q) confer to spike protein the capability to increase its binding strength to ACE2 receptor (X. Yu *et al.*, 2022). Additionally, the P681R mutation, located near the furin cleavage site, enhanced the entry and the viral fusion into host

cells, contributing to increased virulence and accelerated replication in the site of infection (Cele *et al.*, 2021).

In contrast to these earlier variants, Omicron lineage (BA.) marked a significant shift in the virus evolution; the first BA. variant was identified in late 2021 and was characterized by over 30 mutations specifically in the RBD and N-terminal domain (NTD) of the S protein leading to a remarkable ability to evade neutralizing antibodies, reducing the effectiveness of existing vaccines and prior immunity from earlier strains (Solanki *et al.*, 2022) (Shrestha *et al.*, 2022). The key mutations (K417N, E484A, and N501Y), previously identified in the Beta and Alpha variants, were present in the BA. variants in combination with new mutations, such as P681H and G142D, which further enhance immune escape and increase transmissibility (Li *et al.*, 2023). Mutations in the BA. variants also play a key role in increasing transmissibility by enhancing binding to the ACE2 receptor, particularly in the upper respiratory tract, where viral replication is most active (Williams *et al.*, 2021) (Karim and Karim, 2021).

These changes in the viral S protein and the resulting effects on cellular entry, replication kinetic and immune evasion suggest a critical shift in the viral behavior between pre-Omicron and Omicron variants. While the pre-Omicron variants displayed limited immune escape and increased transmissibility, Omicron variants provided a broader capacity for immune escape and enhanced infectivity (VanBlargan *et al.*, 2022). The ability of Omicron variants to evade immunity from previous infection or vaccination, combined with their increased efficiency in infecting cells, enabled global spread, even in populations with prior immunity (Chavda *et al.*, 2022) (Rashid *et al.*, 2022).

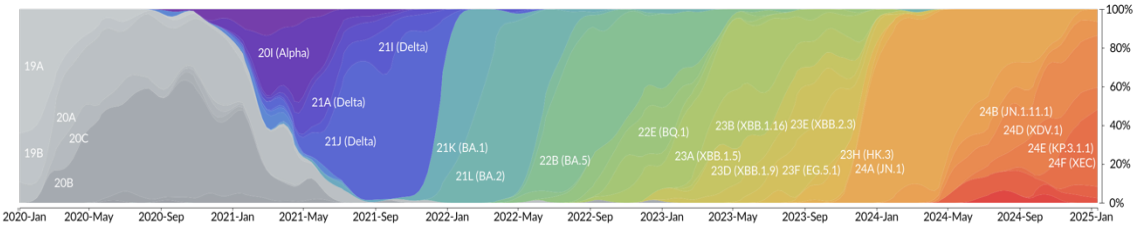


Figure 15 Temporal distribution of SARS-CoV variants. The graph depicts the emergence and relative prevalence of various SARS-CoV-2 variants over time, from the early 2020 to January 2025. Curves represent the frequency of each variant, illustrating their temporal dynamics and shifts in dominance. This graph clary illustrates the ongoing evolution of SARS-CoV-2 in response to selective pressures and public health interventions. Open access Update on Omicron --- who.int, no date

This viral evolution highlighted the adaptation process of the virus into human host and underscored the need for continuous surveillance to address emerging variants (Markov *et al.*, 2023).

Briefly, BA.1 variants was first identified on November 2021, in South Africa and was categorized as a VOC on 26th November 2021 (Viana *et al.*, 2022) (*Update on Omicron --- who.int*, no date). Compering to Whuan-sequence the BA.1 Omicron genome had 30 amino acid substitutions, three in-frame deletions, and an insertion of three amino acids (ins214EPE) resulting in 35 mutations. Many of the mutations occurring in the RBD (15 of the 35 mutations) have reported in the previously variants as the del69-70 found in Alpha, T95I and G142D in Delta. These RBD mutations may confer an evolutionary advantage to the virus, either by strengthening its interaction with the ACE2 receptor or by promoting immune escape mechanisms (Chen *et al.*, 2022) (Liu *et al.*, 2021).

In the early 2022 BA.2 is overtaking BA.1 as a globally dominant variant (Shrestha *et al.*, 2022) (*Update on Omicron --- who.int*, no date). BA.2 emerged as a sublineage of B.1.1.529, which was identified in late 2021. While BA.2 shares many mutations with BA.1, it has additional 8 unique mutations such as S371F, T376A, and D405N. These mutations contributed to increased transmissibility, making BA.2 more contagious than its predecessor, BA.1, although both variants demonstrated similar clinical severity, with most infections being mild or asymptomatic (J. Yu *et al.*, 2022).

Following the emergence of the BA.2 sublineage SARS-CoV-2 continued to evolve, giving rise to several new variants exhibiting mutations that altered transmissibility, immune evasion, and, in some cases, disease severity. BA.2 evolved into BA.4 and BA.5, which harbored additional mutations in the spike protein, such as L452R and F486V, enhancing their ability to evade pre-existing immunity (Maxmen, 2022) (Pung *et al.*, 2021). These variants led to higher rates of reinfection and breakthrough cases in vaccinated individuals, becoming dominant in many regions due to their increased transmissibility.

By 2023, subvariants derived from BA.5, including BF.7, BQ.1, and BQ.1.1, continued to circulate, maintaining significant immune escape capabilities. However, their clinical impact remained similar to that of previous BA. variants, with most cases being mild or moderate. During the same period, the XBB. variant, a recombinant of two BA.2 subvariants (BJ.1 and BM.1.1.1), emerged and represented about 80% of deposited viral sequences, were XBB.1, and the EG.5.1 sublineage; in particular, the XBB.1 subvariant became a major circulating strain, contributing to higher rates of reinfection and evolved generating the XBB.1.5 subvariant which rapidly spread due

to mutations that further increased its ability to bind to the ACE2 receptor, enhancing transmissibility (Miller *et al.*, 2023) (Wang *et al.*, 2023).

EG.5.1 descending from XBB.1.9.2 was identified in May (Uraki *et al.*, 2023). In October 2023 this novel variant acquired the S486P and F456L occurred in more than 65% of genomes published on the GISAID repository, suggesting an epidemiological advantage in this genomic background (Uraki *et al.*, 2023).

In contrast, in August 2023 a new lineage the BA.2.86 emerged and represented an important evolutionary jump, prompting its classification as a VOI by the WHO (*World Health Organization (WHO) --- who.int*, no date) activities/tracking-SARS-CoV-2-variants. BA.2.86 spike carries a novel and unprecedented combination of mutations which confer a stronger affinity for ACE and immune evasion mechanisms, correlating to a high transmissibility (reported in 85% in home setting outbreak) (Reeve *et al.*, 2023) (Herder *et al.*, 2023) (Tamura *et al.*, 2024).

The BA.2.86 variants evolved into the JN.1 sub-lineage, and by September 2023, JN.1 had become the dominant strain in Europe and the USA, driving the epidemic surge towards the end of 2023 and into the beginning of 2024. Epidemiological data suggest that JN.1 has a 2.3-fold growth advantage over EG.5.1.1, increasing immune evasion and a reducing the affinity for ACE2 (Uraki *et al.*, 2023) (Zhang *et al.*, 2024) (Yang *et al.*, 2024).

Lastly, the most recent variant is the XEC with the earliest sample collected on 26 June 2024 and emerged as a recombinant derived from the JN.1 descendent lineages. XEC is currently the only SARS-CoV-2 variant under monitoring (VUM) with increasing prevalence globally. Considering the available evidence, the additional public health risk posed by XEC is evaluated as low at the global level. Therefore, the continued spread of this variant alone is unlikely to increase the burden on national public health systems compared to other Omicron sub-lineages (*Tracking SARS-CoV-2 variants --- who.int*, no date) (*Coronavirus Disease (COVID-19) Situation Reports --- who.int*, no date).



Figure 16 Mutations in the SARS-CoV-2 spike protein and identification of Variants of Concern (VOCs). This figure highlights key mutations in the S protein that have facilitated the identification of the different SARS-CoV-2 VOCs over time. The mutations are annotated on the S1 and S2 subunits, including the RBD, and the FP. Open access (*Sars-CoV-2 circulating variants*, no date)

This complex panorama highlights the essential and crucial role of surveillance. The premature identification of viral variants is essential to contain their spread and avoid dramatic *sequelae.*

Transmission mechanisms

As with other respiratory viruses, the human-to-human transmission of SARS-CoV-2 can occur primarily through respiratory droplets, but aerosol transmission, contact with contaminated surfaces, and fecal-oral routes have also been observed during the epidemic (Figure 17) (Yu *et al.*, 2004) (Otter *et al.*, 2016) (Li *et al.*, 2005).

According to reports from the WHO, respiratory droplets (particles with a diameter greater than 5 μm) are the most likely source of COVID-19 transmission, as early signs of the infection, such as cough and lung opacities, were observed in affected individuals (Zhou *et al.*, 2020) (J. Peiris *et al.*, 2003) (C. Huang *et al.*, 2020). Droplets transmission occurs when an infected person coughs, sneezes, or talks, releasing viral particles into the air. These droplets can then be inhaled or land on the eyes, mouth, or nose of a nearby susceptible person (within 1 meter), potentially resulting in infection (J. S. M. Peiris *et al.*, 2003). This mode of transmission is supported by evidence of active viral replication in both the upper and lower respiratory tracts, as well as the growing number of cases where the virus spread through close contact, particularly among individuals actively coughing (Chan *et al.*, 2020) (Hui *et al.*, 2020) (Qun Li *et al.*, 2020). Another mode of transmission, less characterized than the others, is indirect contact. When infected individuals release viral particles into the air, these particles can persist on surfaces and potentially cause infection. Previous studies have examined the survival time of viral particles from various respiratory viruses on surfaces (Abdelrahman, Li and Wang, 2020). Similar to influenza viruses, as well as other human coronaviruses (SARS-CoV and MERS-CoV), SARS-CoV-2 can survive on different surfaces for hours to days (Abdelrahman, Li and Wang, 2020). Exposure to fomites (contaminated objects), followed by direct contact with respiratory mucosa, may lead to infection (Beig Parikhani *et al.*, 2021).

Furthermore, aerosol transmission has been indicated as a source of infection: fine droplets with a diameter less than 5 μm (aerosols) remained suspended in the air for long periods and spread further away, especially in enclosed indoor setting and not adequately ventilated spaces (Harrison, Lin and Wang, 2020).

Fecal-oral transmission remains a debated route, though SARS-CoV-2 RNA has been found in rectal swabs and nearby toilet areas during the initial outbreak in China (Xiao *et al.*, 2020).

Unlike SARS-CoV, SARS-CoV-2 can spread even before symptoms appear, allowing for presymptomatic and asymptomatic transmission. This has significantly contributed to its rapid spread (Zou *et al.*, 2020). Asymptomatic transmission has

been observed throughout the pandemic, underscoring the importance of understanding transmission dynamics to implement effective public health measures, including mask-wearing, contact tracing, and physical distancing (Chan *et al.*, 2020) (Zou *et al.*, 2020) (Mizumoto *et al.*, 2020). Indeed, the correct use of face masks dramatically reduced the spread of droplets and aerosol, and the social distance contributes to protection in the case of nearby infected subjects (Kucharski *et al.*, 2020).

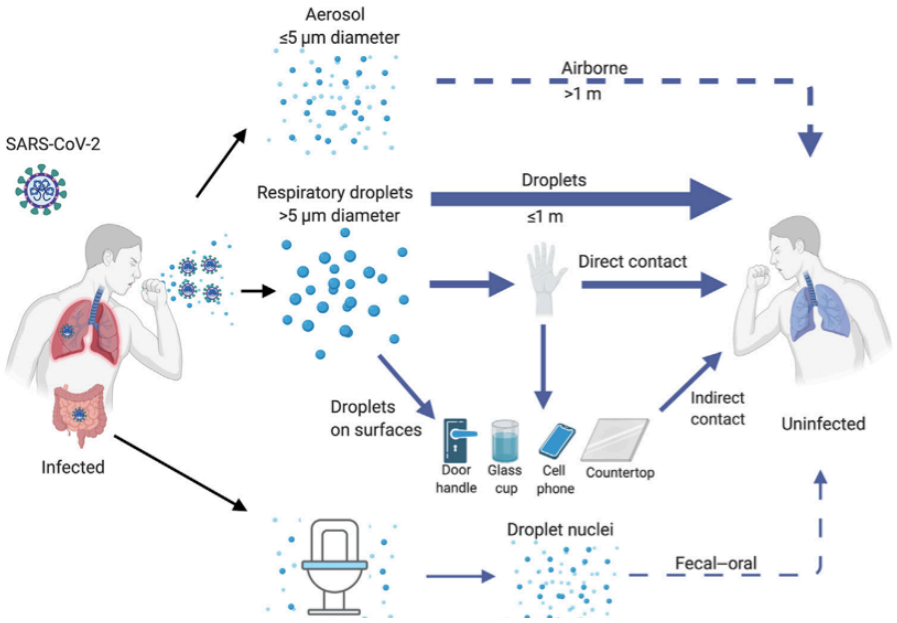


Figure 17 Transmission Routes of SARS-CoV-2. The ongoing COVID-19 pandemic has highlighted several transmission routes for SARS-CoV-2. Droplet transmission (particles >5 µm) is the most widely recognized and significant mode of spread. Direct contact between infected and uninfected individuals, particularly in close settings like households, is another major route. Although less frequent, transmission via fomites (e.g., door handles) is also being investigated as a contributing factor. Airborne and fecal-oral transmissions, observed in past coronaviruses (like SARS-CoV), have not been confirmed for SARS-CoV-2. Open access (Harrison, Lin and Wang, 2020).

Pathogenesis

Since its first appearance in December 2019, substantial efforts have been made to understand the disease caused by SARS-CoV-2. COVID-19, initially considered a self-limiting infection, has proven to present a wide spectrum of clinical severity and progression

Clinic manifestations

The clinical course varies, with some individuals experiencing mild symptoms, while others may progress to severe or critical illness.

The incubation period, known as the time between exposure and the onset of symptoms for the pre-Omicron variants ranges from 4 to 11 days, while for Omicron variants there was a slightly shorter incubation period with symptoms often appearing around 3 to 5 days post-exposure (Galmiche *et al.*, 2023). This difference may be attributed to pre-existing immunity, either from prior vaccination or previous infections, which likely influenced the faster onset of symptoms in individuals exposed to Omicron variants.

During the incubation period, infected individuals can still spread the virus, complicating case tracking and containment efforts. This "silent transmission" has been particularly challenging for controlling the spread of SARS-CoV-2 variants (Sah *et al.*, 2021)

The picture of COVID-19 essentially has four possible clinical evolutions (Ortiz-Prado *et al.*, 2020):

Asymptomatic Infection: some infected subjects would remain completely asymptomatic for all the time of infection. Being asymptomatic means that the person is infected by the virus, but he has subclinical manifestations of the disease. This clinical manifestation was common for Omicron infections. While asymptomatic, these individuals can still spread the virus, which complicates transmission control efforts (Sah *et al.*, 2021).

Mild to Moderate Acute Infection: symptoms in mild cases are diverse and can include anosmia (loss of smell), ageusia (loss of taste), fever, cough, wheezing, fatigue, and muscle pain. Some patients report gastrointestinal issues, sore throat,

rhinorrhea, headache, and confusion prior to the onset of fever. Omicron has been associated with milder symptoms compared to the original strain, though these can still require hospitalization for individuals with pre-existing conditions (Puhach *et al.*, 2022).

Severe Infection and Critical Illness: severe cases may involve respiratory complications such as pneumonia and acute respiratory distress syndrome (ARDS), along with cardiovascular issues, including thrombosis and ischemia, or neurological manifestations. For these patients, oxygen supplementation, non-invasive ventilation, or intubation is required. Omicron variants, while generally associated with less severe illness, can still lead to critical conditions, particularly in individuals who are unvaccinated or immunocompromised (Hu *et al.*, 2023).

Recovery or Exitus: patients are considered to have recovered once they test negative on two consecutive PCR tests, 24 hours apart. However, long-term *sequelae,* known as "long COVID," remain a significant concern. Research indicates that long-term symptoms, such as fatigue, cognitive impairment, and difficulty breathing, are still present in a subset of individuals, even those who experienced mild or moderate disease (Al-Aly and Rosen, 2024).

Collecting data suggest that approximately 80% of individuals infected with SARS-CoV-2 exhibit mild or asymptomatic disease, with symptoms typically confined to the upper respiratory tract. In contrast, 20% of infected individuals experience more severe illness, requiring hospitalization, and around 5% require mechanical ventilation in an insensitive care units (ICU) setting (Domingo *et al.*, 2020). With the emergence of Omicron variants has contributed to a higher number of cases globally, but the variant is generally associated with a lower risk of severe outcomes compared to the pre-Omicron variant. This could be due to increased vaccination coverage, prior infection immunity, and the intrinsic characteristics of the Omicron variant itself. However, the overall burden on healthcare systems remains significant, particularly in areas with lower vaccination rates (Bálint, Vörös-Horváth and Széchenyi, 2022) (Ren *et al.*, 2023).

Immune mediate injury

In addition to the viral characteristics, the spectrum of clinical manifestations is influenced by key factors such as age and the patient's pre-existing health status.

An important clinical consequence for COVID-19 patients is the immune-mediate injury that results from dysregulation of the immune response (Figure 18). It could damage lung tissue due to an abnormal infiltration of inflammatory cells, an excess of pro-inflammatory cytokines secretion, and/or dysregulation in the feedback loop. Lung damage is not only the direct result of viral replication, but it could also be the consequence of uncontrolled inflammation and an excess release of pro-inflammatory cytokines (cytokines storm) or cytokine release syndrome (CRS) (Clementi *et al.*, 2021).

Current studies evidenced how the SARS-CoV-2 infects ciliated cells in the upper airways, from where it spreads down the bronchial tree to the alveoli. This progression is driven by a lack immune responses, particularly in IFN-I and III signaling. Alveolar damage may occur directly thought the infection of alveolar type 2 (AT2) cells or indirectly through inflammatory responses that activate the endothelial cells. In response to lung injury, AT2 cells adopt a damage-associated transient progenitor (DATP) phenotype, which impedes their full differentiation and exacerbates the injury. This disruption of the epithelium and endothelium lung cells allows fluid leakage into the alveoli (Lucas *et al.*, 2020). The exposed extracellular matrix attracts platelets, triggering coagulation and fibrin deposition. Simultaneously, monocytes and neutrophils are recruited, but their dysfunction worsens both inflammation and coagulation. In severe COVID-19, there is an increase in immature neutrophil populations, which promote microthrombi formation and enhancing a proinflammatory response with elevated cytokines such as IL-1, IL-6, CXCL8, and TNF (Muus *et al.*, 2021). The result is an elevated cytokines and chemokines production in the bronchoalveolar lavage fluid (BALF) and the bloodstream, especially in the second week of illness. The excessive inflammatory response can lead to ARDS, pulmonary edema, epithelial cell apoptosis, and multi-organ failure. Elevated cytokine levels in severe cases correlate with increased clinical markers, such as ALT, LDH, CRP, ferritin, and D-dimers (Muus *et al.*, 2021). The combination of TNF and IFNg elevation can trigger inflammatory cell death, contributing to tissue damage and higher mortality. Additionally, the simultaneous upregulation of IFNg and IL-10, particularly in mild cases, is a hallmark of COVID-19 (Sposito *et al.*, 2021). These complications have been detected more in subjects with at least one comorbidity than in a healthy population (Tay *et al.*, 2020).

A comprehensive understanding of how the host immune system responds to SARS-CoV-2 infection is essential for advancing both therapeutic interventions and diagnostic methods. Insights into immune mechanisms such as innate and adaptive immune responses, cytokine profiles, and immune evasion strategies employed by

the virus can facilitate the development of more targeted and effective treatments. Additionally, a deeper knowledge of immune responses can lead to the identification of biomarkers that enable early detection, more accurate disease progression monitoring, and personalized treatment plans, ultimately improving patient outcomes. Moreover, this knowledge is pivotal for the design of future vaccines and antiviral therapies, optimizing their efficacy in different patient populations and against emerging viral variants.

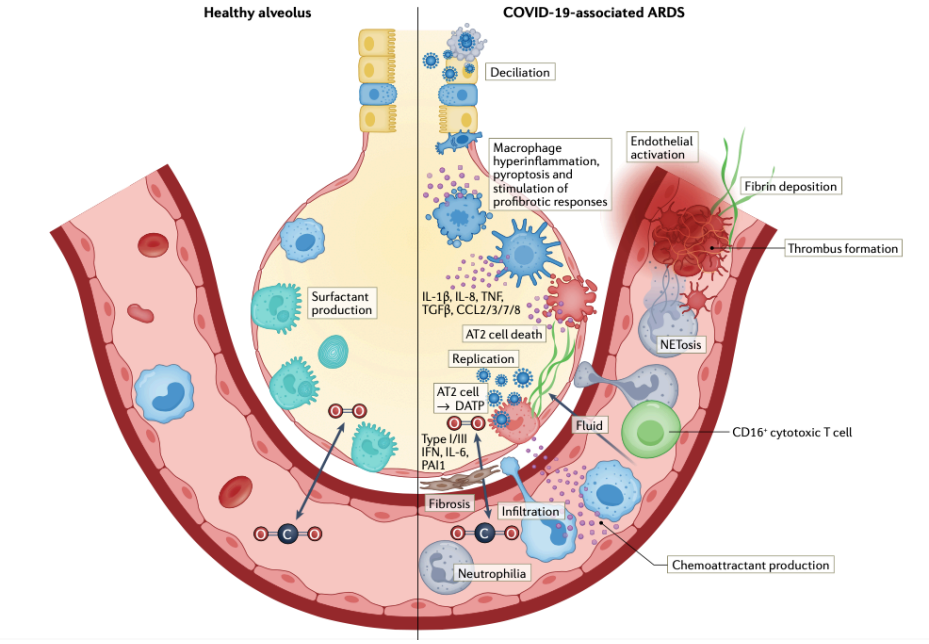


Figure 18 COVID-19-Associated ARDS Development Model SARS-CoV-2 infects the upper airways and spreads to the alveoli, triggering a disrupted immune response. This leads to alveolar damage, fluid leakage, platelet activation, and microthrombi formation. Dysfunctional immune cells, including neutrophils and macrophages, exacerbate inflammation and coagulation. The resulting lung injury impairs oxygen exchange, causing hypoxemia and acute respiratory distress syndrome (ARDS). Open access (Lamers and Haagmans, 2022).

Comorbidities

Retrospective studies have shown that approximately 25% of SARS-CoV-2 positive individuals have at least one comorbidity. Furthermore, 60-90% of hospitalized patients have underlying health conditions (Wiersinga *et al.*, 2020). This highlights the increased risk for individuals with pre-existing health conditions to develop more severe forms of COVID-19. Among hospitalized patients, the most common comorbidities include hypertension (48-57%), diabetes (17-34%), cardiovascular

diseases (21-28%), and chronic pulmonary diseases (4-10%) (Wiersinga *et al.*, 2020). Additionally, 6-8% of hospitalized COVID-19 patients have a history of malignancy (Wiersinga *et al.*, 2020). Moreover, retrospective analysis on data from infected subjects revealed that approximately 25% of SARS-CoV-2 positive people have at least one comorbidity. Indeed, it is estimated that 60-90% of hospitalized infected patients have a previous illness (Wiersinga *et al.*, 2020). This data underlined the increased risk of people with pre-existing pathologies developing a more severe form of COVID-19.

Analyzing comorbidities in hospitalized patients, the most common is hypertension (account for 48-57%), then there are diabetic patients (17-34%), but also patients with cardiovascular (21-28%) or chronic pulmonary (4-10%) diseases (Wiersinga *et al.*, 2020). Lasts, 6-8% of hospitalized COVID-19 patients had malignancy (Wiersinga *et al.*, 2020).

Long COVID condition

Long COVID, or post-acute *sequelae* of COVID-19, is a multisystem condition affecting at least 65 million estimated cases, though this number is likely an underestimation. Is generally defined as multiorgan symptoms which persist for 3 months or more after COVID-19 syndrome (Mateu *et al.*, 2023). It can affect individuals of all ages and severities, with the highest incidence in people aged 36-50 years which had non-hospitalized and mild initial illness.

People affected by long COVID often report an initial acute illness that may have been either minimally symptomatic (cough, fever, and breathlessness) or multisymptomatic (fatigue, cognitive impairments, anosmia and ageusia, chest pain, myalgia and arthralgia, gastrointestinal issues, and skin rashes) (Mateu *et al.*, 2023). Long COVID was documented in individuals who had no symptoms during their initial infection(Ma *et al.*, 2023). After the acute phase, individuals may experience a partial or temporary recovery before new symptoms arise, often described as unusual, exhausting, and in many cases, fluctuating over time (Ladds *et al.*, 2020).

Fatigue is a predominant symptom of long COVID, typically worsening after physical or mental exertion, a phenomenon known as post-exertional symptom exacerbation (Jason and Dorri, 2022). This fatigue is often linked with disturbances in sleep along with increased pain and cognitive impairments (commonly referred to as "brain fog"), especially affecting memory and complex cognitive tasks like multitasking or decision-making (Zhao *et al.*, 2024) (Ladds *et al.*, 2024).

Common allergic reactions in long COVID include rashes watery eyes, and nasal congestion. Throat and gastrointestinal symptoms can involve changes in voice, difficulty swallowing, nausea, and altered eating habits, leading to weight changes and nutritional deficiencies (Rizvi *et al.*, 2023). Some individuals may also experience dizziness, orthostatic hypotension (low blood pressure upon standing), or tachycardia, which can be attributed to dysfunction of the autonomic nervous system (Espinosa-Gonzalez *et al.*, 2023). Mental health issues, such as anxiety and depression, frequently occur alongside long COVID, particularly when there are multiple symptoms present (Zawilska and Kuczyńska, 2022).

Several recent studies identify biochemical and cellular pathways disrupted in individuals with persistent and severe long COVID symptoms. These disruptions are grouped into three primary mechanistic cluster.

The first cluster involves virus-related mechanisms, which include the persistence virus genome or its S-N proteins within tissues. These viral components may directly damage target organs and tissues, and the reactivation of other viruses, such as Epstein-Barr, has also been observed. This viral persistence is likely driven by ineffective immune responses or other underlying mechanisms (Menezes *et al.*, 2024) (Buonsenso and Tantisira, 2024).

The second cluster focuses on immunoinflammatory mechanisms, marked by dysregulated immune responses. Key features include exhausted T-helper cells, high level of cytotoxic T cells and increased cytokine levels. These abnormalities lead to immunopathology, which can damage bystander tissues and contribute to autoimmunity, exacerbating long COVID symptoms (Klein *et al.*, 2023).

The third cluster relates to endothelial inflammation and immune thrombosis, which can disrupt vascular function and lead to tissue injury. Both immunoinflammatory responses and endothelial inflammation can also dysregulate the complement cascade, leading to further tissue damage (Santoro *et al.*, 2023).

Diagnosis

The clinical characteristics of COVID-19 were initially difficult to distinguish from those caused by other respiratory viruses, especially given that many symptoms of mild cases overlapped. To control the spread of SARS-CoV-2, it became clear that rapid and reliable diagnostic tests were crucial for accurately identifying infected individuals and isolating them appropriately.

Diagnostic tests for SARS-CoV-2 can be classified into two main categories: direct and indirect tests.

In detail, the direct diagnostic tests detect the virus in samples either through amplification of its nucleic acids or by identifying viral antigens (antigen tests). The nucleic acid amplification tests (NAATs) allow for the detection of even very small amounts of SARS-CoV-2 RNA in patient samples, making these tests highly sensitive and specific. Due to their reliability, Real-Time RT-PCR (Reverse Transcription Polymerase Chain Reaction) is considered the gold standard for diagnosing COVID-19. This method amplifies specific regions of the viral genome (e.g., E, N, S, or RdRP genes), and the primers can be adapted to identify new viral variants as they emerge (Rahimi, Mirzazadeh and Tavakolpour, 2021). In fact, primers can be modified to recognize mutations in the viral genome as soon as a new viral variant is detected, ensuring ongoing surveillance.

However, despite its advantages, RT-PCR also has several limitations. First, viral RNA can be detected even in individuals who are not contagious, meaning that a positive result may not necessarily correlate with the ability to spread the virus. Furthermore, although RT-PCR is an automated process, one significant limitation of this methodology is the restricted number of samples that can be processed within a single plate and the time-consuming (Rahimi, Mirzazadeh and Tavakolpour, 2021). The time between sample collection and diagnosis may also be affected by logistical issues. Additionally, sample collection and storage, along with the timing of exposure to SARS-CoV-2, can all impact test results. For instance, research by Kucirka *et al.* suggested that the sensitivity of RT-PCR is 33% four days after exposure, 62% at symptom onset, and 80% when performed three days after symptoms begin (Kucirka *et al.*, 2020).

On the other hand, antigen tests detect viral proteins found on the surface of the virus. This method typically involves an immunoassay and can identify replicating virus in patient samples (Krüttgen *et al.*, 2021). Antigen tests are faster, more cost-

effective, and require less time than RT-PCR, making them a good choice for screening programs or situations where nucleic acid amplification tests are not feasible. However, while antigen tests have similar specificity to RT-PCR, they tend to have lower sensitivity. Therefore, a negative result may require confirmation through a Real-Time RT-PCR test to rule out infection (Krüttgen *et al.*, 2021).

Indirect diagnostic tests assess the host's immune response to the viral infection. One common method is serological testing, which detects the presence of antibodies produced by the immune system in response to SARS-CoV-2 infection (Augustine *et al.*, 2020).

Serological tests are valuable for understanding past exposure to the virus and the development of immunity over time. These tests can identify whether a person has developed antibodies (IgM and IgG) in response to the infection (Galipeau *et al.*, 2020). However, while useful for epidemiological studies and understanding the dynamics of viral spread, serological tests are less helpful in the acute phase of infection, as antibodies take several days or weeks to develop (Andreata-Santos *et al.*, 2022). Moreover, with the widespread adoption of vaccination and the possibility of booster shots, serological tests became less reliable for determining whether an individual was currently infected, as they could not differentiate between vaccination-induced immunity and infection-induced immunity (Andreata-Santos *et al.*, 2022).

Therapeutic and prophylactic strategies

Since the outbreak in China, the development of treatment for COVD-19 patients has become a central aim for the scientific community. In March 2020, in response to the emerging COVID-19 pandemic, the Food and Drug Administration (FDA) established the Coronavirus Treatment Acceleration Program (CTAP) to expedite the development of drugs and biological products (excluding vaccines) aimed at treating COVID-19.

Some strategies focused on the capability to hamper different steps of the viral lifecycle, from viral attachment to RNA replication. An example of a drug that interferes with viral replication is Remdesivir, a nucleotide analog that specifically inhibits RNA-dependent RNA polymerase and prevents viral replication, used as a therapy against the Ebola virus. Randomized, double-blind clinical trials have evaluated the safety and the efficacy of Remdesivir in treating COVID-19 (Beigel *et al.*, 2020) (Spinner *et al.*, 2020). The results suggested that the administration of this drug in hospitalized patients could reduce the time to recovery [245] (Beigel *et al.*, 2020) .

On October 22, 2020, the FDA approved remdesivir for the treatment of hospitalized COVID-19 patients aged 12 years and older. More recently, Molnupiravir, a ribonucleoside analog inhibitor originally developed for influenza viruses, was submitted for Emergency Use Authorization for the treatment of mild-to-moderate COVID-19. Early preclinical studies in ferrets demonstrated that oral administration of Molnupiravir reduced SARS-CoV-2 viral load in the upper respiratory tract and completely suppressed viral transmission to untreated contact animals. In human trials, preliminary data indicated that Molnupiravir could shorten the time to SARS-CoV-2 clearance in nasopharyngeal swabs and was generally safe and well-tolerated in symptomatic adults infected with the virus (Fischer *et al.*, 2022) . However, the Italian Medicines Agency (AIFA) suspended the use of Molnupiravir following the negative opinion issued by the European Medicines Agency's (EMA) Committee for Medicinal Products for Human Use (CHMP) on February 24, 2023. This decision was based on the lack of sufficient evidence to demonstrate a clinical benefit in terms of reducing mortality and hospitalizations (*AIFA suspension of lagevrio-molnupiravir* , no date).

Other antiviral agents have been tested against SARS-CoV-2 infection, for example, Hydroxychloroquine. Despite its *in vitro* activity against this virus, clinical trials revealed that it has no benefit in hospitalized patients (‘Effect of Hydroxychloroquine in Hospitalized Patients with Covid-19’, 2020).

To neutralize the virus in infected subjects, a first emergence strategy was the administration of convalescent plasma to patients and the development of monoclonal antibodies (mAbs) (Katz, 2021).

Several anti-S mAbs have been developed and enrolled in clinical trials to prove their safety and efficacy (Weinreich *et al.*, 2021) (Dougan *et al.*, 2021) . Two monoclonal antibody products had Emergency Use Authorizations (EUAs) from Food and Drug Administration (FDA) for the treatment of COVID-19 patients at high risk for progressing to severe disease. These products are:

1. Bamlanivimab and etesevimab (Eli Lilly), which are neutralizing mAbs that bind two overlapping epitopes of RBD. This formulation was clinically evaluated in non-hospitalized COVID-19 patients (Dougan *et al.*, 2021) .
2. Casirivimab plus imdevimab (Regeneron), two high-affinity, mAbs which bind two non-overlapping epitopes of RBD of S protein. The first results highlighted its capability to reduce viral load especially before the initiation of the immune response (Weinreich *et al.*, 2021).

As of August 2022, twelve monoclonal antibodies targeting the spike protein of SARS-CoV-2 have been authorized for clinical use to treat individuals infected with or exposed to the virus. Monoclonal antibodies (mAbs) targeting the RBD of the SARS-CoV-2 spike protein was used both prophylactically and therapeutically for COVID-19. Animal studies, including those with mAbs like pemivibart and adintrevimab, have shown that these antibodies can inhibit viral replication in the lower respiratory tract, reducing virus-induced damage (Cox *et al.*, 2023).

One advantage of mAbs is their ability to protect individuals who do not respond to vaccination, with immediate protection following infusion. The FDA previously granted Emergency Use Authorization (EUA) for tixagevimab/cilgavimab (Evusheld) for pre-exposure prophylaxis (Cox *et al.*, 2023).

However, the emergence of new SARS-CoV-2 variants has led to reduced effectiveness of many mAbs, as shown by *in vitro* neutralization assays with live and pseudotyped viruses (Table1). These assays are used to predict the effectiveness of mAbs, guiding the decisions of FDA on their withdrawal or continued EUA status. Importantly Bebtelovimib (LY-CoV1404) showed no neutralizing effect against the BQ variants and the most recent VOCs (Sun *et al.*, 2023) .

However, the epidemiological picture has become more complex due to the emerge of viral variants. Single and combination therapies with mAbs have been tested to evaluate their efficacy against VOCs. Unfortunately, VOCs are less sensitive

to mAbs that target spike protein than G614D (Planas *et al.*, 2021) (Chen *et al.*, 2021).

Table 1 Neutralization activites of monoclonal antibodies (mAbs) against VOCs. Open access (Cox *et al.*, 2023)**.**

		Alpha	Beta	Delta	Gamma	Variant				
						BA.1	BA.2	BA.1.1	BA.4/BA.5	BA.2.12.1
Class 1	Amubarvimab	0.38	0.62	0.8	0.49	180	200	220	85	97
	Casirivimab	0.91	110	0.71	89	630	670	910	710	1000
	DXP-604	0.75	8.1	1.7	0.55	19	17	18	570	19
	Etesevimab	9.3	320	0.52	270	410	460	530	320	510
	Regdanvimab	1.5	53	37	73	590	830	1000	1000	n.d.
	Tixagevimab	1.4	4.7	1.1	4	360	540	400	860	420
Class 2	Bamlanivimab	1.1	660	650	700	700	660	910	520	580
	Cilgavimab	0.73	1	3.2	0.82	220	2.7	820	11	3.6
Class 3	Bebtelovimab	1	0.84	1.5	1	1.1	0.91	1.1	0.97	1.1
	Imdevimab	0.52	0.62	2.2	0.54	600	230	1000	450	380
	Romlusevimab	0.32	6.7	n.d.	0.7	0.74	8.1	21	27	27
	Sotrovimab	1.8	1	1.1	0.79	3.3	21	2.4	20	18
Cocktails	Amu + Rom	0.89	1.5	2.5	2.5	12	83	200	110	88
	Bam + Ete	1.6	520	1.1	410	740	750	1000	670	740
	Cas + Imd	0.77	2.2	1.1	1.4	840	300	1000	730	620
	Cil + Tix	0.95	2.1	0.93	0.99	75	7.3	310	74	21

<1 <3 <10 <100 >100 n.d.

Since the emergence of the Omicron BA.2 subvariant, no monoclonal antibody has proven effective against these variants. Currently, on March 2024, the FDA has granted EUA for pemivibart (Pemgarda, Invivyd) as pre-exposure prophylaxis for COVID-19 in immunocompromised adults and adolescents, based on positive results from the CANOPY trial, which demonstrated its safety, tolerability, and ability to produce high serum neutralizing antibody levels against recent circulating SARS-CoV-2 variants as JN.1

Conversely, given that an excessive immune response is a critical factor contributing to disease progression in COVID-19 patients, various immunomodulatory therapies have been evaluated as potential treatment options to mitigate this hyperinflammatory response and curb the progression of the disease.

They are not specific drugs against SARS-CoV-2, but their mechanism of action is based on the control of the over-activation of the immune response, with the consequent limitation of the immune-mediated damage. Corticosteroids, JAK inhibitors, mAbs that block IL-6 (Tocilizumab), IL-1 receptor antagonists are the

strategies that have been proven to be effective in dampening hyper- activation of immune response (Stone *et al.*, 2020) (Burrage, Koushesh and Sofat, 2020).

Anyway, the absence of a tailored therapy and the wide-spread of the virus around the world highlighted the urgent need for a prophylactic strategy against SARS-CoV-2. The identification of S as the immunodominant protein, together with its importance in viral entry, explains the efforts of the prophylactic measures to induce an immune response against this viral protein. Several vaccines have been developed to produce neutralizing antibodies against the S protein. Currently approved COVID-19 vaccines can be divided into four main categories (*WHO – COVID19 Vaccine Tracker --- https://covid19.trackvaccines.org*, no date):

(1) RNA vaccines as Moderna and Pfizer-BioNTech's Comirnaty
(2) Vector-based vaccines as AstraZeneca, Covishield and Johnson & Johnson-Janssen
(3) Protein subunit-based vaccines as Novavax and Covovax
(4) Inactivated whole genome virus

These different classes of vaccines have distinct formulations; in particular, they vary in how they deliver the antigen, or the genetic material needed to produce it.

The first two categories include vaccines with mRNA or DNA encoding the SARS-CoV-2 S protein, thereby prompting host cells to synthesize the protein. In contrast, the third category comprises protein-based vaccines, which directly deliver the S protein, typically in combination with adjuvants to augment the immunogenic response. Lastly, the fourth category includes chemically inactivated SARS-CoV-2 viral particles.

In addition, these different vaccine formulations can be distinguished by their immunogenicity, which refers to the ability to activate the innate immune system, thereby triggering an adaptive immune response and generating immunological memory. The primary difference in immunogenicity among the four vaccine types is that mRNA and vector-based vaccines are considered "self-adjuvanted" triggering an immune response. In contrast, protein subunit and inactivated whole-virus vaccines have an external adjuvant molecule to enhance immune activation.

Lastly, all vaccine types have proven highly effective in preventing severe disease of COVID-19 and death (*WHO – COVID19 Vaccine Tracker --- https://covid19.trackvaccines.org*, no date). However, as previously discussed, the widespread deployment of vaccines has introduced selective pressure on the virus,

facilitating the emergence of new variants that exhibit varying degrees of resistance to immune responses.

Immunogenic variations: innate immune responses induced by different vaccines

COVID-19 vaccines employ various strategies to induce immune responses. mRNA vaccines deliver functional mRNA, which is translated by host machinery into the S protein, activating also an immune response (Rosa *et al.*, 2021) (Pardi, Hogan and Weissman, 2020). To balance the immune activation and minimize reactogenicity, the mRNA is modified reducing recognition by TLRs and RLRs. Additionally, lipid nanoparticles (LNPs) protect the mRNA, enhance its delivery to lymphatic tissues, and contribute to immune activation by acting as adjuvants (Figure 19-1) (Pardi *et al.*, 2018).

In comparison, adenovirus vector-based DNA vaccines (AdV) involve a more complex process, requiring intranuclear transcription and RNA processing to produce functional mRNA and spike protein. AdVs activate innate immune responses through different pathways, with their viral DNA detected by TLR2-4, and -9, as well as cytosolic sensors like cGAS. This leads to the production of type-I interferons (Bos *et al.*, 2020). Current AdV vaccines use modified adenoviruses, where the early E1 gene is replaced with the SARS-CoV-2 spike gene, ensuring vaccine safety (Figure 19-2) (Kovesdi and Hedley, 2010).

Recombinant protein subunit vaccines, such as the Novavax, use the trimeric S protein produced in insect cells. These vaccines require adjuvants like Matrix M, which activates innate immune cells at the injection site and in draining lymph nodes, triggering the release of cytokines and amplifying the immune response. Matrix M also activates the NLRP3 inflammasome, promoting the secretion of IL-1β and IL-18 (Figure 19-3) (Bangaru *et al.*, 2020) (Dunkle *et al.*, 2022).

Inactivated vaccines, derived from the entire SARS-CoV-2 virus, are inactivated using physical or chemical agents (e.g., UV radiation, formalin) (Tirelli *et al.*, 2023). Like protein subunit vaccines, these vaccines require adjuvants such as Covaxin, a TLR7/8 agonist, which enhances Th1 responses and suppresses Th2 responses. TLR activation in innate immune cells stimulates type-I IFN production and proinflammatory cytokine release. Inactivated vaccines induce broader immune

responses due to the presence of additional viral proteins, leading to polyclonal T cell responses (McMenamin *et al.*, 2022).

This diversity in vaccine platforms reflects different strategies to modulate immune responses for optimal protection against SARS-CoV-2.

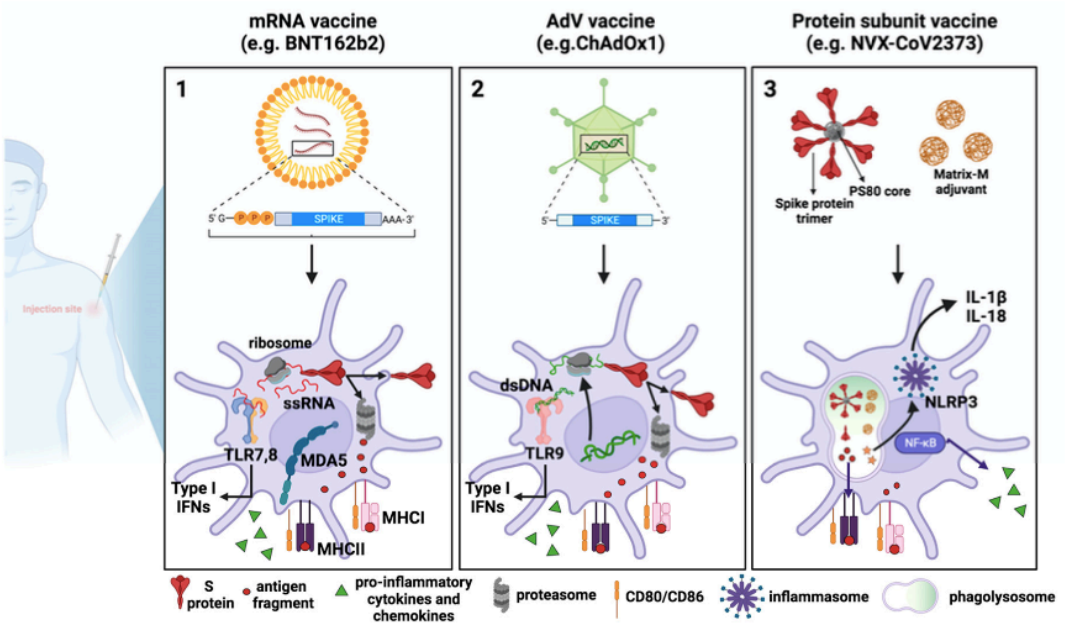


Figure 19 COVID-19 vaccines and immune activation. This schematic figure depicts the mechanisms of action of the three SARS-CoV-2 vaccine platforms: **(1)** mRNA vaccines, where mRNA encoding the S protein **(2)** adenovirus (AdV) vector vaccines, where the S protein is encoded by a DNA sequence; and **(3)** recombinant protein-based vaccines, where SARS-CoV-2 S proteins are assembled on nanoparticles design to mimic structure of the virus. All three vaccine types are processed by dendritic cells in a similar manner; after internalization, the S protein is degraded by dendritic cells and presented by MHC class I and II. The main difference lies in how the S protein is produced. Open access (Manfrini et al., 2024).

AIM OF THE WORK

This study aims to provide an in-depth analysis of the key virological factors that drive the propagation of SARS-CoV-2, including viral entry mechanisms, replication kinetics, immune evasion strategies, and transmission dynamics. By considering the evolving landscape of SARS-CoV-2 and the emergence of new variants, we will investigate these factors across 11 variants of concern (VOCs).

A particular focus will be placed on one of the lesser-studied modes of transmission: indirect contact through contaminated surfaces. Given the variability in transmissibility and infectivity across these VOCs, we will explore their persistence on various materials and their potential to reinfect a susceptible *in vitro* model.

Specifically, the study will examine how key mutations in the spike protein and other viral regions influence the entry mechanism, replication efficiency, and immune evasion properties of each VOC. Using well-established *in vitro* cell models, we will assess how these mutations modulate viral behavior, including their interaction with both innate and adaptive immune responses.

In parallel, we will investigate the persistence of these variants on commonly encountered surfaces, highlighting how specific mutations may impact the stability of each variant. Furthermore, we will evaluate their susceptibility to disinfectants currently recommended for infection control.

By providing a detailed examination of these factors, the study aims to offer crucial insights into the transmission dynamics of SARS-CoV-2 variants, their environmental stability, and the effectiveness of disinfection protocols.

RESULTS

Insights into the replication kinetics of 11 SARS-CoV-2 variants

We conducted an analysis of the replication kinetics of 11 SARS-CoV-2 variants, including pre-Omicron variants (G614D, Alpha, Beta, Gamma, and Delta) and Omicron sublineages (BA.1, BA.2, BA.4, BQ.1.1, XBB.1, and XBB.1.5). These variants were classified as VOCs by the WHO over time but are currently being de-escalated due to their decline in circulation as reported by the European Centre for Disease Prevention and Control (ECDC) (*SARS-CoV-2 variants of concern as of 20 December 2024 --- ecdc.europa.eu*, no date). To evaluate the viral replication dynamics, human lung epithelial carcinoma cells (Calu-3) were utilized as a model to mimic the site of primary infection. For viral replication assessment, RNA genome was extracted from the supernatant of Calu-3 and quantified using Real-Time PCR. Six different time points were selected to characterize the infection kinetics.

The results demonstrate that the different variants exhibit distinct replication profiles, as evidenced by varying areas under the curve (AUC) values (DCt/hpi). Notably, viral RNA copy numbers in the supernatant increased rapidly during the first 24 hours post-infection (hpi) and subsequently plateaued around 72 hpi.

Focusing on the pre-Omicron family variants (Figure 20A), Beta and Gamma variants demonstrated the fastest kinetics, with very similar AUC values (689.5 and 687.1, respectively), followed by Delta (659.3) and Alpha (643.7), and finally G614D exhibited the slowest replication rate, with a small AUC value (512.3). Statistically significant differences in replication kinetics were observed comparing Beta and Gamma to G614D and Alpha ($p < 0.05$); no statistically significant differences were found comparing the Delta with the other variants.

For the Omicron family variants (Figure 20B), BA.2 exhibited the fastest replication kinetics (719.6), followed by XBB.1.5 (639.4). The BA.1, BA.4, and XBB.1 variants showed similar AUC values (499.2, 527.8 and 532.4, respectively), all higher than BQ.1.1 which displayed the lowest replication rates (438.4). Statistical analysis revealed significant differences in replication rates for BA.2, BQ.1.1, and XBB.1.5 compared to all other VOCs, while no significant differences were observed when comparing the replication rates of BA.1, BA.4, and XBB.1.

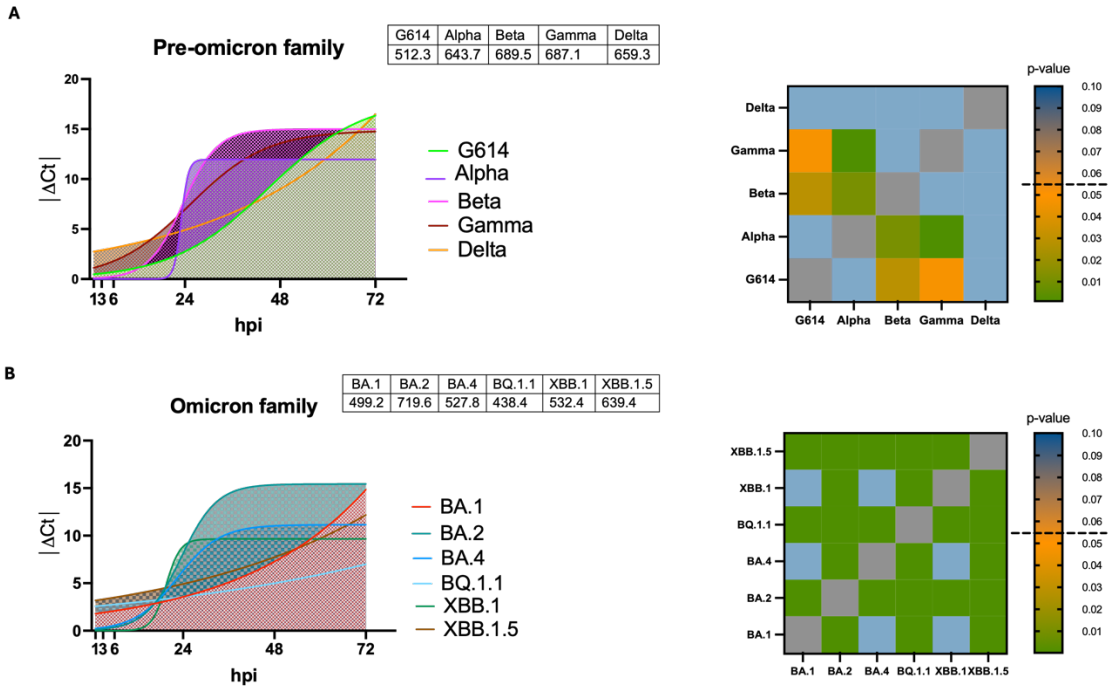


Figure 20. Replication kinetics of 11 SARS-CoV-2 VOCs in Calu-3 cells. Viral genomes copy numbers in the supernatant were measured at six time points post-infection (0.001 MOI). (A) Pre-Omicron VOCs: G614D, Alpha, Beta Gamma and Delta replication kinetics. Statistically significant differences were observed between Beta/Gamma and G614D/Alpha (**p < 0.01). (B) Omicron family variants: BA.1, BA.2, BA.4, BQ.1.1, XBB.1, and XBB.1.5 were assessed for viral replication. Significant differences were observed between BA.2, BQ.1.1, and XBB.1.5 (***p < 0.001), with no significant differences among BA.1, BA.4, and XBB.1 (p > 0.1). The viral RNA levels were quantified by Real-Time PCR and expressed as ΔCt values, with mean ± SD for each variant for three experimental replicates and two experimental sessions. Statistically significant differences in replication kinetics were determined, with **p < 0.01, ***p < 0.001, and ****p < 0.0001. Ct: threshold cycle.

Replication kinetics may be driven by distinct entry efficacy

Considering the different replication kinetic of the VOCs, we investigated how the entry mechanism could affect the replication kinetic. We set up a lentiviral based pseudoviruses protocol for 3 pre-Omicron (G614D, Beta, Delta), and 3 Omicron (BA.1, XBB.1 and XBB.1.5) variants, engineered to express the full-length S protein and ZsGreen or luciferase to monitor infection.

Firstly, we investigated the production of pseudoviruses by evaluating, through immunofluorescence, the presence of the G614D spike protein 48 hpi in HEK mCherry cell line; the results confirmed that the cells were effectively transduced with G614D (Figure 21A). Immunofluorescence was performed exclusively for the G614D variant, so we proceeded to validate the pseudovirus production system by transducing the VeroE6/TMPRSS2 cell line with pseudovirus preparations from different production batches. After 72 hours of trasduction, we assessed luciferase activity detecting the relative luminescence units (RLU) to confirm the reproducibility of the protocol.

The obtained data validated the experimental protocol, although the RLU intensity varied between batches, as confirmed by Two-way Anova analysis. Notably, we observed higher production efficiency for the Beta variant, followed by Delta, XBB.1.5, G614D, XBB.1, and finally BA.1, which exhibited the lowest RLU signal. These results suggest that differences in pseudovirus production could be influenced by batch-to-batch variations in the preparation process.

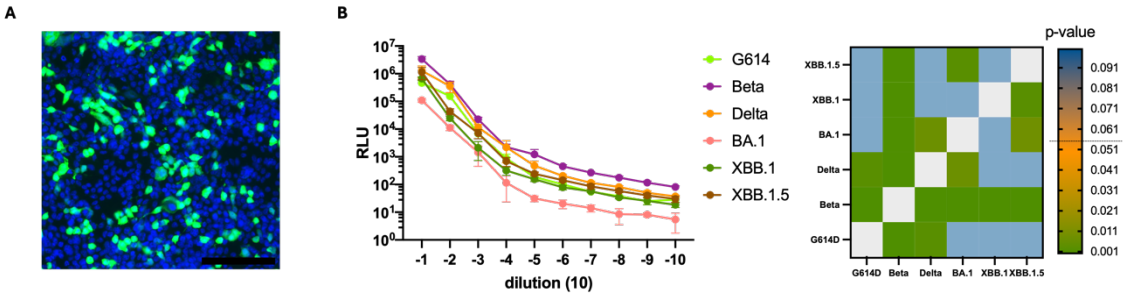


Figure 21 Validation of Pseudovirus System Production. To investigate the entry mechanisms of SARS-CoV-2 VOCs, we employed a lentiviral-based pseudovirus system expressing full-length S protein and ZsGreen or luciferase for trasduction monitoring. We validated the system trasducting susceptible cell lines. **(A)** G614D pseudovirus production was assessed by examining mCherry-positive cells under 20x magnification detecting the GFP (green) signal. Nuclei were counterstained with Hoechst 33342 (blue). Scale bar: 100 µm. **(B)** VOCs pseudovirus production was valitaed trasducting the VeroE6/TMPRSS2 cells using 10 different dilutions, followed by measurement of luminescence signal units (RLU) at 37°C for 72 h. Data from six replicates are shown as the mean ± SD, of six different experimental replicates. Two-way ANOVA ** $p<0.01$ ****, $p < 0.0001$. The luminescence signal confirmed successful production of the various spike proteins**.**

To rule out any potential bias in the entry assay caused by differences in production, we quantified the total protein content in the various pseudovirus stocks using a BCA protein assay. The results shown in Figure 22A demonstrate that the Beta variant stock contains a higher total protein concentration compared to the other variants.

However, based on these data, we confirmed that the amount of S protein was equal across all pseudovirus stocks (Figure 22B). To confirm this hypothesis, we applied the same protein concentration to all pseudovirus preparations and measured the S protein levels using an ELISA assay with an anti-S antibody. These additional controls allowed us to ensure that the differences in entry efficiency couldn't be due to discrepancies in spike protein amounts. The ELISA results showed that the amount of S protein was the same across all VOCs, except for the G614D variant, which exhibited a statistically significant difference compared to the other pseudoviruses ($p < 0.0001$). This discrepancy could be attributed to a higher affinity of the anti-S antibody for detecting the G614D variant.

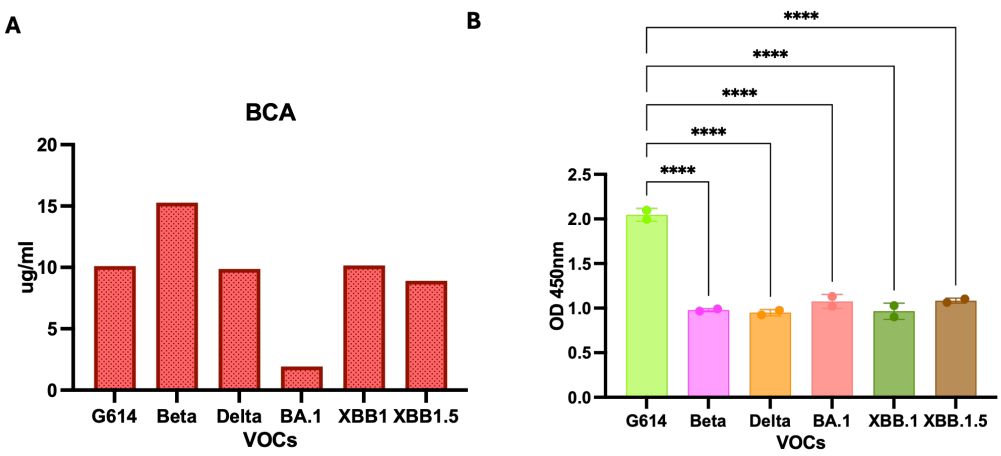


Figure 22 BCA Protein Assay for Quantification of Total Protein in Different Pseudovirus Batches. (A)The total protein concentration (ug/ml) of pseudovirus stocks was determined using a BCA protein assay. The results highlight variability in the protein content across different batches, with the Beta variant stock showing a significantly higher total protein concentration compared to the other variants. (B) The spike protein levels in various pseudovirus variants were quantified using an ELISA assay with an anti-S antibody. The S- detection was reported as mean values ± SD, considering two different experimental replicates. One-way ANOVA ** $p<0.01$ ****, $p < 0.0001$.

Then, we performed the entry experiments on the Calu-3 using an equivalent amount of different pseudovirus constructs based on RLU signal and normalized for total protein concentration of the specific pseudovirus obtained from BCA

experiments (Figure 23A). The obtained results (Figure 23B) clearly illustrate that the VOCs exhibit distinct entry mechanisms. Specifically, the Beta and Delta variants displayed the fastest entry kinetics ($p < 0.0001$), followed by XBB.1.5 ($p<0.0001$). In contrast, the G614D, BA.1, and XBB.1 variants showed comparable relative luminescence unit (RLU) signals, suggesting similar entry profiles. Statistical analysis further confirmed that no significant differences were observed between Beta and Delta, nor between G614D, BA.1, and XBB.1. However, the entry kinetics of XBB.1.5 were significantly different from all other variants ($p < 0.0001$).

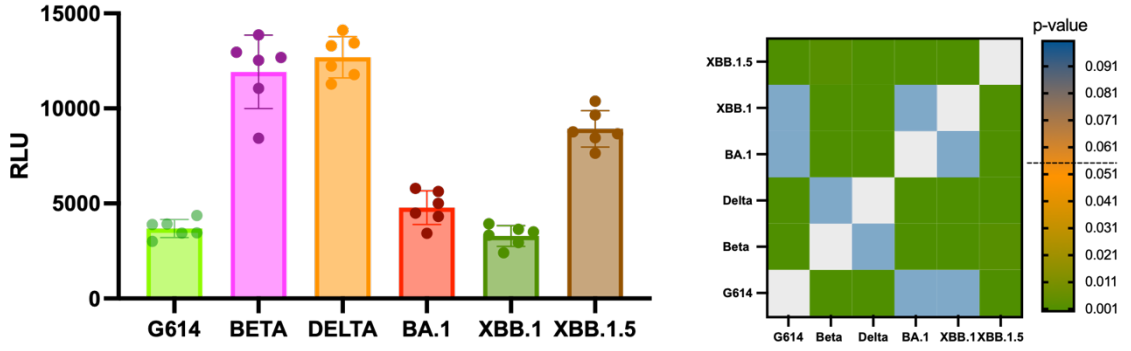


Figure 23 Entry mechanisms of different VOCs on Calu-3 models. Entry experiments were performed using the pseudovirus carrying different S-proteins to infect Calu-3 cells at equal doses, and luciferase activity (Relative luminescence units, RLU) was detected after incubation at 37°C for 72 h. Data from six replicates are shown as the mean ± SD, **** $p < 0.0001$.

To deeply discover the entry process, we examined the involvement of the early and the late pathways for all the lentiviral based pseudoviruses, evaluating the inhibitory effect of bafilomycin A1 (BFLA-1), and camostat mesylate (CAM), alone or combined (Figure 24). Notably, BFLA-1, a vacuolar H^+-ATPase inhibitor, prevented the cleavage of the S protein and exposure of the FP domain by disrupting the acidic environment required for cathepsin L activation, while CAM targeted the early pathway by inhibiting TMPRSS2 activity and preventing direct fusion between the viral envelope and the host membrane (Peacock *et al.*, 2021) (Hoffmann *et al.*, 2020) (Cheng *et al.*, 2020).

As shown in the graph, the selective interference of either the late or the early pathway had not the same effect.

A significant inhibitory effect was observed with CAM treatment (93.6 ± 2.4% of infection inhibition) across all pseudoviruses, while inhibition of endosomal acidification by BFLA-1 only partially hindered pseudovirus entry (70.5 ± 17.4%).

This result was particularly evident in G614D and Delta pseudoviruses (48.5 ± 2.12%).

These results suggested that all the SARS-CoV-2 VOCs examined mainly relied on early pathway if TMPRSS2 was expressed on the host cell membranes. The combination of both inhibitors led to 99.9 ± 0.1% of inhibition, suggesting a complete hampering of the viral entry step.

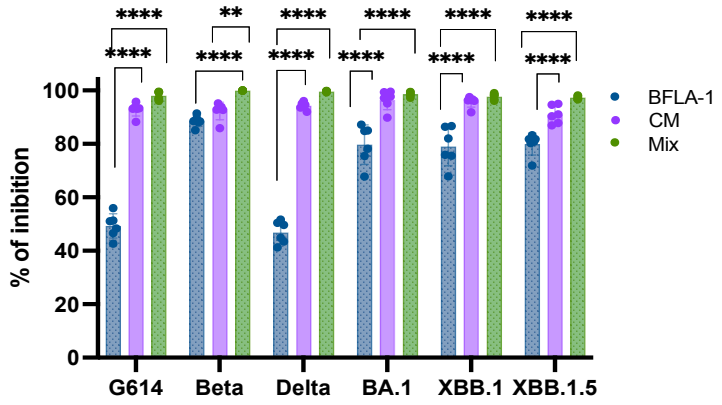


Figure 24 Characterization of the two different entry mechanisms in Calu-3 models. Mechanisms used by the virus to infect Calu-3 thought endocytosis and direct fusion with plasma membrane were selectively hampered by chemical compounds. Targeting only one of the two entry mechanism resulted in different degree of infection inhibition. The infection inhibition percentages were reported as mean values ± SD of six different experimental replicates, ** $p<0.01$ ****, $p < 0.0001$.

Immuno-escape: how the antiviral response impact on the replication kinetic

Based on the kinetic replication and the entry mechanism results, we focused on the role of the innate immunity of the Calu-3 cell lines exploring how this may influence both these virological aspects. Therefore, we evaluated the first host defense against virus infection the type-I-IFN-response released by cells through a signaling cascade started with the activation of RIG-I or RLRs upon interaction with viral products. We evaluated the mRNA expression of RIG-I, IFNβ and the downstream ISGs (IFIT1, MX1, MX2, ISG15) using qPCR at different time point (1, 3, 6 and 24 hpi).

The obtained results showed (Figure 25) how the mRNA expression of IFNβ and the ISGs significantly increased upon SARS-CoV-2 infection in Calu-3 compared to uninfected control.

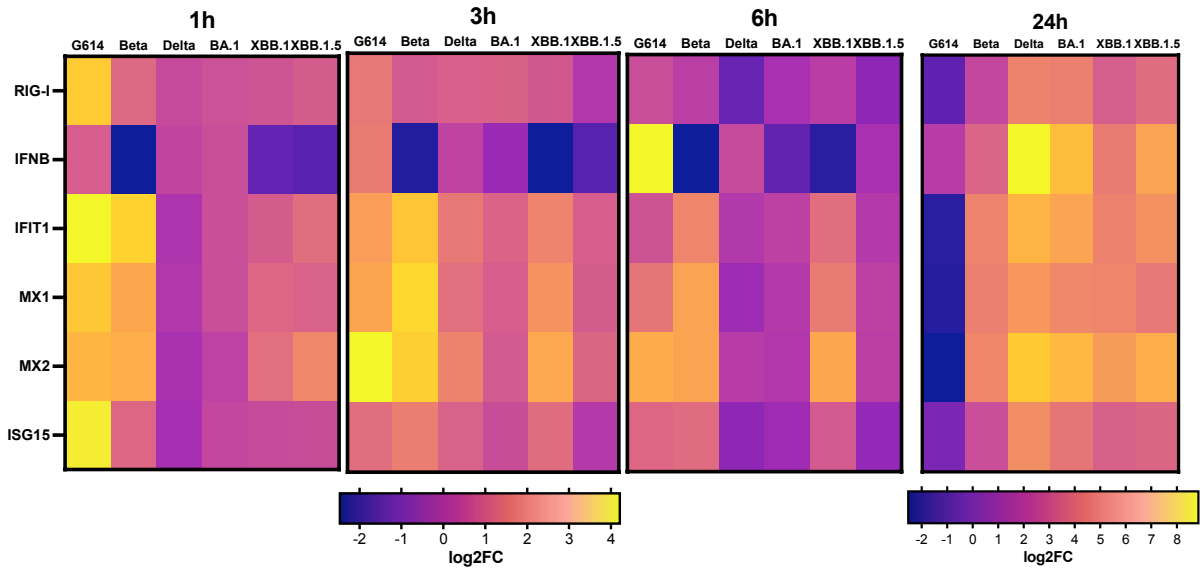


Figure 25 Different immune-escape mechanisms for VOCs. Heatmap showing the activation of the interferon signaling pathway following infection with 0.1 MOI. The activation (value > 1) or downregulation (value < 1) of IFN-related genes was calculated by subtracting the Ct values of specific genes from the Ct values of the housekeeping gene (GAPDH), yielding the ΔCt. Gene expression is presented as log2 fold change relative to uninfected cells (ΔΔCt). Monitoring the immune response at different time points provided insights into how specific VOCs may mediate distinct activation or suppression path. The results were obtained from three different replicates and two different experimental sessions.

Specifically, considering the immune response after 1 hpi we observed that G614D was rapidly recognized, triggering an immune response as demonstrated by the upregulation of mRNA levels of RIG-I, IFIT-1, MIX1, MIX2, and ISG15 with statistically significant differences ($p < 0.001$) when compared to the other variants.

Considering the IFNβ response was similar between G614D, Delta and BA.1 and downregulated in Beta ($p<0.0001$), XBB.1 ($p<0.01$) and XBB.1.5 ($p<0.001$) comparing to the other variants (Figure 26).

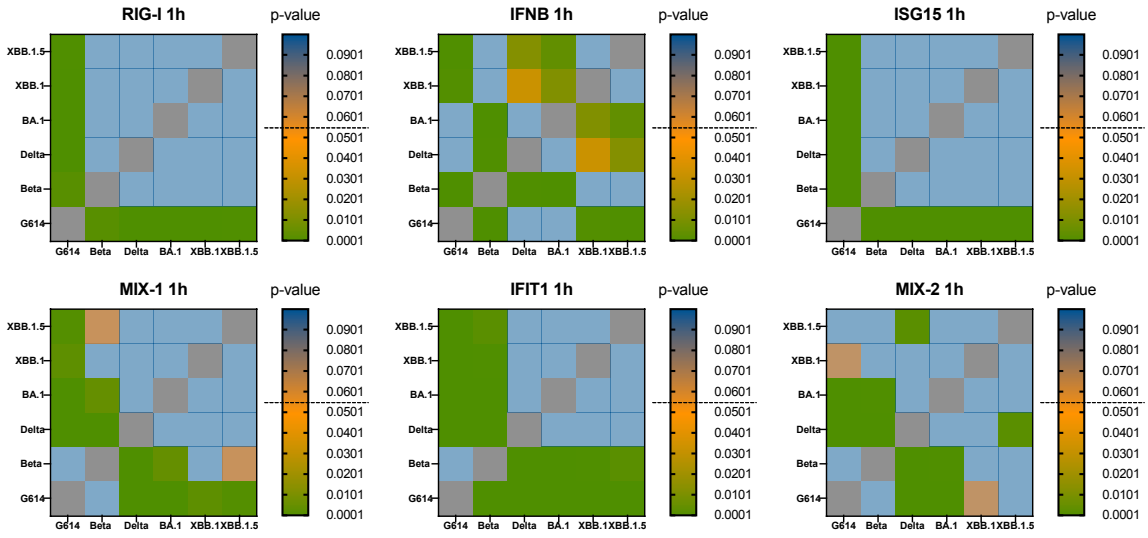


Figure 26 Statistical analysis of immune response. Study of gene expression levels in the Calu-3 model at 1 hours post-infection (hpi) with six SARS-CoV-2 variants.

Notably, 3 hpi with G614D, the levels of RIG-I and ISG15 decrease and return to baseline, with no significant difference compared to the other variants. In contrast, IFN-β expression was significantly elevated at 3 hpi in both G614D and Delta variants compared to other VOCs (Figure 25). Specifically, the expression level of IFN-β showed statistically significant differences compared G614D to Beta, XBB.1 ($p < 0.0001$), BA.1 ($p < 0.01$), and XBB.1.5 ($p < 0.001$), while Delta exhibited significant differences when compared to Beta ($p < 0.01$) and XBB.1 ($p < 0.001$) (

Figure **27**).

Considering the ISGs expression, the IFIT-1, MIX1, and MIX2 genes were upregulated in G614D, Beta, Delta, and XBB.1, but downregulated in BA.1 and XBB.1.5. Statistical analysis confirmed that IFIT-1 and MIX1 were significantly different between BA.1 and XBB.1 compared to Beta ($p < 0.0001$), while MIX2 was upregulated in both G614D and Beta. G614D showed a significant difference when compared to Delta ($p < 0.01$), BA.1, and XBB.1 ($p < 0.0001$). Beta was statistically different when compared to BA.1 ($p < 0.001$) and XBB.1.5 ($p < 0.0001$).

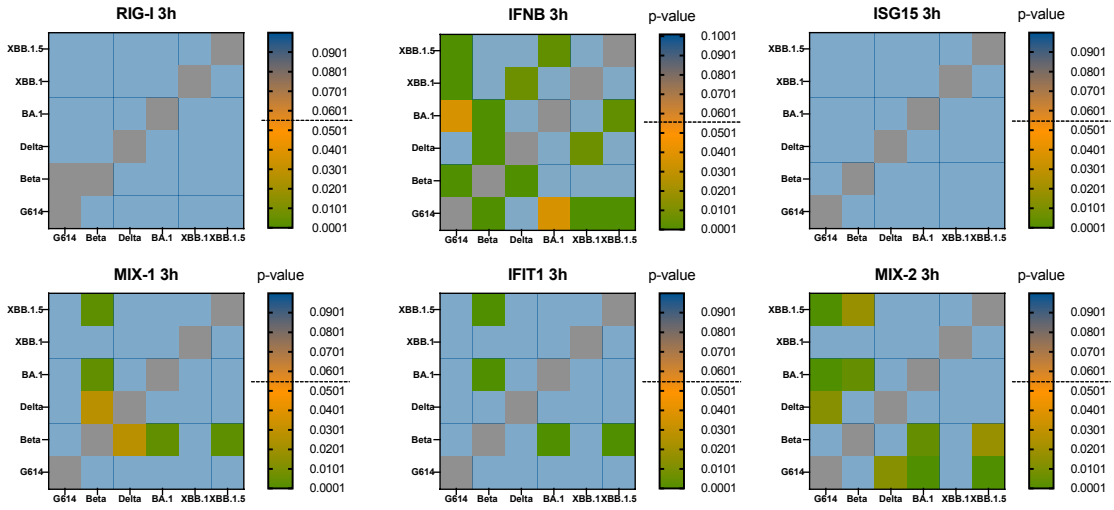


Figure 27 Statistical analysis of immune response. Study of gene expression levels in the Calu-3 model at 3 hours post-infection (hpi) with six SARS-CoV-2 variants.

G614D reached its peak expression at 6 hpi, and the upregulation of IFN-β was statistically significant compared to all VOCs ($p < 0.0001$). Moreover, IFN-β upregulation in Delta resulted in a statistically significant difference from all VOCs ($p < 0.0001$), excluding XBB.1.5 ($p > 0.1$). In addition to the upregulation of IFN-β, both Delta and XBB.1.5 showed a downregulation of RIG-I compared to G614D and Beta.

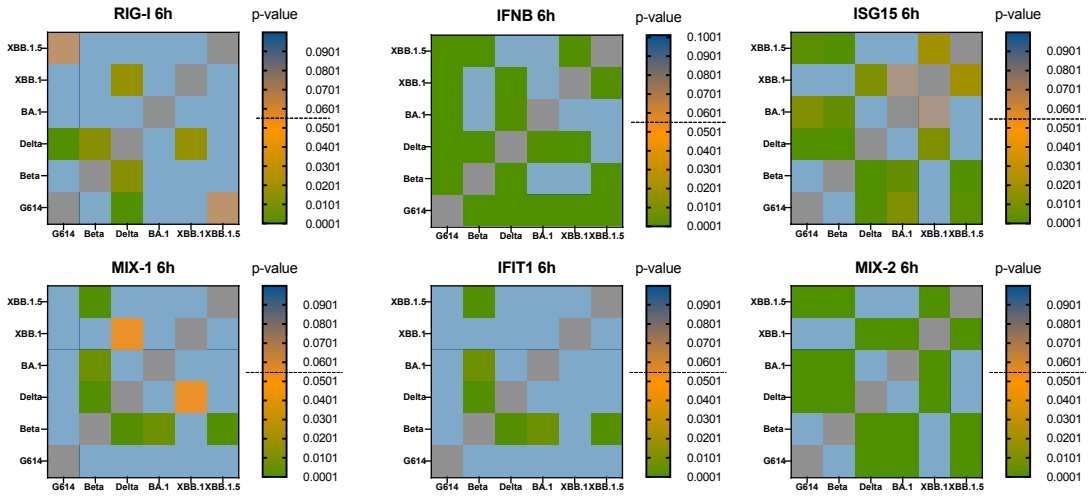


Figure 28 Statistical analysis of immune response. Study of gene expression levels in the Calu-3 model at 6 hours post-infection (hpi) with six SARS-CoV-2 variants.

Furthermore, an upregulation of downstream genes involved in the interferon response was observed in G614D, Beta, and XBB.1 compared to other variants. Specifically, G614D exhibited an upregulation of ISG15 expression compared to Delta, XBB.1.5 ($p < 0.0001$), and BA.1 ($p < 0.01$), and of MIX2 compared to Delta, BA.1, and XBB.1.5 ($p < 0.0001$). Beta showed an upregulation of ISG15, MIX1, MIX2, and IFIT1, with statistically significant higher expression compared to Delta, BA.1, and XBB.1.5 (p-values ranged from < 0.0001 to < 0.001).

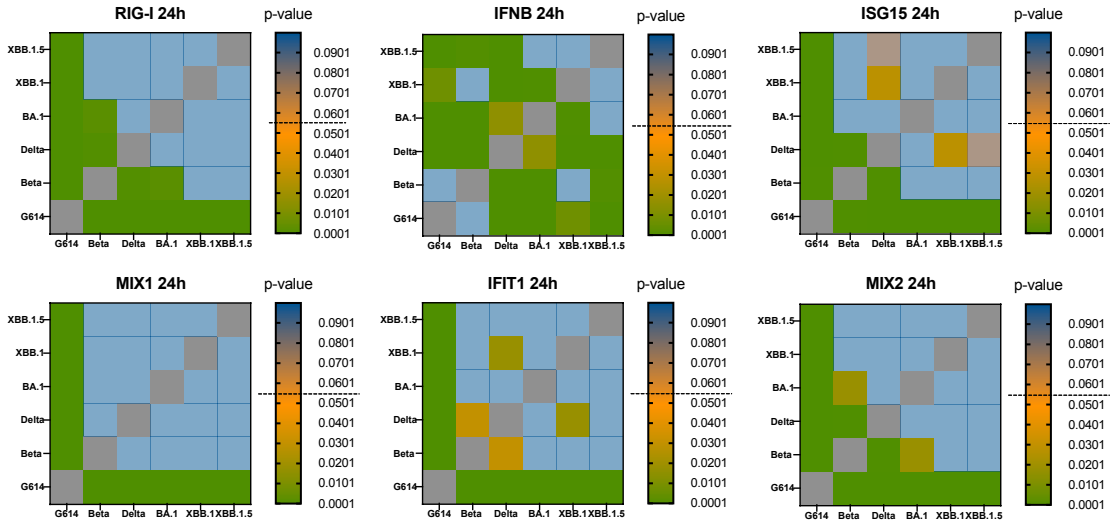


Figure 29 Statistical analysis of immune response. Study of gene expression levels in the Calu-3 model at 24 hours post-infection (hpi) with six SARS-CoV-2 variants

At the 24-hour time point, G614D exhibited a downregulation of IFNβ and ISGs ($p < 0.0001$), which may correlate with the resolution of the infection.

In contrast, all other variants displayed an increased expression of IFNβ ($p < 0.0001$). Notably, Beta didn't exhibit further upregulation of RIG-I, IFIT1, MIX1, MIX2, and ISG15 compared to earlier time points, whereas the levels of these genes continue to rise in all other VOCs ($p<0.0001$).

Considering the three different virological aspects (viral entry mechanisms, replication kinetics, and the immune escape) we analyzed, we conducted a multivariable analysis to identify potential correlations between these factors (Figure 30). The results revealed a strong positive correlation between viral entry mechanisms and replication kinetics (r = 0.95), indicating that variants with faster viral entry also exhibit higher replication rates. This suggests a direct link between the efficiency of viral entry into host cells and the subsequent replication processes.

However, when evaluating the abundance of the IFN response at 24 hpi in relation to viral replication and entry mechanisms, no significant correlation was observed (r < 0.5). This lack of correlation implies that the induction of the interferon (IFN) response does not appear to directly influence the viral entry or replication rates within the time frame studied, suggesting that these processes may be regulated independently or that the IFN response may require a longer time to manifest a measurable effect on viral dynamics.

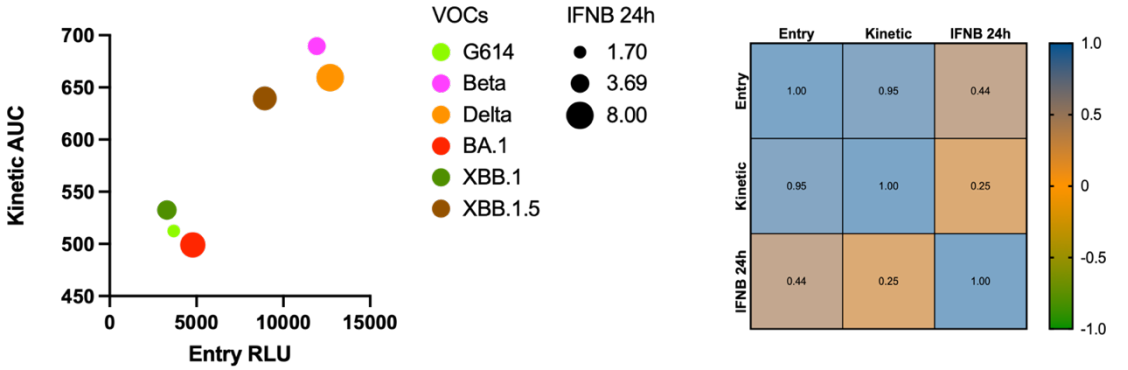


Figure 30 Correlation analysis of entry, replication and immune escape mechanisms. Correlation analysis was performed on 11 VOCs, considering entry values (x-axis), replication kinetics (y-axis), and immune response (size). Entry values are indicated by the RLU signal, replication kinetics are represented by the AUC value, and immune escape is reflected by the upregulation of IFNB levels at 24 hpi. Pearson correlation analysis is shown in the heatmap, highlighting a strong correlation between entry and replication mechanisms (0.95).

Study the persistence mechanisms of SARS-CoV-2 variants

After assessing the virological aspects in terms of viral entry, replication kinetics, and immune response, we aimed to study transmission through contaminated objects: fomites.

To obtain these results, we set up an experimental protocol to investigate the persistence of 11 SARS-CoV-2 variants on three selected materials: polystyrene-plastic, aluminum, and copper.

Briefly, we selected a reasonable viral load (1.5×10^6 $TCID_{50}$/ml) that could be deposited on a surface by an infected individual, based on a previous study (Criscuolo *et al.*, 2021). We then examined viral recovery at three time points: 15, 60, and 120 minutes. After each time point, we recovered the viral particles from the surface and back titrated them using the Vero/TMPRSS2 permissive cell model. The obtained results allowed us to draw two main observations: none of the tested variants were able to persist for more than 15 minutes on copper a material known for its antimicrobial and antiviral properties (Figure 31A). For polystyrene-plastic and aluminum, which are non-porous and non-charged materials, we observed that some variants were able to persist (Figure 31B-C).

In this case, the persistence is not dependent on the material, but rather on the variant: the same variants that persist remain stable on both materials. At the first time point of 15 minutes, Gamma was the most persistent variant, with a detected viral load of 91.6 ± 2.8% compared to the stock on aluminum and polystyrene-plastic, followed by Delta with a viral load of 78.3 ± 5.7% on aluminum and 67.3 ± 2.5% on polystyrene-plastic. Among the Omicron variants, BA.1, XBB.1 and XBB.1.5 exhibited the similar persistence value; the detected viral load of BA.1 was 55 ± 1% on aluminum and 73.3 ± 2.8% on polystyrene-plastic, while for the XBB variants was 62.6 ± 8.08% on aluminum and 64.2 ± 10.7% on polystyrene-plastic. After 120 minutes, Gamma showed a persistence rate of 81.6 ± 6.3% on aluminum and 43.3 ± 2.8% on polystyrene-plastic, while Delta showed 20 ± 5% persistence on polystyrene-plastic. The BA.1 and XBB.1 variants had 15 ± 2.6% persistence on polystyrene-plastic, while only BA.1 persisted on aluminum with 7.6 ± 4%. XBB.1.5 did not persist further. Lastly, after 6 hours, no variants remained detectable on either material. We performed a two-way ANOVA to analyze the variance in persistence mechanisms at 15 minutes for all VOCs across the two materials. The persistence rates of the variants were significantly different, with a p-value < 0.01 compared to other VOCs as showed in the heatmap.

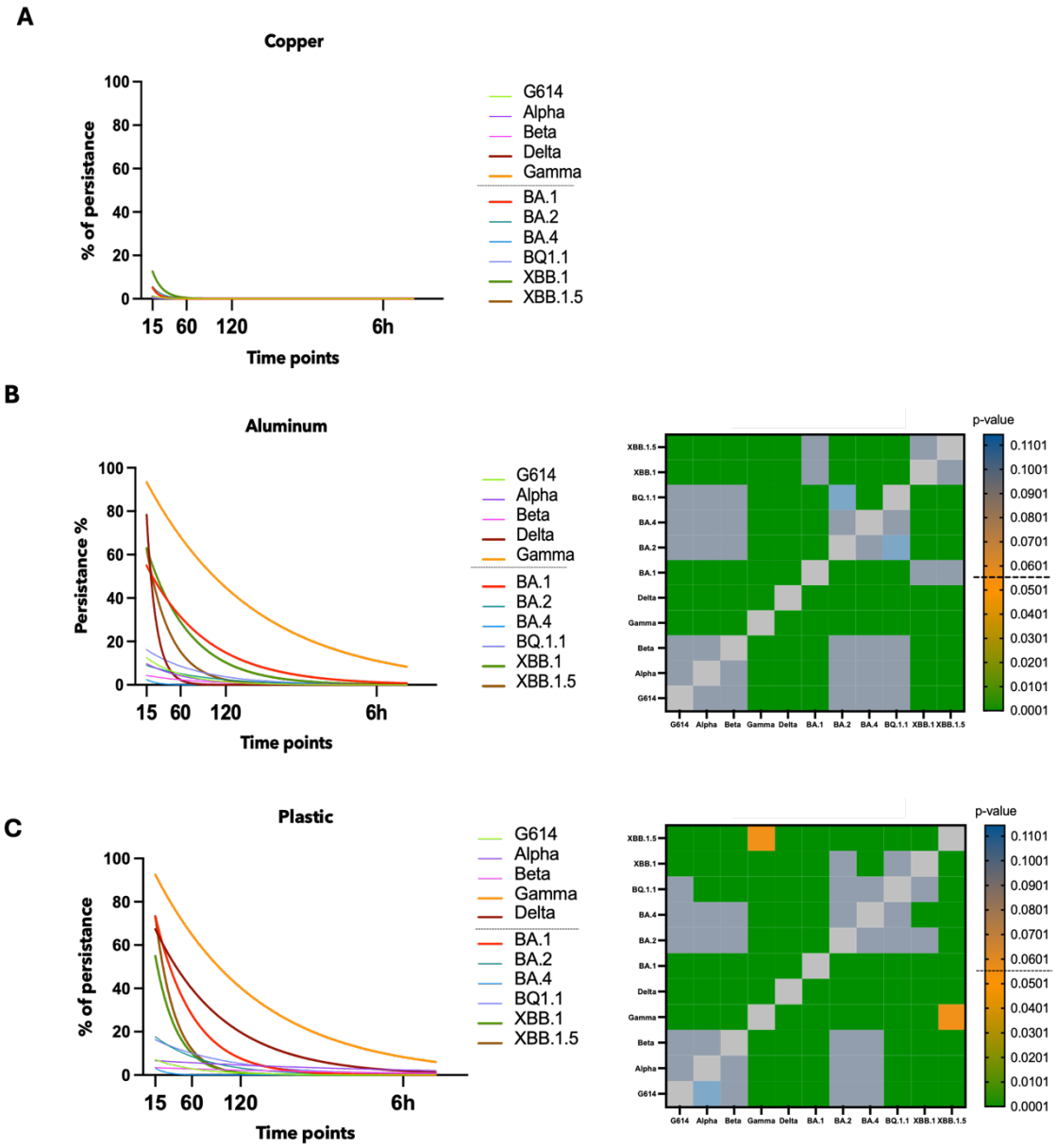


Figure 31 Persistence mechanism as an alternative transmission route of SARS-CoV-2 variants. Fomite transmission was studied on copper, polystyrene-plastic and aluminum surfaces at different time points. The persistence percentage was calculated based on the detected viral load ($TCID_{50}$/ml) at each time point, relative to the titer of viral stock ($TCID_{50}$/ml). The decrease in viral load was estimated by fitting a logistic growth curve. Data are shown as the mean ± SD of three replicates and three experimental sessions, **** $p < 0.0001$.

Implication of different mutations in the persistence mechanism

To investigate the impact of mutations on the persistence mechanisms of SARS-CoV-2 variants, we performed a variant calling analysis on the S, E and M proteins of the sequenced isolates, using the D614G strain as a reference control. The results, presented in Table 2 highlighted the presence of various mutations within the analyzed regions.

Table 2 Variant calling and mutation analysis across the Genome of 11 VOCs.

	S1			S2	E	M
	NTD	RBD				
G614D	–	–	–	–	–	–
Alpha	del 69-70; del 144	**N501Y**; A570D; P681H		T716I; S982A; D1118H		
Beta	**L18F**; D80A; **T95I**; D215G; del 241-242	**K417N**; E484K; **N501Y**		**A701V**		
Gamma	**L18F**; T20N; **P26S**; **D138Y**; R190S	K417T; E484K; **N501Y**;	**H655Y**	**T1027I**; V1176F	**P71L**	
Delta	T19R; E156G; del 157-158	**L452R**; T478K; P681R		D950N; D1084H		**I82T**; S94G
BA.1	**A67V**; del 69-70; **T95I**; **G142D**; del 143-145; del 211; L212I; ins EPE	G339D; S371L; S373P; S375F; **K417N**; N440K; **G446S**; **S477N**; T478K; E484A; Q493R; G496S; Q498R; **N501Y**; Y505H; T547K	**H655Y**; N679K; **P681H**;	**A701V**; N764K; **D796Y**; N856K; Q954H; N969K; L981F	**T9I**	D3G; Q19E; A63T;
BA.2	T19I; del 24-26; A27S; **G142D**; V213G	G339D; S371F; S373P; S375F; T376A; D405N; R408S; **K417N**; N440K; **S477N**; T478K; E484A; Q493R; **N501Y**; Y505H	**H655Y**; N679K; **P681H**;	N764K; **D796Y**; Q954H; N969K	**T9I**	Q19E; A63T;
BA.4	T19I; del 24-26; A27S; del 69-70; **G142D**; V213G	S371F; S373P; S375F; T376A; D405N; R408S; **K417N**; N440K; T478K; E484A; F486V; Q498R; **N501Y**; Y505H	**H655Y**; N679K; **P681H**;	N764K; **D796Y**; Q954H; N969K	**T9I**	D3N; Q19E; A63T;
BQ.1.1	T19I; del 24-26; A27S; del 69-70; **G142D**; V213G	G339D; R346T; S371F; S373P; S375F; T376A; D405N; R408S; **K417N;** N440K; K444T; **L452R**; E484A; F486V; Q498R; **N501Y**; Y505H	**H655Y**; N679K; **P681H**;	N764K; **D796Y**; Q954H; N969K	**T9I**	D3N; Q19E; A63T;
XBB.1	T19I; del 24-26; A27S; V83A; **G142D**; del 144; V213G; G252V	G339H; R346T; S371F; S373P; S375F; T376A; D405N; R408S; **K417N**; N440K; V445P; **G446S**; T478K; E484A; F486S; F490S; Q498R; **N501Y**; Y505H;	**H655Y**; N679K; **P681H**;	N764K; **D796Y**; Q954H; N969K; S982A	**T9I**	Q19E; A63T;
XBB.1.5	T19I; del 24-26; A27S; V83A; **G142D**; del 144; V213G; G252V	G339H; R346T; S371F; S373P; S375F; T376A; D405N; R408S; **K417N**; N440K; V445P; **G446S**; T478K; E484A; F486P; F490S; Q498R; **N501Y**; Y505H;	**H655Y**; N679K; **P681H**;	N764K; **D796Y**; Q954H; N969K; S982A	**T9I**	Q19E; A63T;

Firstly, the significance of each mutation was evaluated in terms of protein stabilization or destabilization, based on a structure-based analysis conducted in a previous study (Mohammad *et al.*, 2021). We then focused on the mutations located in the exposed domains of the S protein (S1 subunit, Receptor-Binding Domain, and S2 subunit) to assess their impact on the overall stability of the protein.

The obtained results highlighted a significant shift in the stability of the S protein during the SARS-CoV-2 evolution. Among the pre-Omicron variants, the G614D S protein exhibited the lowest stability (-0.027 kcal/mol, r = 0.817), whereas the Gamma variant displayed the highest stability (-0.933 kcal/mol, r = 0.885), consistent with the results of the persistence experiment where the viral load of the Gamma remained more stable over time compared to the other variants (Figure 32).

The stability of the Alpha, Beta, and Delta variants was similar, with a value of -0.46 ± 0.11 kcal/mol and r = 0.82; however, the Delta variant exhibited a longer persistence compared to Alpha and Beta.

In the Omicron family, it is noteworthy that the BA.1 variant, the most persistent among the BA lineage (-0.955 kcal/mol, r = 0.79), showed the most stable conformation.

In contrast, subsequent Omicron variants exhibited either positive stability values or values close to zero, suggesting a more unstable S conformation (0.85 ± 0.5

kcal/mol, r = 0.78). This observation further supports the persistence of BA.1, indicating a more stable structural conformation that may contribute to its persistence over time. Conversely, the XBB variants, which show greater persistence than other BA variants, display increased instability, likely due to the mutations present in their S proteins.

The obtained results suggest that the mutations influencing the stability of the S protein may also contribute to mechanisms of persistence.

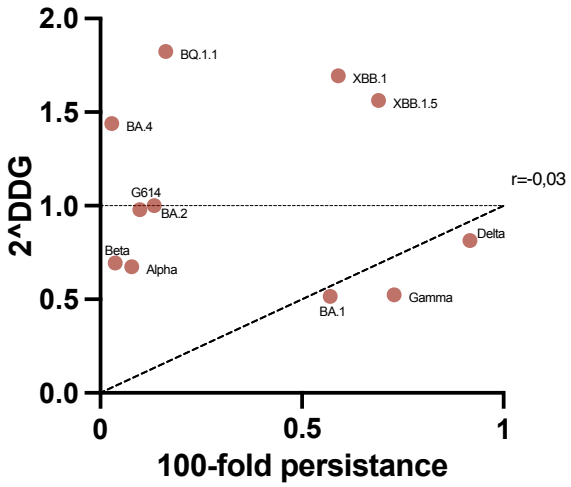


Figure 32 Correlation between persistence values and stability conformation. The graph shows persistence value (x-asses) expressed as 100-fold and the DDG obtained from MAESTRO analysis (y-asses) and expressed as 2^DDG considering the value from 0-1 spike conformation with higher stability while value from 1-2 spike conformation with lowest stability. The Spearman's correlation analysis (dotted line, r =- 0.03, p = 0.9) is shown.

Focusing on the variant calling Table 2, the persistence variants (Gamma, Delta, BA.1, XBB.1, and XBB.1.5) exhibited stabilized and destabilized mutations. Gamma carried 2 destabilizing and 5 stabilizing mutations, including *D138Y* and *T1027I* in the S protein domains, which were not conserved. Delta had 1 destabilizing mutation and a single stabilizing mutation, *I82T* in the E domain, which was not present in other variants.

BA.1 showed 2 destabilizing mutations and 7 stabilizing mutations (*A67V, S477N, H655Y, P681H, A701V* and *D796Y* on the S and *T9I* on the E) all of which were also found in non-persistent variants. Similarly, XBB.1 and XBB.1.5 each had 3 destabilizing mutations and 4 stabilizing mutations (*H655Y, P681H* and *D796Y* on the S and *T9I* on the E), which were already present in non-persistent variants.

To investigate the persistence mechanisms of the three persistent Omicron variants, we focused on mutations that were neither destabilizing nor conserved in

other non-persistent variants. The only mutation conserved across all persistent Omicron variants was G446S in the RBD domain. The role of this mutation in protein stability had not been characterized in previous studies, although the G446V mutation in the same region was identified as stabilizing (Mohammad *et al.*, 2021). Moreover, considering the virological significance of the G446S mutation, particularly its role in immune escape and neutralization sensitivity (Qu *et al.*, 2022), we further investigated its function using a lentiviral pseudovirus approach.

Starting with the XBB.1.5 mutant S protein, we reverted the mutation to the wild-type form using a PCR-based protocol with specific primers.

We next evaluated the titer of both wild-type and mutated pseudoviruses, which was used to determine the equivalent quantity of pseudoparticles for the persistence experiments. As shown in the corresponding graph (Figure 33A), no statistically significant difference was observed between the two pseudoviruses. We then performed the persistence experiment, and the obtained data confirmed that the pseudovirus carrying the wild-type S mutation exhibits significantly lower persistence compared to the G446S pseudovirus (Figure 33B).

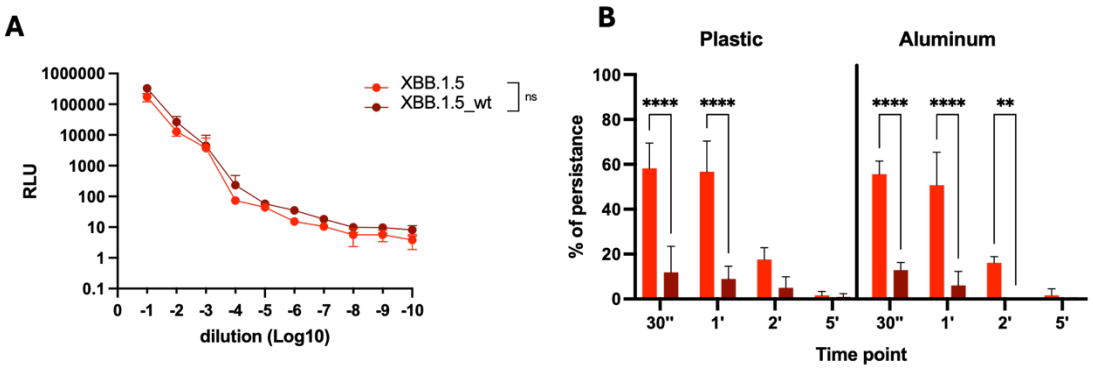


Figure 33 Characterization of the G446S mutation in the persistence mechanism. (A) Pseudovirus particles carrying XBB.1.5 or XBB.1.5_wt S proteins were used to infect Calu-3 cells, and luciferase activity (RLU) was measured after 72 hours of incubation at 37°C. Data from six replicates are presented as mean ± SD and are not statistically different (p = ns). **(B)** An equal amount of pseudoviruses was used in persistence experiments, where the recovered pseudoparticles was used to infect Calu-3 cells, and RLU signals were measured after 72 hours of incubation at 37°C. The data are presented as mean and ± SD and T-test analysis was performed on the six different replcates and the two experimental sessions, ** $p < 0.01$ **** $p < 0.0001$.

At the first time point (30 seconds), the mutated pseudovirus demonstrated a persistence rate of 56.6 ± 12% on polystyrene-plastic and 55.6 ± 5% on aluminum, compared to the wild-type pseudovirus, which showed a persistence rate of 10.7 ± 3.7% on polystyrene-plastic and 12.8 ± 3% on aluminum. After 1 minute, no significant difference in persistence percentage was observed between the two pseudoviruses or on either surface. At 2 minutes, the G446S pseudovirus exhibited

a persistence percentage of 16.7 ± 3.8%, while the wild-type pseudovirus dropped to less than 5% on polystyrene-plastic and was completely absent on aluminum. At both 5 and 30 minutes, no detectable pseudovirus load was observed on either surface. These findings suggest that the G446S mutation may enhance the stability of the spike protein, potentially playing a key role in the persistence mechanism of the pseudovirus.

To further validate the role of this mutation in the persistence mechanism, we performed molecular modeling to determine the specific location of the G446S mutation within the RBD. The obtained structure revealed that the mutation occurs in an exposed region of the RBD, which may facilitate interactions with surfaces, potentially enhancing persistence (Figure 34).

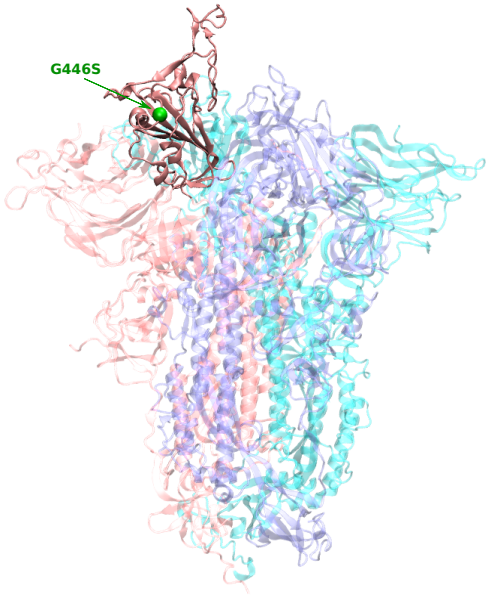


Figure 34 3D modeling of G446S mutation. Representative structure of the G614D spike protein in the 1-up state to map the location of the G446S mutation within the RBD domain and assess its potential role in increased persistence.

Evaluating the efficacy of "green" disinfectants

As a final aspect, we assessed the disinfectant efficacy of persistent variants using naturally derived disinfectants such as tea tree oil (TTO) and quercetin (QRE), as well as biomolecules such as daptomycin (DAP). In addition to the naturally derived compounds, we also included two positive disinfectant controls: 90% alcohol and UV-C light. Considering the significance of fomite transmission, we tested whether other respiratory viruses (as influenza A/Puerto Rico/H1N1 (PR) strain and A/Hong Kong/H3N2 (HK) strain) could persist for shorter or longer periods compared to SARS-CoV-2 variants. The persistence assay results highlighted that both influenza strains were able to persist longer than the SARS-CoV-2 variants over time (Figure 35).

In particular, the PR strain maintained 100% persistence up to 120 minutes, and at 6 hours, its persistence remained above 10% on all surfaces tested, except copper. In contrast, the HK strain exhibited approximately 50% persistence at 60 minutes; however, after 120 minutes and at the 6-hour time point, its persistence dropped to below 10% on all surfaces tested.

Based on these results, these two influenza strains were used as positive controls for evaluating disinfectant efficacy.

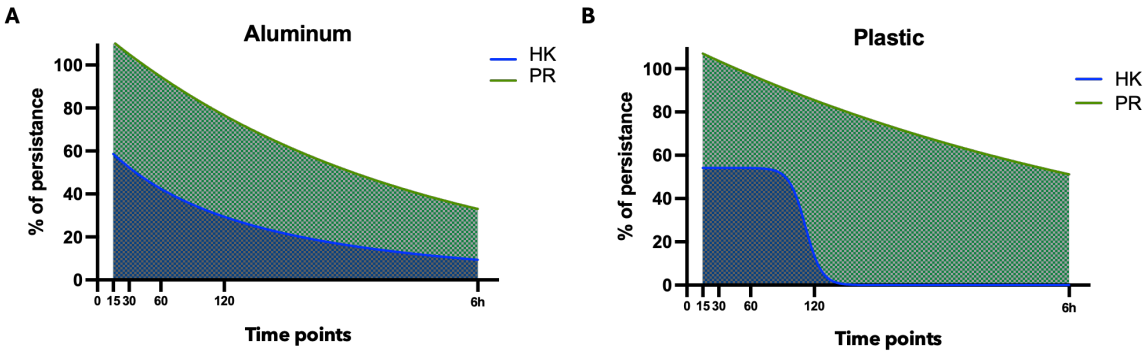


Figure 35 Persistence mechanisms of influenza strains on aluminum and polystyrene-plastic. Persistence assays was calculated by infecting MDCK cells with recovered viral particles, and viral load was expressed as the fold change in TCD_{50}/ml relative to the starting stock titer. The decrease in viral load was estimated by fitting a logistic growth curve. Data are shown as the mean ± SD for three experimental replicates and two experimental sessions.

For the assessment of disinfectant activity, we repeated the persistence experiment using the Gamma, Delta, BA.1, and XBB.1 variants, PR and HK strains evaluating the antiviral efficacy of the compounds within a 15-minute persistence

window, with time points at 1, 5, and 10 minutes, on both polystyrene-plastic and aluminum surfaces (Figure 36).

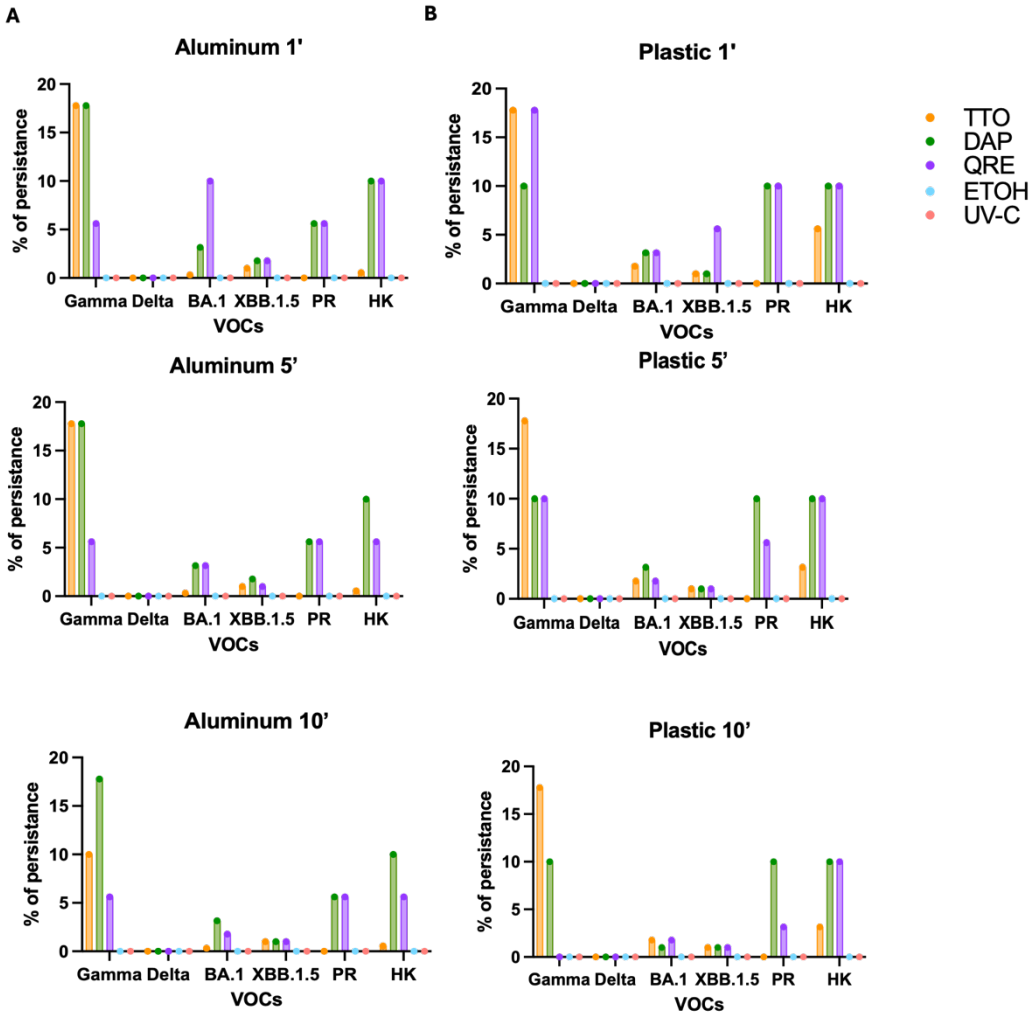


Figure 36 Assessment of disinfectant efficacy against persistent SARS-CoV-2 variants and influenza strains. The efficacy of disinfectants, including TTO, QRE, DAP, and two positive controls (alcohol and UV-C), was tested on polystyrene-plastic and aluminum surfaces at 1, 5, and 10-minute time points. All disinfectants reduced viral load by up to 80% after 1 minute. TTO, DAP, and QRE achieved >95% reduction in viral load for SARS-CoV-2 variants, with TTO being the most effective on aluminum (1.88 ± 0.36%) and polystyrene-plastic (8.4 ± 2.08%) at 1 minute. Alcohol and UV-C achive complete disinfection within 1 minute. Data are shown as the mean ± SD of three different replicates and two experimental sessions.

We can conclude that all disinfectants demonstrate a broad spectrum of antimicrobial activity, effectively achieving up to 80% reduction in viral load after just 1 minute of exposure.

Excluding the Gamma variant, all other SARS-CoV-2 variants and influenza strains were disinfected by more than 95% using TTO. Specifically, on aluminum, the

percentage of residual viral load detected at 1 to 10 minutes was 1.88 ± 0.36%, while on polystyrene-plastic, the residual % was 8.4 ± 2.08% at 1 minute, decreasing to 5.9 ± 1.19% at both 5 and 10 minutes.

The disinfection efficacy of DAP and QER was higher for SARS-CoV-2 variants compared to influenza strains. For SARS-CoV-2 VOCs, the residual percentage of viral load after 10 minutes of treatment with DAP was 1.38 ± 1.29% on aluminum and 0.66 ± 0.47% on polystyrene-plastic. In contrast, for influenza strains, the residual viral load was 7.81 ± 2.19% on aluminum and 10.00% on polystyrene-plastic.

After treatment with QER, the residual viral load for SARS-CoV-2 VOCs was 0.92 ± 0.72% on both aluminum and polystyrene-plastic surfaces. In comparison, influenza strains showed a % of residual viral load of 5.62% on aluminum and 6.58 ± 3.42% on polystyrene-plastic.

Gamma, unlike the other variants, was more effectively disinfected by QER, with only 17% of the viral load detected on aluminum and complete disinfection on polystyrene-plastic after 10 minutes. In contrast, TTO and DAP exhibited similar residual viral loads after 10 minutes, with 10% detected on metal and 17% on polystyrene-plastic.

Notably, both positive controls (alcohol and UV) were able to achieve complete disinfection (100%) of all viruses after just 1 minute of treatment.

DISCUSSION

The continuous evolution of SARS-CoV-2 has resulted in the emergence of new variants, each characterized by unique features that impact their replication dynamics, immune evasion mechanisms, and transmission. In this study, we comprehensively dissected and studied these different virological aspects of 11 SARS-CoV-2 variants, including both pre-Omicron and Omicron sublineages. Our results, in conjunction with existing literature, highlighted significant differences in the biological behavior of these variants, providing valuable insights into their transmissibility, immune escape, and persistence, as well as their implications for public health strategies.

Our first aim was to evaluate the replication kinetics of SARS-CoV-2 variants using an *in vitro* model that closely mimics the primary site of viral infection: human-derived lung adenocarcinoma cells, specifically Calu-3 cells. These cells express the ACE2 receptor and the TMPRSS2 protease, both essential for SARS-CoV-2 infection, making them a well-established model for studying viral entry and replication. The obtained results highlighted how pre-Omicron variants, particularly Beta, Gamma, and Delta, exhibited faster replication kinetics compared to earlier strains, highlighting how occurred mutations may enhance viral fitness and may contribute to more rapid replication kinetic (Zhou *et al.*, 2021) (Mlcochova *et al.*, 2021).

Conversely, the Omicron variants, including BA.1, XBB.1, and XBB.1.5, exhibited slow replication kinetics; this could be associated with the higher number of mutations in the spike protein, particularly in the RBD, they may not confer an advantage in terms of replication rate as observed with the pre-Omicron variants. Interestingly, several studies reported that while Omicron variants exhibit higher transmissibility, their replication in lung tissue appears to be less efficient compared to earlier variants, which aligns with our findings (Park *et al.*, 2023) (Qianqian Li *et al.*, 2020). This may reflect a shift in viral evolution favoring mucosal transmission over lung pathology, a factor that likely contributes to the distinct disease profiles observed with Omicron infections, including lower rates of hospitalization and severe disease.

Taken together, these results support the hypothesis that specific mutations, particularly in the S protein, may enhance viral replication by optimizing the replication machinery or facilitating more efficient viral entry.

To assess the impact of these mutations on the entry process, we set a lentiviral pseudovirus system to express variant-specific S proteins. The results were

consistent with the replication kinetics: variants exhibiting faster replication also demonstrated more efficient entry, thereby establishing a clear correlation between these two processes. These findings underscore the critical role of S protein mutations in modulating both entry efficiency and replication dynamics, which could have significant implications for the transmissibility and pathogenicity of SARS-CoV-2 variants. In particular, the Beta and Delta had the fastest entry compared to G614D, and to Omicron. To better dissect the entry dynamics of SARS-CoV-2 VOCs we treated the Cau-3 cells with the two inhibitors that selectively interfere with the two viral entry processes: camostat mesylate and BFLA-1. Camostat mesylate acts by inhibiting TMPRSS2, thereby preventing the cleavage of the S protein and blocking the direct fusion of the viral envelope with the host cell membrane. To target the late entry route, we employed BFLA-1, an inhibitor of H+-pump ATPase. The acidic environment within the endosomal compartment is essential for the activation of cathepsins (L and B), which cleaves the S protein and exposes the fusion peptide. By inhibiting phagosome-lysosome fusion, this approach effectively reduces the entry of SARS-CoV-2. The results indicated that selectively inhibiting either pathway provided varying levels of protection against infection by SARS-CoV-2 variants, suggesting that these variants do not utilize both entry mechanisms to the same extent. Specifically, inhibition of TMPRSS2 activity exhibited a more pronounced inhibitory effect compared to targeting endosomal acidification across all variants, confirming the essential role of TMPRSS2 in facilitating viral entry via direct fusion with host cell membranes (Hoffmann *et al.*, 2020). Different studies suggest that the duration of the viral entry process is dependent on the pathway utilized (Koch *et al.*, 2021); the endocytic pathway, which involves multiple mechanisms, is slower compared to the direct fusion of the viral envelope with the plasma membrane (Koch *et al.*, 2021). Based on our findings, this may account for the discovered differences in the replication kinetics of the variants under investigation. Both the Delta and Beta variants, which exhibited faster replication kinetics and more rapid entry, were inhibited by over 90% with camostat. Notably, the Delta variant showed less than 50% inhibition when treated with BFLA-1, highlighting its preference for direct fusion and supporting its increased transmissibility.

In contrast, Omicron variants were inhibited by more than 80% with BFLA-1, suggesting that their slower replication kinetics and reduced entry efficiency are likely due to reliance on the late entry pathway. This may reflect conformational changes in the spike protein that influence the efficiency of membrane fusion and receptor binding, as previously proposed (Harbison *et al.*, 2022) (Criscuolo *et al.*, 2024). Unexpectedly, for the G614D variant, BFLA-1 inhibited the entry mechanism by only

50%, despite this variant exhibiting relatively slow entry kinetics. This discrepancy underscores the importance of considering the specific entry pathway and highlights the critical role of S protein cleavage rates, which directly impact viral entry, transmissibility, and infectivity (Harbison *et al.*, 2022) . Several studies suggest that pre-activation of the S protein via furin cleavage may facilitate subsequent processing by TMPRSS2, thereby promoting direct fusion between the viral envelope and the host cell membrane, instead of relying solely on the endocytic pathway (Le Bert *et al.*, 2020) (Zahradník *et al.*, 2021). In contrast, other studies propose that variants with lower furin cleavage efficiency may rely more heavily on endocytosis and subsequent cathepsin-mediated activation (Yao *et al.*, 2024). The G614D variant exhibited reduced cleavage efficiency compared to other variants, which may explain its altered interaction with TMPRSS2 and its relatively lower susceptibility to BFLA-1 inhibition (Korber *et al.*, 2020) (Johnson *et al.*, 2021). These findings suggest that variations in the cleavage efficiency of the spike protein could contribute to differences in the viral entry mechanisms and, consequently, the replication kinetics and infectivity of different SARS-CoV-2 variants.

Considering the key factors contributing to the increased transmissibility and infectivity of SARS-CoV-2 variants, such as entry mechanisms and replication kinetics, we also observed one additional critical aspect: the immune response. The ability of the virus to escape antibody recognition significantly contributed to its rapid circulation and evolution, giving rise to multiple variants (Korber *et al.*, 2020) (Wibmer *et al.*, 2021). Studies showed that immune escape, particularly from neutralizing antibodies, is a critical driver of viral evolution (Yao *et al.*, 2024).

In our experimental setting, we assessed virological escape by evaluating the host's first line of defense: the interferon response at different time points after infecting the Calu-3 cells. Interferons play a pivotal role in the early detection of viral infections by activating pattern recognition receptors that detect viral RNA and subsequently initiate antiviral immune responses (Schneider, Chevillotte and Rice, 2014). This early response triggers a cascade of antiviral mechanisms, including the activation of innate immune cells and the establishment of an environment that restricts viral replication (Diamond and Kanneganti, 2022). The interferon response also primes the host for a more robust adaptive immune response, including the recruitment of T cells and the production of specific antibodies (Sa Ribero *et al.*, 2020). We evaluated the Type I interferon (IFN-I) defense mechanism. Is well understood that upon detection of viral RNA by pattern recognition receptors (PRRs) such as RIG-I, signaling pathways are triggered, leading to the activation of transcription factors promoting the expression of IFN-β, which binds to the IFN-α/β

receptor (IFNAR) on cells. The activation of the JAK-STAT signaling pathway drives the expression of interferon-stimulated genes (ISGs) as MX1, MIX2, IFIT1, and ISG15 inhibiting viral replication and enhancing immune responses (Loo and Gale, 2011) (Minkoff and tenOever, 2023).

Our results highlighted that SARS-CoV-2 variants elicit differential interferon responses in Calu-3 cells. The G614D variant triggered a rapid immune activation, marked by a strong upregulation of RIG-I and other ISGs within the first time points, coherently with the findings of previous studies (Sun *et al.*, 2022). This rapid detection of the G614D variant suggests a robust immune sensing mechanism, potentially contributing to its slower replication kinetics.

In contrast, variants like Beta and XBB.1 exhibited a delayed or diminished IFN-β response, a feature commonly associated with immune evasion mechanisms. Studies have shown that some variants, particularly Beta, demonstrate a greater ability to modulate the host immune response, allowing for more efficient viral replication and immune escape (Mlcochova *et al.*, 2021) (Harvey *et al.*, 2021). Our observation of the downregulated of IFN- at 3 hpi by Beta correlated with the knowledge that immune evasion is a key feature of its pathogenesis. Omicron variants, including BA.1 and XBB.1.5, also displayed an active IFN response at later time points, which may enhance their ability to persist in the host and evade immune surveillance(Shrestha *et al.*, 2022) (Schreiber, 2020) (Hoffmann *et al.*, 2021).

Interestingly, the sustained IFN-β response in variants like G614D and Delta, particularly at 6 hpi, supports the knowledge that these variants are less efficient in immune evasion. This observation may explain why G614D, and Delta exhibit more controlled replication compared to Beta, as a prolonged IFN response can help limit viral replication (Rashid *et al.*, 2022).

Understanding how SARS-CoV-2 variants evade the interferon response is crucial for developing strategies to limit the viral evolution and persistence in the population. The differential activation of the interferon response across variants could help explain the observed differences in their replication kinetics, immune evasion capabilities, and overall transmissibility (Minkoff and tenOever, 2023).

To better characterize the transmissibility and infectivity of SARS-CoV-2 variants, we studied another less-characterized aspect: the stability of the virus on surfaces. This factor plays a crucial role in transmission, particularly in indoor settings such as healthcare environments, where fomites may contribute to indirect infection (*World Health Statistics 2020*, no date). According to the World Health Organization (WHO), while the primary mode of transmission was via respiratory droplets and aerosols, contact with contaminated surfaces remained a potential risk for the spread of the

virus, especially in high-touch areas and hospital settings where vulnerable individuals may be at greater risk (*World health statistics 2021*, no date). Understanding the environmental stability of SARS-CoV-2 variants was essential for improving infection control measures and public health strategies aimed at reducing transmission.

Furthermore, studies demonstrated that the persistence of SARS-CoV-2 on surfaces is influenced by several factors, including surface type, temperature, and humidity (Tang *et al.*, 2020). Considering this aspect, we assessed the persistence of SARS-CoV-2 variants in a controlled experimental setting with consistent temperature and humidity, focusing on three common materials: polystyrene-plastic, aluminum, and copper. These materials exhibit distinct chemical and physical properties that can influence viral stability. While all three are non-porous, aluminum and copper are non-ferrous metals (Govind *et al.*, 2021) (Rai *et al.*, 2012), whereas polystyrene-plastic is a highly durable polymer that can provide a more stable surface for virus retention (Aboubakr, Sharafeldin and Goyal, 2020). The varying surface characteristics of these materials—such as conductivity, surface charge, and resistance to degradation—could significantly impact the persistence of the virus, highlighting the importance of material composition in assessing transmission risk, particularly in indoor or healthcare environments (van Doremalen *et al.*, 2020) . The obtained results corroborated the antimicrobial and antiviral properties of copper, which rapidly inactivated the virus, with no detectable viral load after 15 minutes (Kampf *et al.*, 2020). In contrast, polystyrene-plastic and aluminum surfaces supported viral persistence, with variants like Gamma and Delta exhibiting higher stability over time. This was in line with the previous research which showed that SARS-CoV-2 could persist on non-porous surfaces like polystyrene-plastic and stainless steel for up to 72 hours (van Doremalen *et al.*, 2020). The results obtained led to the following conclusions: despite using the same viral load in the persistence experiments, the variants exhibited similar persistence on both materials, suggesting that material-dependent factors do not influence viral stability. The variants that showed the greatest persistence over time were Gamma, Delta, BA.1, XBB.1, and XBB.1. These findings are consistent with studies indicating that environmental persistence is largely determined by viral characteristics rather than the type of surface (Aboubakr, Sharafeldin and Goyal, 2020). From these data, we hypothesized that the increased or decreased persistence of the different variants might be linked to specific mutations that could lead to greater or lesser stabilization of the entire spike protein.

To explore this further, we performed a stability prediction analysis of the spike protein using the ΔΔG which is a computational metric that quantifies the change in stability of a protein due to a mutation. It represents the difference in Gibbs free energy (G) between the mutated and wild-type protein (Mohammad *et al.*, 2021). This analysis confirmed that pre-Omicron variants, such as Gamma and Delta, exhibited DDG values much closer to zero, indicating greater stability of the S protein. In contrast, within the Omicron lineage, only BA.1 showed stability values comparable to those of Gamma and Delta. The other two XBB. variants, which demonstrated increased persistence on surfaces, showed a high positive value of DDG indicating instability of the spike (Sinha, Sangeet and Roy, 2023).

To further investigate and clarify the persistence mechanism of the XBB variants, we expanded our analysis beyond just the ΔΔG energy changes to a variant calling analysis; we used D614G as a reference to highlight the aminoacidic changes of the clinical isolates. Multiple sequence alignment allowed to identification of shared mutations across the persistent Omicron sublineages, focusing on mutations that were absent in non-persistent variants. This analysis involved both the S protein and other structural proteins, such as the E and M proteins, which may contribute to viral interactions with surfaces. Interestingly, we identified a conserved mutation, G446S, present in the persistent Omicron variants. This mutation had not been previously associated with altered stability, but its conservation across the variants suggested a potential role in viral persistence. Notably, this mutation, located in an exposed region of the RBD, may facilitate interactions with surfaces, contributing to the virus's persistence in the environment. This finding is consistent with prior structural studies that suggested how mutations in the RBD can stabilize the spike protein, potentially enhancing both immune escape and environmental persistence (Mohammad *et al.*, 2021) (Minkoff and tenOever, 2023). To further investigate the role of the G446S mutation in the persistence mechanism, we reverted the mutation to the wild-type form and studied the persistence dynamics using a variant-specific S pseudovirus model. The data obtained from this experimental setup revealed that the pseudovirus containing the wild-type mutation persisted much less on surfaces compared to the variant with the G446S mutation. This finding suggests that the G446S mutation could be directly involved in the persistence mechanism observed in Omicron variants, highlighting its potential role in enhancing the virus's ability to remain infective on surfaces for longer periods.

Considering the ability of different SARS-CoV-2 variants to persist on surfaces, we investigated the disinfectant activity of natural compounds like TTO and QRE and

biomolecule DAPTO. Briefly, the antiviral activity of TTO was primarily attributed to its ability to inhibit the S protein from binding to the ACE2 receptor, preventing viral entry into host cells. Additionally, TTO destabilizes the viral membrane, reducing the viral replication mechanisms and persisting on surfaces. Studies combined experimental and computational approaches to show that TTO interferes with the viral structure, blocking the interaction between the spike protein and host cell receptors (Bailey *et al.*, 2021) (Romeo *et al.*, 2022). Moreover, QRE is a plant-derived flavonoid that exhibits multiple mechanisms of action that could limit viral infection and replication. Molecular docking studies demonstrated that quercetin binds with high affinity to several key SARS-CoV-2 proteins, including the S protein, and interacts with host cell proteins like ACE2 and TMPRSS2 reducing viral infection efficiency and preventing viral spread (Roy *et al.*, 2024)

Then DAP, a cyclic lipopeptide antibiotic, was primarily known for its potent antimicrobial activity, particularly against Gram-positive bacteria. However, recent studies explored its antiviral properties, particularly its ability to disrupt viral envelope-forming complexes that cause membrane depolarization, leading to cellular dysfunction which could interfere with viral entry and replication (Shekunov *et al.*, 2023).

Considering the antiviral and antimicrobial properties of TTO, QRE, and DAP, we evaluated their effectiveness in disinfecting respiratory viruses, specifically persistent variants of SARS-CoV-2 and two distinct strains of influenza, both of which demonstrated prolonged persistence on surfaces. Our results highlighted that TTO, QRE, and DAP demonstrated broad-spectrum antiviral activity, achieving up to 90% reduction in viral load after just 10 minutes of exposure. Moreover, to validate the effectiveness of these compounds, we compared them to commonly used disinfection techniques, such as UV-C light and alcohol-based disinfectants, which are well-established for their ability to rapidly inactivate viral pathogens (Minkoff and tenOever, 2023) (Scepankova *et al.*, 2021). Under controlled experimental conditions, both UV-C light and alcohol-based disinfectants provided complete viral inactivation within 1 minute, validating their virucidal activity. These findings underscore the superior efficacy of UV-C radiation and alcohol-based disinfectants in comparison to natural disinfectants for microbial deactivation. However, it is important to consider the potential negative effects of these disinfection methods on both human health and environmental integrity. Prolonged or unprotected exposure to UV-C radiation may pose significant risks to human skin and ocular tissues as well as the overuse of alcohol-based disinfectants. Furthermore, improper disposal or excessive application of these agents may result in environmental contamination,

affecting ecosystems and non-target organisms. These considerations highlight the necessity of balancing disinfection efficacy with the evaluation of associated health and ecological risks. For these reasons, natural compounds such as TTO, QRE, and DAP could represent a non-toxic and safe alternative for disinfection and lastly, and alternative to conventional disinfectants.

Despite the valuable insights gained from our study, certain methodological limitations must be acknowledged. Firstly, while lentiviral pseudovirus systems are commonly employed to study viral entry, the complexities of live virus infection are not fully replicated by this system. Specifically, various structural and non-structural viral components that may influence entry dynamics, replication efficiency, and host-virus interactions are absent in the pseudovirus system. Furthermore, although the inhibitor-based approach provided insight into entry pathways, the relative contribution of TMPRSS2- and endocytosis-mediated entry may vary across different cellular contexts, potentially limiting the broader applicability of the findings. Additionally, the *in vitro* cellular models used may not accurately replicate the physiological environment of the human respiratory tract, thus hindering the direct translation of the findings to *in vivo* conditions. Lastly, the use of pharmacological inhibitors to delineate entry pathways may introduce off-target effects, potentially altering cellular mechanisms beyond viral entry, which could influence the interpretation of the results.

CONCLUSION

This study provides a comprehensive evaluation of the virological properties of SARS-CoV-2 variants, revealing significant differences in their replication kinetics, entry mechanisms, immune evasion strategies, and persistence on surfaces. The findings emphasize the complexity of SARS-CoV-2 evolution and highlight the need for continued surveillance of new variants to inform public health strategies. The differential immune responses observed across variants, along with their ability to persist on surfaces, underscore the importance of timely disinfection and the need for targeted interventions. Natural disinfectants like TTO and QRE, in addition to conventional measures such as alcohol and UV-C light, demonstrate promise in controlling SARS-CoV-2 transmission, offering complementary options for infection control. As SARS-CoV-2 continues to evolve, understanding the interplay between viral mutations, host immune responses, and environmental persistence will be critical in shaping effective strategies for controlling the pandemic.

MATERIALS AND METHODS

Cell lines

Vero E6 (Vero C1008, clone E6; ATCC CRL-1586), HEK-293T ^{CD81KO} (Human epithelial kidney cancer cell line, kindly provided by the Grove of The Royal Free Hospital, University College London 307)[307], MDCK (Madin-Darby canine kidney, ATCC CCL-34), and 293T-ACE2/TMPRSS2 (Homo sapiens embryonic kidney epithelial cells expressing human angiotensin-converting enzyme 2 and transmembrane protease serine 2, BEI Resources, NIAID, NIH: NR-55293) were cultured in Dulbecco's modified Eagle medium (DMEM) supplemented with non-essential amino acids (NEAA), penicillin/streptomycin (P/S, 100 U/mL), HEPES buffer (10 mM), and 10% (v/v) heat-inactivated fetal bovine serum (FBS). For the Vero E6 cell line, 1 mg/mL of Geneticin (G418) was added to the medium to maintain stable expression (Vero E6/TMPRSS2, NIBSC 100978). Calu-3 (human lung adenocarcinoma cell line, ATCC HTB-55) was cultured in Minimum Essential Medium (MEM) supplemented with 1× NEAA, P/S (100 U/mL), 1 mM sodium pyruvate, and 10% (v/v) heat-inactivated FBS. All cell lines were incubated at 37°C with 5% CO_2 in a humidified atmosphere. Regular mycoplasma testing was performed for all cell lines using the Lonza Mycoplasma Detection Kit (LT07-218).

Virus isolation

As recently published in our paper (Criscuolo *et al.*, 2024) we perform virus isolation starting from 1 mL of the nasopharyngeal swab transport medium (COPAN's UTM® universal viral transport medium) and mixing it in a 1:1 ratio with DMEM supplemented with penicillin/streptomycin (P/S) and Amphotericin B. This mixture was then added to a monolayer of Vero E6 cells at 80% confluence, cultured in a 25 cm^2 tissue culture flask. The viral adsorption step was carried out for 3 hours at 37°C, after which 2 mL of DMEM supplemented with 2% FBS and Amphotericin B was added to the monolayer. At one day post-infection (dpi), the monolayer was washed with PBS, and 3 mL of DMEM supplemented with 2% FBS and Amphotericin B was added. The cytopathic effect (CPE) was monitored using an inverted phase-contrast microscope (Olympus CKX41). The supernatant was collected once the monolayer was fully disrupted (3 dpi), aliquoted, and stored at -80°C (P1).

For virus-specific PCR, viral stocks were heat-inactivated at 56°C for 30 minutes. The viral RNA was extracted using the QIAamp Viral RNA Mini Kit (Qiagen, 52906) according to the manufacturer's instructions. cDNA synthesis and PCR amplification were performed using the Superscript® III One-Step RT-PCR System (Invitrogen, 12574026) with Platinum Taq DNA polymerase. The reaction was carried out in a single tube using RNA-dependent RNA polymerase (RdRp) primers for SARS-CoV-2 (Table 3). The thermal cycling conditions were as follows: 50°C for 20 minutes, followed by 50 cycles of 95°C for 2 minutes, 55°C for 20 seconds, 68°C for 30 seconds, and a final extension at 68°C for 5 minutes.

Virus sequencing

We used the same viral isolates reported in our recent studies (Criscuolo *et al.*, 2024).

The viral RNA was extracted from 200 µL of heat inactivated viral stock using the ELITe InGeniusTM workstation (ELITechGroup). Targeted RNA enrichment for Illumina sequencing was then performed using the BS-Paragon CleanPlex SARS-CoV-2 Flex Panel (Paragon Genomics) following the manufacturer's instructions. The purified genetic material was quantified using the Qubit double-stranded DNA (dsDNA) HS Assay Kit on a Qubit 2.0 Fluorometer (Thermo Fisher) and samples were diluted and pooled to a final concentration of 2 nM. Then, 50 pM of the library pool was sequenced on the iSeq Illumina platform using the iSeq 100 i1 Reagent v2 (300-cycle). The obtained data were then analyzed using the coronavirus antiviral and resistance database of Stanford University (*Stanford Coronavirus Antiviral & Resistance Database (CoVDB) --- covdb.stanford.edu*, no date) through which the consensus sequence of viral stock was obtained. Then the FASTA sequences were also verified through Nextclade software (*Nextclade --- clades.nextstrain.org*, no date) and deposited on GSAID with the following accession ID: D614D (GSAID accession ID: EPI_ISL_413489), Alpha (GSAID accession ID: EPI_ISL_1924880), Beta (GSAID accession ID: EPI_ISL_1599180), Gamma (GSAID accession ID: EPI_ISL_1925323), Delta (GSAID accession ID: EPI_ISL_4198505), Omicron BA.1 (GSAID accession ID: EPI_ISL_12188061), Omicron BA.2 (GSAID accession ID: EPI_ISL_13285445), Omicron BA.4 (GSAID accession ID: EPI_ISL_13878328) Omicron BA.5 (GSAID accession ID: EPI_ISL_16355612), Omicron BQ.1.1 (GSAID accession ID: EPI_ISL_16355615), Omicron XBB.1 (GSAID accession ID:

EPI_ISL_16526278), Omicron XBB.1.5 (GSAID accession ID: EPI_ISL_18537906), Omicron EG.5 (GSAID accession ID: EPI_ISL_18540450).

Virus titration

SARS-CoV-2 and influenza virus stocks were titrated using Endpoint Dilutions Assay (EDA, $TCID_{50}$/mL). Either Vero E6, Vero/TMPRSS2, or MDCK cells were seeded into 96-well plates and infected at approximately 95% confluence with serial 10-fold dilutions of the virus stock. After 1 h of adsorption at 37 °C, the cell-free virus was removed, cells were washed with PBS, and complete medium supplemented with 2% FBS was added for Vero cells and DMEM no FBS supplemented with TPCK-trypsin (1:200) for MDCK cells. After 72 h, cells were observed in inverted phase-contrast microscopy (Olympus CKX41) to evaluate the presence of a cytopathic effect (CPE). $TCID_{50}$/mL of viral stocks were then determined with the Reed–Muench formula.

Kinetic profiles

Calu-3 ($3 \cdot 10^5$ $cells/_{mL}$) were seeded in 96-well plates and cultured for 3 days at 37°C and 5% CO_2 in a humidified atmosphere. Then, the cells were infected with 0.001 multiplicity of infection (MOI) of variants isolated in triplicate. After 1 hour of adsorption, the cells were washed three times with PBS to remove any unbound virus and cell supernatants were collected at 6 time points: 1, 3, 6, 24, 48 and 72 hpi. Viral genome from the collected supernatants was extracted with QIAamp Viral RNA Mini Kit (52904, QIAGEN). The Superscript® III First-Strand system for RT-PCR (18080-051, Invitrogen) was used to synthesized cDNA from purified RNA following manufacturer's instructions. Then, Real-Time PCR was performed using SYBR Green PCR Master Mix (4309155, Applied Biosystems), N2 primers reported in Table 3. The thermal cycling conditions are the following: 95°C 2 min, 45 cycle of 95°C 20 sec, 55°C 20 sec, 72°C 30 sec and then 72°C 10 min.

Immune-response

Calu-3 cells ($3 \cdot 10^5$ $cells/_{mL}$) were seeded into 96-well plates and cultured for 24 hours at 37°C with 5% CO_2 in a humidified atmosphere. Subsequently, the cells were infected in triplicate with 0.1 MOI of the G614D, Delta, Beta, BA.1, XBB.1, and XBB.1.5 isolated variants. After 1 hour of adsorption, the cells were washed three

times with PBS to remove any cell-free virus. Supernatants were then collected at six time points: 1-, 3-, 6-, and 24 hpi. For RNA extraction, Calu-3 cells were lysed using RLT buffer, and total cellular RNA was extracted using the RNeasy kit (74104, Invitrogen) according to the manufacturer's instructions. Reverse transcription was performed using the First-Strand cDNA Synthesis System (18080-051, Invitrogen) with oligo(dT) primers to generate cDNA from the coding RNA. Quantitative RT-PCR analysis of ISG transcripts and human GAPDH was conducted using Power SYBR Green PCR Master Mix (4309155, Applied Biosystems, UK) with the following cycling conditions: initial denaturation at 95°C for 10 minutes, followed by 40 cycles of 95°C for 15 seconds and 60°C for 1 minute. The sequences of the primers used are listed in the table below.

Table 3 List of primers used for RNA identification, immune response and pseudovirus G446S mutation

	FW	REV
RdRp	CAAGTGGGGTAAGGCTAGACTTT	CTTAGGATAATCCCAACCCAT
IFNB	TCCAAATTGCTCTCCTGTTG	GCAGTATTCAAGCCTCCCAT
IFIT1	TCTCAGAGGAGCCTGGCTAA	TGACATCTCAATTGCTCCAGA
MX1	CCAGCTGCTGCATCCCACCC	AGGGGCGCACCTTCTCCTCA
MX2	CAGAGGCAGCGGAATCGTAA	TGAAGCTCTAGCTCGGTGTTC
ISG15	CGCAGATCACCCAGAAGATCG	TTCGTCGCATTTGTCCACCA
RIG-I	ATCCCAGTGTATGAACAGCAG	GCCTGTAACTCTATACCCATGTC
GAPDH	TGGGCTACACTGAGCACCAG	GGGTGTCGCTGTTGAAGTCA
G446S	CAGCAAGCCGGGCGGCAACTACAAC	TCCAGCTTGTTGCTGTTC
N2	TTACAAACATTGGCCGCAAA	GCGCGACATTCCGAAGAA

Pseudovirus generation and titration

Lentiviral pseudoviruses were generated using the following spike proteins: G614D (NR-53765, BEI Resource), Beta strain (170449, Addgene), Delta strain (172320, Addgene), BA.1 (194602, Addgene), XBB.1.5 (196585, Addgene) and XBB.1, obtained by reverting the single mutation difference in XBB.1.5 using specific primers (Crawford *et al.*, 2020).

Briefly, HEK-293T ^{CD81KO}, an improved *in vitro* model for pseudovirus production due to the absence of the CD81, were seeded in a 75 cm^2 tissue culture flask to be at 60-70% confluent the next day. 24 hours after cells were co-transfected with 5

plasmids from BEI Resource: 1.25 µg pHAGE with CMV-driven Luciferase-IRES-ZsGreen (NR-52516)

0.275 µg pHDM with HIV Gag-Pol (NR-52517), 0.275 pHDM with HIV Tat (NR-52518), 0.275 pRC with CMV-driven HIV Rev (NR-52519) and 0.425 µg pHDM- the previously S protein with C-term 21 bp. PEI (919012, Sigma-Aldrich) was mixed with DNA in a 1:3 ratio and incubated at room temperature for 30 minutes to allow complex formation prior to transfection. After 6 hours, the transfection medium was replaced with DMEM without FBS. At 48 hours post-transfection, the medium was collected and replaced, and the process was repeated at 72 hours post-transfection. Pseudovirus-containing media were then pooled and subjected to ultracentrifugation through a 20% sucrose cushion at 20,000 xg for 1 hour at 4°C using a Beckman 328 SW28 rotor. The pseudoviruses were aliquoted and stored at -80°C for further use.

Pseudovirus titer was determined by a luciferase assay. Vero/TMPRSS2 cells ($3 \cdot 10^5$ $cells/_{mL}$) were seeded in a 96-well plate and incubated at 37°C for 24 hours. Serial 1:10 dilutions of pseudovirus were added to the cells, and the plate was spinoculated at 800 xg for 1 hour at 37°C for adsorption. Afterward, the pseudovirus-containing media were removed and replaced with fresh medium supplemented with 2% FBS.

72 hpi, cell supernatants were removed, and cells were lysed with 100 µL of Glo Lysis Buffer (E2661, Promega) for 15 minutes at room temperature with gentle agitation. Cell lysates were transferred to a luminometer plate, and 100 µL of Bright-Glo Assay Reagent (E2620, Promega) was added before measuring luminescence using a Victor3 luminometer (Perkin Elmer). For further assays, the dilution corresponding to Relative Luminescence Units (RLUs) greater than 1000-fold above background was selected.

Pseudovirus mutation

To investigate the role of the G446D mutation in the persistence mechanism, we used the plasmid encoding the spike protein of XBB.1.5 (196585, Addgene). Specific primers were designed to amplify the entire spike gene and revert the D446G mutation to the wild-type form sequences (Table 3). High-fidelity AccuPrime polymerase (12339016, Invitrogen) was used for amplification with the following thermal cycling conditions: 94°C 2 min, 35 cycle of 94°C 30 sec, 55°C 20 sec, 68°C 12 min and then 68°C 5 min. The amplification products were verified by agarose gel electrophoresis (1%), and the band corresponding to the full-length plasmid was

excised. The plasmid was then digested with DpnI (R0176S, New England Biolabs) for 15 minutes at 37°C to remove methylated parental DNA. Electrocompetent *E. coli* (XL1-Blue; 200228, Agilent) cells were transformed and after 1 hour of recovery in SOC medium at 37°C with shaking, cells were plated on agar plates and incubated overnight at 37°C. Single colonies were picked, and plasmid DNA was extracted using the QIAprep Spin Miniprep Kit (27104, Qiagen).

The mutation was confirmed by Sanger sequencing (ABI 3100*,* SeqGen).

Once the mutation was verified, the wild-type XBB.1.5 (XBB.1.5_wt) was used to transfect the HEK-293T ^{CD81KO} as previously described. The pseudovirus titer was determined using the luciferase assay on Vero/TMPRSS2 cells and compared to the titer of XBB.1.5.

Quantification of spike protein in pseudoviruses assay

BCA Total protein concentrations were determined using the BCA Protein Assay Kit (A65453, Thermo Scientific, Pierce), following the manufacturer's instructions. Briefly, a standard curve was prepared using serial dilutions of bovine serum albumin (BSA) in PBS, with concentrations ranging from 0 to 2 mg/mL. For protein sample quantification, samples were diluted in PBS to fall within the linear range of the standard curve, using 10-20 µL per well. In a 96-well plate, 200 µL of BCA working reagent was added to each well and the plate was incubated at 37°C for 30 minutes. After incubation, the absorbance was measured at 562 nm using a microplate reader (Multiskan GO, Thermo Scientific). Protein concentrations (µg/mL) were determined by comparing the absorbance of each sample to the standard curve.

ELISA ELISA (Enzyme-Linked Immunosorbent Assay) Equal amount of total proteins (25 ng) of each pseudovirus was coated onto 96-well plates and incubated overnight at 4°C, allowing for antigen attachment. Following coating, the plates were blocked with Protein-Free Blocking Buffer (37572, Thermo Fisher Scientific) to prevent non-specific binding. After blocking, the plates were incubated for at least 1 hour with primary antibodies specific for the SARS-CoV-2 spike protein (anti-S rabbit 40150-R007, Sino Biological). Subsequently, the plates were washed three times with PBS-T to remove unbound antibodies. A horseradish peroxidase (HRP)-conjugated anti-rabbit secondary antibody A24470, Invitrogen;) was then added for 1 hour to enable detection. Following secondary antibody incubation, the signal was developed by adding TMB (3,3',5,5'-Tetramethylbenzidine) substrate solution (N301,

Thermo Fisher Scientific), and the reaction was stopped by adding sulfuric acid (410577000, Carlo Erba) to block the signal.

The absorbance was measured at 450 nm using a Multiskan GO plate reader (Thermo Scientific). The presence of spike variants was indicated by the level of absorbance, which was proportional to the amount of bound antibody, reflecting the pseudovirus spike protein interaction.

XTT Assay for determination of cell viability and cytotoxicity

Cell viability was assessed using the Cell Proliferation Kit II (XTT) (11465015001, Roche Diagnostics, Merck). In this assay, the tetrazolium salt XTT (2,3-bis-(2-methoxy-4-nitro-5-sulfophenyl)-2H-tetrazolium-5-carboxanilide) is metabolized by viable cells to form an orange formazan dye, which can be quantified photometrically at 450 nm.

For entry experiment, Vero/TMPRSS2 cells ($3 \cdot 10^5$ $^{cells}/_{mL}$) were seeded in 96-well plates and incubated for 24 hours. The culture medium was then replaced with medium containing different concentrations of the inhibitors Bafilomycin A1 (BFLA-1 1; SML1661, Merck) and Camostat mesylate (SML0057, Merck) and cells were incubated for an additional 2 hours at 37°C (Hoffmann *et al.*, 2020) (Clementi *et al.*, 2020). Following treatment, XTT reagent was added to each well, and the plates were incubated for 4 more hours. The optical density (OD) was measured at 450 nm (with a reference wavelength of 650 nm) using a Multiskan GO plate reader (Thermo Scientific).

For disinfection experiments, Vero/TMPRSS2 cells ($3 \cdot 10^5$ $^{cells}/_{mL}$) were seeded in 96-well plates and incubated for 24 hours. The culture medium was then replaced with medium containing different concentrations of natural compound as Tea tree oil, (TTO, W390208, Sigma-Aldrich), Daptomycin (DAP, SBR00014, Sigma-Aldrich) and Quercitin (QRE, PHR1488, Sigma-Aldrich). After 2h of incubation a 37°C the optical density was measure at 450nm and 650 nm using Multiskan GO plate reader (Thermo Scientific).

Inhibition of pseudovirus entry process

To selectively inhibit different cell proteases involved in SARS-CoV-2 entry, two compounds were used: BFLA-1 and Camostat mesylate.

Calu-3 cells ($3 \cdot 10^5$ $^{cells}/_{mL}$) were seeded in 96-well plates and cultured for three days at 37°C with 5% CO_2. Prior to pseudovirus transduction, cells were pretreated for 1 hour with either BFLA-1 (100 nM), Camostat mesylate (100 µM), or a combination of both. The pseudovirus transduction was performed using 100,000 RLU for each variant, as determined by titration. A positive control, pseudovirus without inhibitors was also included. Cells were centrifuged at 800 xg for 1 hour at 37°C for adsorption and then incubated for 3 days at 37°C and 5% CO_2. After incubation, cells were lysed with 100 µL of Glo Lysis Buffer (E2661, Promega) for 15 minutes at room temperature. Cell lysates were transferred to a luminometer plate, and 100 µL of Bright-Glo Assay Reagent (E2620, Promega) was added just before luminescence detection using a Victor3 luminometer (Perkin Elmer).

Six biological replicates were performed for each condition. To evaluate the capability of the compounds to inhibit pseudoviral entry, transduction was normalized against uninfected cells (set as 100%) and untreated infected cells (set as 0%).

Immunofluorescence

293T-ACE2/TMPRSS2 cells were seeded on glass coverslip for 1 day at 37°C and 5% CO_2. Then, cells were fixed and permeabilized with ice-cold methanol-acetone (1:1) for 15 minutes at room temperature. After three washes with PBS, cells were incubated with the primary antibody (40150-MM08, Sino Biological; anti-S) for 1 hour at 37°C. Subsequentially, cells were washed three times with PBS and cells nuclei were stained with Hoechst 33342 (94403, Sigma-Aldrich) for 15 minutes at 37°C. The images were acquired with Zeiss Axio Observer.Z1 microscope with QImaging Exi-Blue (Carl Zeiss, Oberkochen, Germany) at a 20-fold magnification. The obtained images were analyzed with ImageJ software (release 1.53).

Persistence experiment

SARS-CoV-2 variants. The persistence assay of 11 isolated SARS-CoV-2 variants were tested on three different materials—polystyrene-plastic, aluminum, and copper—. Prior to use, all materials were thoroughly disinfected. The same amount of the virus ($1.5 \cdot 10^6$ $^{TCID_{50}}/_{mL}$) in 50 µL was tested for each material on a 24-well plate; following the inoculation, the virus was recovered from the surface by adding an equivalent volume of DMEM (10 times the volume of the inoculum) after 15, 30 minutes, 1 and 2 hours. The recovered virus was then aliquoted and stored at -80°C.

To determine the viral persistence over the time, the recovered virus was re-titrated using a back-titration assay on Vero/TMPRSS2 ($3 \cdot 10^5$ $cells/_{mL}$); after 1h of adsorption, cells were washed with PBS to remove cell-free virus, and complete medium was added to cells supplemented with 2% FBS. After 72 hpi the CPE was evaluated in inverted phase-contrast microscopy (Olympus CKX41) and $TCID_{50}/_{mL}$ of persistent viruses was determined with the Reed–Muench formula. The infectious titer reduction rates were calculated as ($1 - 1/_{10log_{10}} . N_0/_{N_t}$) . 100 (%) where Nt is the titer of the post persistence sample, and N0 is the titer of the stock before the persistence (Inagaki *et al.*, 2020).

Influenza strains The persistence of influenza strains was tested on polystyrene-plastic, aluminum and copper using the same amount of virus ($1.5 \cdot 10^6$ $TCID_{50}/_{mL}$) in each material following the inoculation, the virus was recovered from the surface by adding an equivalent volume of DMEM (10 times the volume of the inoculum) after 15, 30 minutes, 1, 2 and 6 hours and then stored at -80°C. MDCK ($3 \cdot 10^5$ $cells/_{mL}$) cells were seeded into 96-well plates and were infected at 95% of confluency with base 10 dilutions of persistence virus. After 72 hpi the CPE was evaluated in inverted phase-contrast microscopy (Olympus CKX41) and $TCID_{50}$/mL of persistent viruses was determined with the titer of stock sample, which was set as 100% and the persistence rates were calculated as reported above.

Pseudovirus XBB.1.5 Vero/TMPRSS2 cells ($3 \cdot 10^5$ $cells/_{mL}$) were seeded in 96-well plates and incubated for 24 hours. Serial 1:10 dilutions of pseudovirus were then added to the cells, followed by centrifugation at 800 xg for 1 hour; after centrifugation, the media was removed, and the cells were washed with PBS. Fresh medium supplemented with 2% FBS was then added. 72 hpi, the cells were lysed with 100 µL of Glo Lysis Buffer (E266, Promega) for 15 minutes, and luminescence was measured by adding 100 µL of Bright-Glo Assay Reagent (E2620, Promega) and detecting signals using a Victor3 luminometer (Perkin Elmer). Based on these results, a standard of 100,000 RLU was selected for each pseudovirus to ensure equal viral input for subsequent persistence assays. Persistence was evaluated on sterilized polystyrene-plastic and aluminum surfaces at time points of 30 seconds, 1 minute, 2 minutes, 5 minutes, and 30 minutes. To recover the pseudovirus, 10 times the volume of DMEM was added to the surface, and the samples were then stored at -80°C. After recovery, the pseudovirus was titrated back on Vero/TMPRSS2 cells, and

persistence was quantified by measuring luciferase activity. For each variant, the persistence value was normalized to the stock titer (set as 100%).

Disinfectant analysis

To evaluate the disinfectant efficacy of the different compounds TTO, DAP, QRE, EtOH 95% and UV-C the persistence experiment was repeated, focusing solely on the persistent viral variants on the two materials previously subjected to sanitation. 50 µL of viral titer was used considering $1.5 \cdot 10^6$ $TCID_{50}/_{ml}$. The experiments were performed within a 15-minute window to ensure that the observed disinfectant effect could be attributed specifically to each disinfectant agent. For all disinfectants tested, the experiment was conducted in 12-well plates, where 50 µL of virus present on the surfaces was mixed with 50 µL of the disinfectant and recovered after 1, 5, and 10 minutes. For the UV-C treatment, used as a positive sanitation control, the samples were irradiated on ice at a dose of approximately 1.8 mW/cm², with a working distance of 20 cm for different exposure times (1, 5, and 10 minutes). After UV treatment, the virus was eluted, stored at -80°C, and subjected to back titration the following day, as described. After 72 hours, the Vero/TMPRSS2 or MDCK cells were examined for cytopathic effects (CPE), and the $TCID_{50}$/mL was calculated according to the previously described method.

In silico characterization

Variant calling analysis Whole genome sequencing of the clinical isolates was performed, and the resulting sequences were aligned against the G614D reference variant. Variant calling analysis was then carried out on the S, M, and E proteins using the online MAFFT alignment program to identify potential mutations and variations (*Extract a specific region from unaligned sequences --- mafft.cbrc.jp*, no date).

Structural Modeling and Stability Analysis of Spike Variants

D614G spikes were constructed and simulated as described in (Castelli *et al.*, 2021). The spike ectodomain (residues 14-1146) were modeled using Modeller10.4 (Šali and Blundell, 1993) in the 1-up and closed state both as S0 and S1-S2 (processed at the furin cleavage site – FCS) using the spike sequence from the clinical isolate described in this study as query and the deposited structures with RCSB ID: GZGI and 7BNN as templates. To study the contribution of all the reported

mutations of each variant, the last frame of each 200 ns trajectory were used for stability calculation using MAESTRO web tool (*MAESTRO --- biwww.che.sbg.ac.at*, no date). More in details, we evaluated stability in terms of free energy changes (ΔΔGbinding = ΔGmutant − ΔGWT), which accounts for contributions from hydrophobic, polar, van der Waals, hydrogen bonding, and electrostatic interactions.

Data analysis and statistics

Data analysis was performed using GraphPad Prism 9 (GraphPad Software, San Diego, CA, USA, www.graphpad.com), and results are expressed as mean values ± standard deviation (SD) unless otherwise specified. To study the replication kinetics of viral variants, ΔCt was calculated by subtracting the cycle threshold (Ct) values of non-infected cells (used as control) from those of infected cells. This approach allowed us to quantify the relative replication of the virus, with the ΔCt reflecting the difference in viral RNA amplification between infected and uninfected cells. The area under the curve (AUC) was then calculated, and nonlinear logistic growth analysis was applied to model the kinetic replication curve.

For the immune activation analysis, ΔCt was calculated by subtracting the Ct of the housekeeping gene from the Ct of the target gene for each sample. To evaluate the fold change of the immune response, the ΔΔCt method was applied, which involved subtracting the ΔCt of uninfected cells from the ΔCt of infected cells. This allowed us to measure the relative change in gene expression and quantify the activation of the immune response following infection. Statistical analysis for both replication kinetics and immune activation was conducted using Two-way ANOVA followed by Tukey's multiple comparisons test.

To assess the inhibition of pseudoviral entry, transduction data were normalized to uninfected cells (set to 100%) and untreated infected cells (set to 0%). The cytopathic effect (CPE) in Vero/TMPRSS2 and MDCK cells was normalized to virus infection controls (set to 0% inhibition) and uninfected cells (set to 100% inhibition). These data were analyzed using Two-way ANOVA and Tukey's multiple comparisons test.

To evaluate the relationships between different variables, two separate Spearman's rank correlation analyses were performed. In the first analysis, Spearman's correlation was used to explore the relationships between viral entry mechanisms, replication kinetics, and immune activation. The correlation coefficients (r) were calculated for each pairwise comparison, with values ranging from -1 (perfect negative correlation) to +1 (perfect positive correlation), and a coefficient of

0 indicating no correlation. In the second analysis, Spearman's correlation was applied to assess the relationship between viral persistence data and the stability of viral spike proteins, where the stability was quantified based on ΔΔG (Delta Delta G) values obtained through computational analysis. This analysis allowed us to examine whether viral persistence could be linked to the stability of the spike variants, providing insight into potential structural determinants of viral persistence. Statistical significance was considered for both analyses at $p < 0.05$.

For the evaluation of the functional mutation G446D in pseudovirus assays, the Mann-Whitney U test was applied to compare the persistence data between infected and uninfected groups.

REFERENCES

Abdelrahman, Z., Li, M. and Wang, X. (2020) 'Comparative Review of SARS-CoV-2, SARS-CoV, MERS-CoV, and Influenza A Respiratory Viruses', *Frontiers in Immunology*, 11. Available at: https://doi.org/10.3389/fimmu.2020.552909.

Aboubakr, H.A., Sharafeldin, T.A. and Goyal, S.M. (2020) 'Stability of SARS-CoV-2 and other coronaviruses in the environment and on common touch surfaces and the influence of climatic conditions: A review', *Transboundary and Emerging Diseases*, 68(2), pp. 296–312. Available at: https://doi.org/10.1111/tbed.13707.

Addetia, A. *et al.* (2023) 'Neutralization, effector function and immune imprinting of Omicron variants', *Nature*, 621(7979), pp. 592–601. Available at: https://doi.org/10.1038/s41586-023-06487-6.

AIFA suspension of lagevrio-molnupiravir (no date). Available at: AIFA: https://www.aifa.gov.it/-/sospensione_utilizzo_lagevrio_molnupiravir (Accessed: 18 January 2025).

Al-Aly, Z. and Rosen, C.J. (2024) 'Long Covid and Impaired Cognition — More Evidence and More Work to Do', *New England Journal of Medicine*, 390(9), pp. 858–860. Available at: https://doi.org/10.1056/nejme2400189.

Amraei, R. *et al.* (2021) 'CD209L/L-SIGN and CD209/DC-SIGN Act as Receptors for SARS-CoV-2', *ACS Central Science*, 7(7), pp. 1156–1165. Available at: https://doi.org/10.1021/acscentsci.0c01537.

Andreano, E. and Rappuoli, R. (2021) 'SARS-CoV-2 escaped natural immunity, raising questions about vaccines and therapies', *Nature Medicine*, 27(5), pp. 759–761. Available at: https://doi.org/10.1038/s41591-021-01347-0.

Andreata-Santos, R. *et al.* (2022) 'Validation of Serological Methods for COVID-19 and Retrospective Screening of Health Employees and Visitors to the São Paulo University Hospital, Brazil', *Frontiers in Cellular and Infection Microbiology*, 12. Available at: https://doi.org/10.3389/fcimb.2022.787411.

Arya, R. *et al.* (2021) 'Structural insights into SARS-CoV-2 proteins', *Journal of Molecular Biology*, 433(2), p. 166725. Available at: https://doi.org/10.1016/j.jmb.2020.11.024.

Augustine, R. *et al.* (2020) 'Rapid Antibody-Based COVID-19 Mass Surveillance: Relevance, Challenges, and Prospects in a Pandemic and Post-Pandemic World', *Journal of Clinical Medicine*, 9(10), p. 3372. Available at: https://doi.org/10.3390/jcm9103372.

Bai, Z. *et al.* (2021) 'The SARS-CoV-2 Nucleocapsid Protein and Its Role in Viral Structure, Biological Functions, and a Potential Target for Drug or Vaccine Mitigation', *Viruses*, 13(6), p. 1115. Available at: https://doi.org/10.3390/v13061115.

Bailey, E.S. *et al.* (2021) 'Essential Oil Disinfectant Efficacy Against SARS-CoV-2 Microbial Surrogates', *Frontiers in Public Health*, 9. Available at: https://doi.org/10.3389/fpubh.2021.783832.

Bálint, G., Vörös-Horváth, B. and Széchenyi, A. (2022) 'Omicron: increased transmissibility and decreased pathogenicity', *Signal Transduction and Targeted Therapy*, 7(1). Available at: https://doi.org/10.1038/s41392-022-01009-8.

Bandyopadhyay, S.K. *et al.* (1995) 'Transcriptional Induction by Double-stranded RNA Is Mediated by Interferon-stimulated Response Elements without Activation of Interferon-stimulated Gene Factor 3', *Journal of Biological Chemistry*, 270(33), pp. 19624–19629. Available at: https://doi.org/10.1074/jbc.270.33.19624.

Banerjee, A.K. *et al.* (2020) 'SARS-CoV-2 Disrupts Splicing, Translation, and Protein Trafficking to Suppress Host Defenses', *Cell*, 183(5), pp. 1325-1339.e21. Available at: https://doi.org/10.1016/j.cell.2020.10.004.

Bangaru, S. *et al.* (2020) 'Structural analysis of full-length SARS-CoV-2 spike protein from an advanced vaccine candidate', *Science*, 370(6520), pp. 1089–1094. Available at: https://doi.org/10.1126/science.abe1502.

Bao, C. *et al.* (2021) 'Natural killer cells associated with SARS-CoV-2 viral RNA shedding, antibody response and mortality in COVID-19 patients', *Experimental Hematology & Oncology*, 10(1). Available at: https://doi.org/10.1186/s40164-021-00199-1.

Beig Parikhani, A. *et al.* (2021) 'The Inclusive Review on SARS-CoV-2 Biology, Epidemiology, Diagnosis, and Potential Management Options', *Current Microbiology*, 78(4), pp. 1099–1114. Available at: https://doi.org/10.1007/s00284-021-02396-x.

Beigel, J.H. *et al.* (2020) 'Remdesivir for the Treatment of Covid-19 — Final Report', *New England Journal of Medicine*, 383(19), pp. 1813–1826. Available at: https://doi.org/10.1056/nejmoa2007764.

Benton, D.J. *et al.* (2020) 'Receptor binding and priming of the spike protein of SARS-CoV-2 for membrane fusion', *Nature*, 588(7837), pp. 327–330. Available at: https://doi.org/10.1038/s41586-020-2772-0.

Le Bert, N. *et al.* (2020) 'SARS-CoV-2-specific T cell immunity in cases of COVID-19 and SARS, and uninfected controls', *Nature*, 584(7821), pp. 457–462. Available at: https://doi.org/10.1038/s41586-020-2550-z.

Bestle, D. *et al.* (2020) 'TMPRSS2 and furin are both essential for proteolytic activation of SARS-CoV-2 in human airway cells', *Life Science Alliance*, 3(9), p. e202000786. Available at: https://doi.org/10.26508/lsa.202000786.

Blanco-Melo, D. *et al.* (2020) 'Imbalanced Host Response to SARS-CoV-2 Drives Development of COVID-19', *Cell*, 181(5), pp. 1036-1045.e9. Available at: https://doi.org/10.1016/j.cell.2020.04.026.

Bos, R. *et al.* (2020) 'Ad26 vector-based COVID-19 vaccine encoding a prefusion-stabilized SARS-CoV-2 Spike immunogen induces potent humoral and cellular immune responses', *npj Vaccines*, 5(1). Available at: https://doi.org/10.1038/s41541-020-00243-x.

Brant, A.C. *et al.* (2021) 'SARS-CoV-2: from its discovery to genome structure, transcription, and replication', *Cell & Bioscience*, 11(1). Available at: https://doi.org/10.1186/s13578-021-00643-z.

Briard, B., Place, D.E. and Kanneganti, T.-D. (2020) 'DNA Sensing in the Innate Immune Response', *Physiology*, 35(2), pp. 112–124. Available at: https://doi.org/10.1152/physiol.00022.2019.

Bruel, T. *et al.* (2023) 'Sotrovimab therapy elicits antiviral activities against Omicron BQ.1.1 and XBB.1.5 in sera of immunocompromised patients', *Med*, 4(10), pp. 664–667. Available at: https://doi.org/10.1016/j.medj.2023.07.007.

Buonsenso, D. and Tantisira, K.G. (2024) 'Long COVID and SARS-CoV-2 persistence: new answers, more questions', *The Lancet Infectious Diseases*, 24(8), pp. 796–798. Available at: https://doi.org/10.1016/s1473-3099(24)00216-0.

Burbelo, P.D. *et al.* (2020) 'Sensitivity in Detection of Antibodies to Nucleocapsid and Spike Proteins of Severe Acute Respiratory Syndrome Coronavirus 2 in Patients With Coronavirus Disease 2019', *The Journal of Infectious Diseases*, 222(2), pp. 206–213. Available at: https://doi.org/10.1093/infdis/jiaa273.

Burrage, D.R., Koushesh, S. and Sofat, N. (2020) 'Immunomodulatory Drugs in the Management of SARS-CoV-2', *Frontiers in Immunology*, 11. Available at: https://doi.org/10.3389/fimmu.2020.01844.

Camargo, S.M.R. *et al.* (2009) 'Tissue-Specific Amino Acid Transporter Partners ACE2 and Collectrin Differentially Interact With Hartnup Mutations', *Gastroenterology*, 136(3), pp. 872-882.e3. Available at: https://doi.org/10.1053/j.gastro.2008.10.055.

Cantuti-Castelvetri, L. *et al.* (2020) 'Neuropilin-1 facilitates SARS-CoV-2 cell entry and infectivity', *Science*, 370(6518), pp. 856–860. Available at: https://doi.org/10.1126/science.abd2985.

Cao, X. (2020) 'COVID-19: immunopathology and its implications for therapy', *Nature Reviews Immunology*, 20(5), pp. 269–270. Available at: https://doi.org/10.1038/s41577-020-0308-3.

Cao, Y. *et al.* (2022) 'Characterization of the enhanced infectivity and antibody evasion of Omicron BA.2.75', *Cell Host & Microbe*, 30(11), pp. 1527-1539.e5. Available at: https://doi.org/10.1016/j.chom.2022.09.018.

Castelli, M. *et al.* (2021) 'Characterization of a Lineage C.36 SARS-CoV-2 Isolate with Reduced Susceptibility to Neutralization Circulating in Lombardy, Italy', *Viruses*, 13(8), p. 1514. Available at: https://doi.org/10.3390/v13081514.

Cele, S. *et al.* (2021) 'Omicron extensively but incompletely escapes Pfizer BNT162b2 neutralization', *Nature*, 602(7898), pp. 654–656. Available at: https://doi.org/10.1038/s41586-021-04387-1.

Cesar-Silva, D. *et al.* (2022) 'The Endolysosomal System: The Acid Test for SARS-CoV-2', *International Journal of Molecular Sciences*, 23(9), p. 4576. Available at: https://doi.org/10.3390/ijms23094576.

Cesta, M.F. (2006) 'Normal Structure, Function, and Histology of Mucosa-Associated Lymphoid Tissue', *Toxicologic Pathology*, 34(5), pp. 599–608. Available at: https://doi.org/10.1080/01926230600865531.

Chalkias, S. *et al.* (2024) 'Interim Report of the Reactogenicity and Immunogenicity of Severe Acute Respiratory Syndrome Coronavirus 2 XBB–Containing Vaccines', *The Journal of Infectious Diseases*, 230(2), pp. e279–e286. Available at: https://doi.org/10.1093/infdis/jiae067.

Chan, J.F.-W. *et al.* (2020) 'A familial cluster of pneumonia associated with the 2019 novel coronavirus indicating person-to-person transmission: a study of a family cluster', *The Lancet*, 395(10223), pp. 514–523. Available at: https://doi.org/10.1016/s0140-6736(20)30154-9.

Channappanavar, R. *et al.* (2016) 'Dysregulated Type I Interferon and Inflammatory Monocyte-Macrophage Responses Cause Lethal Pneumonia in SARS-CoV-Infected Mice', *Cell Host & Microbe*, 19(2), pp. 181–193. Available at: https://doi.org/10.1016/j.chom.2016.01.007.

Channappanavar, R. *et al.* (2019) 'IFN-I response timing relative to virus replication determines MERS coronavirus infection outcomes', *Journal of Clinical Investigation*, 129(9), pp. 3625–3639. Available at: https://doi.org/10.1172/jci126363.

Chattopadhyay, S. and Sen, G.C. (2016) 'RIG-I-like receptor-induced IRF3 mediated pathway of apoptosis (RIPA): a new antiviral pathway', *Protein & Cell*, 8(3), pp. 165–168. Available at: https://doi.org/10.1007/s13238-016-0334-x.

Chavda, V. *et al.* (2022) 'The Delta and Omicron Variants of SARS-CoV-2: What We Know So Far', *Vaccines*, 10(11), p. 1926. Available at: https://doi.org/10.3390/vaccines10111926.

Chen, J. *et al.* (2022) 'Omicron Variant (B.1.1.529): Infectivity, Vaccine Breakthrough, and Antibody Resistance', *Journal of Chemical Information and Modeling*, 62(2), pp. 412–422. Available at: https://doi.org/10.1021/acs.jcim.1c01451.

Chen, R.E. *et al.* (2021) 'In vivo monoclonal antibody efficacy against SARS-CoV-2 variant strains', *Nature*, 596(7870), pp. 103–108. Available at: https://doi.org/10.1038/s41586-021-03720-y.

Chen, Z. *et al.* (2005) 'Function of HAb18G/CD147 in Invasion of Host Cells by Severe Acute Respiratory Syndrome Coronavirus', *The Journal of Infectious Diseases*, 191(5), pp. 755–760. Available at: https://doi.org/10.1086/427811.

Cheng, Y.-W. *et al.* (2020) 'Furin Inhibitors Block SARS-CoV-2 Spike Protein Cleavage to Suppress Virus Production and Cytopathic Effects', *Cell Reports*, 33(2), p. 108254. Available at: https://doi.org/10.1016/j.celrep.2020.108254.

Christgen, S. and Kanneganti, T.-D. (2020) 'Inflammasomes and the fine line between defense and disease', *Current Opinion in Immunology*, 62, pp. 39–44. Available at: https://doi.org/10.1016/j.coi.2019.11.007.

Clementi, N. *et al.* (2020) 'Combined Prophylactic and Therapeutic Use Maximizes Hydroxychloroquine Anti-SARS-CoV-2 Effects in vitro', *Frontiers in Microbiology*, 11. Available at: https://doi.org/10.3389/fmicb.2020.01704.

Clementi, N. *et al.* (2021) 'Viral Respiratory Pathogens and Lung Injury', *Clinical Microbiology Reviews*, 34(3). Available at: https://doi.org/10.1128/cmr.00103-20.

Cohen, B. *et al.* (1995) 'Ligand-Induced Association of the Type I Interferon Receptor Components', *Molecular and Cellular Biology*, 15(8), pp. 4208–4214. Available at: https://doi.org/10.1128/mcb.15.8.4208.

Cohen, K.W. *et al.* (2021) 'Longitudinal analysis shows durable and broad immune memory after SARS-CoV-2 infection with persisting antibody responses and memory B and T cells', *Cell Reports Medicine*, 2(7), p. 100354. Available at: https://doi.org/10.1016/j.xcrm.2021.100354.

Coronavirus Disease (COVID-19) Situation Reports --- who.int (no date). Available at: https://www.who.int/emergencies/diseases/novel-coronavirus-2019/situation-reports (Accessed: 12 January 2025).

COVID-19 deaths | WHO COVID-19 dashboard --- data.who.int (no date). Available at: https://data.who.int/dashboards/covid19/deaths?n=c (Accessed: 12 January 2025).

COVID-19 Map - Johns Hopkins Coronavirus Resource Center --- coronavirus.jhu.edu. (no date). Available at: https://coronavirus.jhu.edu/map.html (Accessed: 12 January 2025).

Cox, M. *et al.* (2023) 'SARS-CoV-2 variant evasion of monoclonal antibodies based on in vitro studies', *Nature Reviews Microbiology*, 21(2), pp. 112–124. Available at: https://doi.org/10.1038/s41579-022-00809-7.

Crawford, K.H.D. *et al.* (2020) 'Protocol and Reagents for Pseudotyping Lentiviral Particles with SARS-CoV-2 Spike Protein for Neutralization Assays', *Viruses*, 12(5), p. 513. Available at: https://doi.org/10.3390/v12050513.

Criscuolo, E. *et al.* (2021) 'Fast inactivation of SARS-CoV-2 by UV-C and ozone exposure on different materials', *Emerging Microbes & Infections*, 10(1), pp. 206–209. Available at: https://doi.org/10.1080/22221751.2021.1872354.

Criscuolo, E. *et al.* (2024) 'Single spike mutation differentiating XBB.1 and XBB.1.5 enhances SARS-CoV-2 cell-to-cell transmission and facilitates serum-mediated enhancement', *Frontiers in Immunology*, 15. Available at: https://doi.org/10.3389/fimmu.2024.1501200.

Crotty, S. (2014) 'T Follicular Helper Cell Differentiation, Function, and Roles in Disease', *Immunity*, 41(4), pp. 529–542. Available at: https://doi.org/10.1016/j.immuni.2014.10.004.

Dai, Y.-J. *et al.* (2020) 'Comprehensive analysis of two potential novel SARS-CoV-2 entries, TMPRSS2 and IFITM3, in healthy individuals and cancer patients', *International Journal of Biological Sciences*, 16(15), pp. 3028–3036. Available at: https://doi.org/10.7150/ijbs.51234.

Deng, X. *et al.* (2017) 'Coronavirus nonstructural protein 15 mediates evasion of dsRNA sensors and limits apoptosis in macrophages', *Proceedings of the National Academy of Sciences*, 114(21). Available at: https://doi.org/10.1073/pnas.1618310114.

Devaraj, S.G. *et al.* (2007) 'Regulation of IRF-3-dependent Innate Immunity by the Papain-like Protease Domain of the Severe Acute Respiratory Syndrome Coronavirus', *Journal of Biological Chemistry*, 282(44), pp. 32208–32221. Available at: https://doi.org/10.1074/jbc.m704870200.

Diamond, M.S. and Kanneganti, T.-D. (2022) 'Innate immunity: the first line of defense against SARS-CoV-2', *Nature Immunology*, 23(2), pp. 165–176. Available at: https://doi.org/10.1038/s41590-021-01091-0.

Domingo, P. *et al.* (2020) 'The four horsemen of a viral Apocalypse: The pathogenesis of SARS-CoV-2 infection (COVID-19)', *EBioMedicine*, 58, p. 102887. Available at: https://doi.org/10.1016/j.ebiom.2020.102887.

van Doremalen, N. *et al.* (2020) 'Aerosol and Surface Stability of SARS-CoV-2 as Compared with SARS-CoV-1', *New England Journal of Medicine*, 382(16), pp. 1564–1567. Available at: https://doi.org/10.1056/nejmc2004973.

Dougan, M. *et al.* (2021) 'Bamlanivimab plus Etesevimab in Mild or Moderate Covid-19', *New England Journal of Medicine*, 385(15), pp. 1382–1392. Available at: https://doi.org/10.1056/nejmoa2102685.

Duan, L. *et al.* (2020) 'The SARS-CoV-2 Spike Glycoprotein Biosynthesis, Structure, Function, and Antigenicity: Implications for the Design of Spike-Based Vaccine Immunogens', *Frontiers in Immunology*, 11. Available at: https://doi.org/10.3389/fimmu.2020.576622.

Dunkle, L.M. *et al.* (2022) 'Efficacy and Safety of NVX-CoV2373 in Adults in the United States and Mexico', *New England Journal of Medicine*, 386(6), pp. 531–543. Available at: https://doi.org/10.1056/nejmoa2116185.

'Effect of Hydroxychloroquine in Hospitalized Patients with Covid-19' (2020) *New England Journal of Medicine*, 383(21), pp. 2030–2040. Available at: https://doi.org/10.1056/nejmoa2022926.

Espinosa-Gonzalez, A.B. *et al.* (2023) 'Orthostatic tachycardia after covid-19', *BMJ*, p. e073488. Available at: https://doi.org/10.1136/bmj-2022-073488.

Extract a specific region from unaligned sequences --- mafft.cbrc.jp (no date). Available at: https://mafft.cbrc.jp/alignment/server/specificregion-last.html (Accessed: 12 January 2025).

Fensterl, V., Chattopadhyay, S. and Sen, G.C. (2015) 'No Love Lost Between Viruses and Interferons', *Annual Review of Virology*, 2(1), pp. 549–572. Available at: https://doi.org/10.1146/annurev-virology-100114-055249.

Fischer, W.A. *et al.* (2022) 'A phase 2a clinical trial of molnupiravir in patients with COVID-19 shows accelerated SARS-CoV-2 RNA clearance and elimination of infectious virus', *Science Translational Medicine*, 14(628). Available at: https://doi.org/10.1126/scitranslmed.abl7430.

Fung, T.S. and Liu, D.X. (2018) 'Post-Translational Modifications of Coronavirus Proteins: Roles and Function', *Future Virology*, 13(6), pp. 405–430. Available at: https://doi.org/10.2217/fvl-2018-0008.

Galipeau, Y. *et al.* (2020) 'Humoral Responses and Serological Assays in SARS-CoV-2 Infections', *Frontiers in Immunology*, 11. Available at: https://doi.org/10.3389/fimmu.2020.610688.

Galmiche, S. *et al.* (2023) 'SARS-CoV-2 incubation period across variants of concern, individual factors, and circumstances of infection in France: a case series

analysis from the ComCor study', *The Lancet Microbe*, 4(6), pp. e409–e417. Available at: https://doi.org/10.1016/S2666-5247(23)00005-8.

Gomes, C.P. *et al.* (2020) 'Cathepsin L in COVID-19: From Pharmacological Evidences to Genetics', *Frontiers in Cellular and Infection Microbiology*, 10. Available at: https://doi.org/10.3389/fcimb.2020.589505.

Gordon, D.E. *et al.* (2020) 'A SARS-CoV-2 protein interaction map reveals targets for drug repurposing', *Nature*, 583(7816), pp. 459–468. Available at: https://doi.org/10.1038/s41586-020-2286-9.

Govind, V. *et al.* (2021) 'Antiviral properties of copper and its alloys to inactivate covid-19 virus: a review', *BioMetals*, 34(6), pp. 1217–1235. Available at: https://doi.org/10.1007/s10534-021-00339-4.

Gruner, H.N. *et al.* (2023) 'SARS-CoV-2 ORF3A interacts with the Clic-like chloride channel-1 (CLCC1) and triggers an unfolded protein response', *PeerJ*, 11, p. e15077. Available at: https://doi.org/10.7717/peerj.15077.

Guo, L. *et al.* (2020) 'Profiling Early Humoral Response to Diagnose Novel Coronavirus Disease (COVID-19)', *Clinical Infectious Diseases*, 71(15), pp. 778–785. Available at: https://doi.org/10.1093/cid/ciaa310.

Hackbart, M., Deng, X. and Baker, S.C. (2020) 'Coronavirus endoribonuclease targets viral polyuridine sequences to evade activating host sensors', *Proceedings of the National Academy of Sciences*, 117(14), pp. 8094–8103. Available at: https://doi.org/10.1073/pnas.1921485117.

Harbison, A.M. *et al.* (2022) 'Fine-tuning the spike: role of the nature and topology of the glycan shield in the structure and dynamics of the SARS-CoV-2 S', *Chemical Science*, 13(2), pp. 386–395. Available at: https://doi.org/10.1039/d1sc04832e.

Harrison, A.G., Lin, T. and Wang, P. (2020) 'Mechanisms of SARS-CoV-2 Transmission and Pathogenesis', *Trends in Immunology*, 41(12), pp. 1100–1115. Available at: https://doi.org/10.1016/j.it.2020.10.004.

Harvey, W.T. *et al.* (2021) 'SARS-CoV-2 variants, spike mutations and immune escape', *Nature Reviews Microbiology*, 19(7), pp. 409–424. Available at: https://doi.org/10.1038/s41579-021-00573-0.

Herder, V. *et al.* (2023) 'The SARS-CoV-2 Omicron sub-variant BA.2.86 is attenuated in hamsters'. Available at: https://doi.org/10.1101/2023.11.10.566576.

Hoffmann, M. *et al.* (2020) 'SARS-CoV-2 Cell Entry Depends on ACE2 and TMPRSS2 and Is Blocked by a Clinically Proven Protease Inhibitor', *Cell*, 181(2), pp. 271-280.e8. Available at: https://doi.org/10.1016/j.cell.2020.02.052.

Hoffmann, M. *et al.* (2021) 'SARS-CoV-2 variants B.1.351 and P.1 escape from neutralizing antibodies', *Cell*, 184(9), pp. 2384-2393.e12. Available at: https://doi.org/10.1016/j.cell.2021.03.036.

Hoffmann, M., Kleine-Weber, H. and Pöhlmann, S. (2020) 'A Multibasic Cleavage Site in the Spike Protein of SARS-CoV-2 Is Essential for Infection of Human Lung Cells', *Molecular Cell*, 78(4), pp. 779-784.e5. Available at: https://doi.org/10.1016/j.molcel.2020.04.022.

Hosseini, A. *et al.* (2020) 'Innate and adaptive immune responses against coronavirus', *Biomedicine & Pharmacotherapy*, 132, p. 110859. Available at: https://doi.org/10.1016/j.biopha.2020.110859.

Hu, B. *et al.* (2020) 'Characteristics of SARS-CoV-2 and COVID-19', *Nature Reviews Microbiology*, 19(3), pp. 141–154. Available at: https://doi.org/10.1038/s41579-020-00459-7.

Hu, F.-H. *et al.* (2023) 'Clinical outcomes of the severe acute respiratory syndrome coronavirus 2 Omicron and Delta variant: systematic review and meta-analysis of 33 studies covering 6 037 144 coronavirus disease 2019–positive patients', *Clinical Microbiology and Infection*, 29(7), pp. 835–844. Available at: https://doi.org/10.1016/j.cmi.2023.03.017.

Hu, Y. *et al.* (2017) 'The Severe Acute Respiratory Syndrome Coronavirus Nucleocapsid Inhibits Type I Interferon Production by Interfering with TRIM25-Mediated RIG-I Ubiquitination', *Journal of Virology*. Edited by S. Perlman, 91(8). Available at: https://doi.org/10.1128/jvi.02143-16.

Huang, C. *et al.* (2020) 'Clinical features of patients infected with 2019 novel coronavirus in Wuhan, China', *The Lancet*, 395(10223), pp. 497–506. Available at: https://doi.org/10.1016/S0140-6736(20)30183-5.

Huang, I.-C. *et al.* (2011) 'Distinct Patterns of IFITM-Mediated Restriction of Filoviruses, SARS Coronavirus, and Influenza A Virus', *PLoS Pathogens*. Edited by R.S. Baric, 7(1), p. e1001258. Available at: https://doi.org/10.1371/journal.ppat.1001258.

Huang, Y. *et al.* (2020) 'Structural and functional properties of SARS-CoV-2 spike protein: potential antivirus drug development for COVID-19', *Acta Pharmacologica Sinica*, 41(9), pp. 1141–1149. Available at: https://doi.org/10.1038/s41401-020-0485-4.

Hui, K.P.Y. *et al.* (2020) 'Tropism, replication competence, and innate immune responses of the coronavirus SARS-CoV-2 in human respiratory tract and conjunctiva: an analysis in ex-vivo and in-vitro cultures', *The Lancet Respiratory*

Medicine, 8(7), pp. 687–695. Available at: https://doi.org/10.1016/s2213-2600(20)30193-4.

Inagaki, H. *et al.* (2020) 'Rapid inactivation of SARS-CoV-2 with deep-UV LED irradiation', *Emerging Microbes & Infections*, 9(1), pp. 1744–1747. Available at: https://doi.org/10.1080/22221751.2020.1796529.

Jackson, C.B. *et al.* (2021) 'Mechanisms of SARS-CoV-2 entry into cells', *Nature Reviews Molecular Cell Biology*, 23(1), pp. 3–20. Available at: https://doi.org/10.1038/s41580-021-00418-x.

Jaimes, J.A. *et al.* (2020) 'Phylogenetic Analysis and Structural Modeling of SARS-CoV-2 Spike Protein Reveals an Evolutionary Distinct and Proteolytically Sensitive Activation Loop', *Journal of Molecular Biology*, 432(10), pp. 3309–3325. Available at: https://doi.org/10.1016/j.jmb.2020.04.009.

Jason, L.A. and Dorri, J.A. (2022) 'ME/CFS and Post-Exertional Malaise among Patients with Long COVID', *Neurology International*, 15(1), pp. 1–11. Available at: https://doi.org/10.3390/neurolint15010001.

Jefferies, C.A. (2019) 'Regulating IRFs in IFN Driven Disease', *Frontiers in Immunology*, 10. Available at: https://doi.org/10.3389/fimmu.2019.00325.

Jeffers, S.A. *et al.* (2004) 'CD209L (L-SIGN) is a receptor for severe acute respiratory syndrome coronavirus', *Proceedings of the National Academy of Sciences*, 101(44), pp. 15748–15753. Available at: https://doi.org/10.1073/pnas.0403812101.

Johnson, B.A. *et al.* (2021) 'Loss of furin cleavage site attenuates SARS-CoV-2 pathogenesis', *Nature*, 591(7849), pp. 293–299. Available at: https://doi.org/10.1038/s41586-021-03237-4.

Kalfaoglu, B. *et al.* (2021) 'T-cell dysregulation in COVID-19', *Biochemical and Biophysical Research Communications*, 538, pp. 204–210. Available at: https://doi.org/10.1016/j.bbrc.2020.10.079.

Kampf, G. *et al.* (2020) 'Persistence of coronaviruses on inanimate surfaces and their inactivation with biocidal agents', *Journal of Hospital Infection*, 104(3), pp. 246–251. Available at: https://doi.org/10.1016/j.jhin.2020.01.022.

Kanneganti, T. (2020) 'Intracellular innate immune receptors: Life inside the cell', *Immunological Reviews*, 297(1), pp. 5–12. Available at: https://doi.org/10.1111/imr.12912.

Karim, S.S.A. and Karim, Q.A. (2021) 'Omicron SARS-CoV-2 variant: a new chapter in the COVID-19 pandemic', *The Lancet*, 398(10317), pp. 2126–2128. Available at: https://doi.org/10.1016/s0140-6736(21)02758-6.

Katiyar, H. *et al.* (2024) 'SARS-CoV-2 Assembly: Gaining Infectivity and Beyond', *Viruses*, 16(11), p. 1648. Available at: https://doi.org/10.3390/v16111648.

Katz, L.M. (2021) '(A Little) Clarity on Convalescent Plasma for Covid-19', *New England Journal of Medicine*, 384(7), pp. 666–668. Available at: https://doi.org/10.1056/nejme2035678.

Kaushal, N. *et al.* (2020) 'Mutational Frequencies of SARS-CoV-2 Genome during the Beginning Months of the Outbreak in USA', *Pathogens*, 9(7), p. 565. Available at: https://doi.org/10.3390/pathogens9070565.

Ke, Z. *et al.* (2020) 'Structures and distributions of SARS-CoV-2 spike proteins on intact virions', *Nature*, 588(7838), pp. 498–502. Available at: https://doi.org/10.1038/s41586-020-2665-2.

Kim, D. *et al.* (2020) 'The Architecture of SARS-CoV-2 Transcriptome', *Cell*, 181(4), pp. 914-921.e10. Available at: https://doi.org/10.1016/j.cell.2020.04.011.

Klein, J. *et al.* (2023) 'Distinguishing features of long COVID identified through immune profiling', *Nature*, 623(7985), pp. 139–148. Available at: https://doi.org/10.1038/s41586-023-06651-y.

Knoops, K. *et al.* (2008) 'SARS-Coronavirus Replication Is Supported by a Reticulovesicular Network of Modified Endoplasmic Reticulum', *PLoS Biology*. Edited by M. Emerman, 6(9), p. e226. Available at: https://doi.org/10.1371/journal.pbio.0060226.

Koch, J. *et al.* (2021) 'TMPRSS2 expression dictates the entry route used by SARS-CoV-2 to infect host cells', *The EMBO Journal*, 40(16). Available at: https://doi.org/10.15252/embj.2021107821.

Konno, Y. *et al.* (2020) 'SARS-CoV-2 ORF3b Is a Potent Interferon Antagonist Whose Activity Is Increased by a Naturally Occurring Elongation Variant', *Cell Reports*, 32(12), p. 108185. Available at: https://doi.org/10.1016/j.celrep.2020.108185.

Korber, B. *et al.* (2020) 'Tracking Changes in SARS-CoV-2 Spike: Evidence that D614G Increases Infectivity of the COVID-19 Virus', *Cell*, 182(4), pp. 812-827.e19. Available at: https://doi.org/10.1016/j.cell.2020.06.043.

Korneeva, N. *et al.* (2023) 'SARS-CoV-2 viral protein Nsp2 stimulates translation under normal and hypoxic conditions', *Virology Journal*, 20(1). Available at: https://doi.org/10.1186/s12985-023-02021-2.

Kovesdi, I. and Hedley, S.J. (2010) 'Adenoviral Producer Cells', *Viruses*, 2(8), pp. 1681–1703. Available at: https://doi.org/10.3390/v2081681.

Krüttgen, A. *et al.* (2021) 'Comparison of the SARS-CoV-2 Rapid antigen test to the real star Sars-CoV-2 RT PCR kit', *Journal of Virological Methods*, 288, p. 114024. Available at: https://doi.org/10.1016/j.jviromet.2020.114024.

Kucharski, A.J. *et al.* (2020) 'Effectiveness of isolation, testing, contact tracing, and physical distancing on reducing transmission of SARS-CoV-2 in different settings: a mathematical modelling study', *The Lancet Infectious Diseases*, 20(10), pp. 1151–1160. Available at: https://doi.org/10.1016/s1473-3099(20)30457-6.

Kucirka, L.M. *et al.* (2020) 'Variation in False-Negative Rate of Reverse Transcriptase Polymerase Chain Reaction–Based SARS-CoV-2 Tests by Time Since Exposure', *Annals of Internal Medicine*, 173(4), pp. 262–267. Available at: https://doi.org/10.7326/m20-1495.

Kuri-Cervantes, L. *et al.* (2020) 'Comprehensive mapping of immune perturbations associated with severe COVID-19', *Science Immunology*, 5(49). Available at: https://doi.org/10.1126/sciimmunol.abd7114.

Ladds, E. *et al.* (2020) 'Persistent symptoms after Covid-19: qualitative study of 114 "long Covid" patients and draft quality principles for services', *BMC Health Services Research*, 20(1). Available at: https://doi.org/10.1186/s12913-020-06001-y.

Ladds, E. *et al.* (2024) 'Cognitive dysfunction after covid-19', *BMJ*, p. e075387. Available at: https://doi.org/10.1136/bmj-2023-075387.

Lamers, M.M. and Haagmans, B.L. (2022) 'SARS-CoV-2 pathogenesis', *Nature Reviews Microbiology*, 20(5), pp. 270–284. Available at: https://doi.org/10.1038/s41579-022-00713-0.

Lan, J. *et al.* (2020) 'Structure of the SARS-CoV-2 spike receptor-binding domain bound to the ACE2 receptor', *Nature*, 581(7807), pp. 215–220. Available at: https://doi.org/10.1038/s41586-020-2180-5.

Latifi-Pupovci, H. (2022) 'Molecular mechanisms involved in pathogenicity of SARS-CoV-2: Immune evasion and implications for therapeutic strategies', *Biomedicine & Pharmacotherapy*, 153, p. 113368. Available at: https://doi.org/10.1016/j.biopha.2022.113368.

Lee, J.S. *et al.* (2020) 'Immunophenotyping of COVID-19 and influenza highlights the role of type I interferons in development of severe COVID-19', *Science Immunology*, 5(49). Available at: https://doi.org/10.1126/sciimmunol.abd1554.

Lei, J., Kusov, Y. and Hilgenfeld, R. (2018) 'Nsp3 of coronaviruses: Structures and functions of a large multi-domain protein', *Antiviral Research*, 149, pp. 58–74. Available at: https://doi.org/10.1016/j.antiviral.2017.11.001.

Lei, X. *et al.* (2020) 'Activation and evasion of type I interferon responses by SARS-CoV-2', *Nature Communications*, 11(1). Available at: https://doi.org/10.1038/s41467-020-17665-9.

Li, Qun *et al.* (2020) 'Early Transmission Dynamics in Wuhan, China, of Novel Coronavirus–Infected Pneumonia', *New England Journal of Medicine*, 382(13), pp. 1199–1207. Available at: https://doi.org/10.1056/nejmoa2001316.

Li, Qianqian *et al.* (2020) 'The Impact of Mutations in SARS-CoV-2 Spike on Viral Infectivity and Antigenicity', *Cell*, 182(5), pp. 1284-1294.e9. Available at: https://doi.org/10.1016/j.cell.2020.07.012.

Li, Y. *et al.* (2005) 'Role of air distribution in SARS transmission during the largest nosocomial outbreak in Hong Kong', *Indoor Air*, 15(2), pp. 83–95. Available at: https://doi.org/10.1111/j.1600-0668.2004.00317.x.

Li, Y. *et al.* (2023) 'Structural Basis for the Enhanced Infectivity and Immune Evasion of Omicron Subvariants', *Viruses*, 15(6), p. 1398. Available at: https://doi.org/10.3390/v15061398.

Li, Z. and Buck, M. (2021) 'Neuropilin-1 assists SARS-CoV-2 infection by stimulating the separation of Spike protein S1 and S2', *Biophysical Journal*, 120(14), pp. 2828–2837. Available at: https://doi.org/10.1016/j.bpj.2021.05.026.

Liao, M. *et al.* (2020) 'Single-cell landscape of bronchoalveolar immune cells in patients with COVID-19', *Nature Medicine*, 26(6), pp. 842–844. Available at: https://doi.org/10.1038/s41591-020-0901-9.

Liu, C. *et al.* (2021) 'Reduced neutralization of SARS-CoV-2 B.1.617 by vaccine and convalescent serum', *Cell*, 184(16), pp. 4220-4236.e13. Available at: https://doi.org/10.1016/j.cell.2021.06.020.

Liu, D.X., Yuan, Q. and Liao, Y. (2007) 'Coronavirus envelope protein: A small membrane protein with multiple functions', *Cellular and Molecular Life Sciences*, 64(16), pp. 2043–2048. Available at: https://doi.org/10.1007/s00018-007-7103-1.

Liu, Jing *et al.* (2020) 'Longitudinal characteristics of lymphocyte responses and cytokine profiles in the peripheral blood of SARS-CoV-2 infected patients', *eBioMedicine*, 55, p. 102763. Available at: https://doi.org/10.1016/j.ebiom.2020.102763.

Loo, Y.-M. and Gale, M. (2011) 'Immune Signaling by RIG-I-like Receptors', *Immunity*, 34(5), pp. 680–692. Available at: https://doi.org/10.1016/j.immuni.2011.05.003.

Lu, X. *et al.* (2010) 'SARS-CoV nucleocapsid protein antagonizes IFN-β response by targeting initial step of IFN-β induction pathway, and its C-terminal region is

critical for the antagonism', *Virus Genes*, 42(1), pp. 37–45. Available at: https://doi.org/10.1007/s11262-010-0544-x.

Lubinski, B. and Whittaker, G.R. (2024) 'Host Cell Proteases Involved in Human Respiratory Viral Infections and Their Inhibitors: A Review', *Viruses*, 16(6), p. 984. Available at: https://doi.org/10.3390/v16060984.

Lucas, C. *et al.* (2020) 'Longitudinal analyses reveal immunological misfiring in severe COVID-19', *Nature*, 584(7821), pp. 463–469. Available at: https://doi.org/10.1038/s41586-020-2588-y.

Lythgoe, K.A. *et al.* (2021) 'SARS-CoV-2 within-host diversity and transmission', *Science*, 372(6539). Available at: https://doi.org/10.1126/science.abg0821.

Ma, Y. *et al.* (2015) 'Structural basis and functional analysis of the SARS coronavirus nsp14–nsp10 complex', *Proceedings of the National Academy of Sciences*, 112(30), pp. 9436–9441. Available at: https://doi.org/10.1073/pnas.1508686112.

Ma, Y. *et al.* (2023) 'Long-Term Consequences of Asymptomatic SARS-CoV-2 Infection: A Systematic Review and Meta-Analysis', *International Journal of Environmental Research and Public Health*, 20(2), p. 1613. Available at: https://doi.org/10.3390/ijerph20021613.

MAESTRO --- biwww.che.sbg.ac.at (no date). Available at: http://biwww.che.sbg.ac.at/MAESTRO (Accessed: 12 January 2025).

Manfrini, N. *et al.* (2024) 'SARS-CoV-2: A Glance at the Innate Immune Response Elicited by Infection and Vaccination', *Antibodies*, 13(1), p. 13. Available at: https://doi.org/10.3390/antib13010013.

Mantlo, E. *et al.* (2020) 'Antiviral activities of type I interferons to SARS-CoV-2 infection', *Antiviral Research*, 179, p. 104811. Available at: https://doi.org/10.1016/j.antiviral.2020.104811.

Markov, P. V *et al.* (2023) 'The evolution of SARS-CoV-2', *Nature Reviews Microbiology*, 21(6), pp. 361–379. Available at: https://doi.org/10.1038/s41579-023-00878-2.

Marques-Pereira, C. *et al.* (2022) 'SARS-CoV-2 Membrane Protein: From Genomic Data to Structural New Insights', *International Journal of Molecular Sciences*, 23(6), p. 2986. Available at: https://doi.org/10.3390/ijms23062986.

Mateu, L. *et al.* (2023) 'Determinants of the onset and prognosis of the post-COVID-19 condition: a 2-year prospective observational cohort study', *The Lancet Regional Health - Europe*, 33, p. 100724. Available at: https://doi.org/10.1016/j.lanepe.2023.100724.

Maxmen, A. (2022) 'Are new Omicron subvariants a threat? Here's how scientists are keeping watch', *Nature*, 604(7907), pp. 605–606. Available at: https://doi.org/10.1038/d41586-022-01069-4.

Mazzoni, A. *et al.* (2020) 'Impaired immune cell cytotoxicity in severe COVID-19 is IL-6 dependent', *Journal of Clinical Investigation*, 130(9), pp. 4694–4703. Available at: https://doi.org/10.1172/jci138554.

McGonagle, D. *et al.* (2020) 'The Role of Cytokines including Interleukin-6 in COVID-19 induced Pneumonia and Macrophage Activation Syndrome-Like Disease', *Autoimmunity Reviews*, 19(6), p. 102537. Available at: https://doi.org/10.1016/j.autrev.2020.102537.

McMenamin, M.E. *et al.* (2022) 'Vaccine effectiveness of one, two, and three doses of BNT162b2 and CoronaVac against COVID-19 in Hong Kong: a population-based observational study', *The Lancet Infectious Diseases*, 22(10), pp. 1435–1443. Available at: https://doi.org/10.1016/s1473-3099(22)00345-0.

Menachery, V.D., Debbink, K. and Baric, R.S. (2014) 'Coronavirus non-structural protein 16: Evasion, attenuation, and possible treatments', *Virus Research*, 194, pp. 191–199. Available at: https://doi.org/10.1016/j.virusres.2014.09.009.

Menezes, S.M. *et al.* (2024) 'Blood transcriptomic analyses reveal persistent SARS-CoV-2 RNA and candidate biomarkers in post-COVID-19 condition', *The Lancet Microbe*, 5(8), p. 100849. Available at: https://doi.org/10.1016/s2666-5247(24)00055-7.

Meyer, B., Drosten, C. and Müller, M.A. (2014) 'Serological assays for emerging coronaviruses: Challenges and pitfalls', *Virus Research*, 194, pp. 175–183. Available at: https://doi.org/10.1016/j.virusres.2014.03.018.

Miao, L. *et al.* (2023) 'SIM imaging resolves endocytosis of SARS-CoV-2 spike RBD in living cells', *Cell Chemical Biology*, 30(3), pp. 248-260.e4. Available at: https://doi.org/10.1016/j.chembiol.2023.02.001.

Milan Bonotto, R. *et al.* (2023) 'Cathepsin inhibitors nitroxoline and its derivatives inhibit SARS-CoV-2 infection', *Antiviral Research*, 216, p. 105655. Available at: https://doi.org/10.1016/j.antiviral.2023.105655.

Miller, J. *et al.* (2023) 'Substantial Neutralization Escape by SARS-CoV-2 Omicron Variants BQ.1.1 and XBB.1', *New England Journal of Medicine*, 388(7), pp. 662–664. Available at: https://doi.org/10.1056/nejmc2214314.

Minkoff, J.M. and tenOever, B. (2023) 'Innate immune evasion strategies of SARS-CoV-2', *Nature Reviews Microbiology* [Preprint]. Available at: https://doi.org/10.1038/s41579-022-00839-1.

Mizumoto, K. *et al.* (2020) 'Estimating the asymptomatic proportion of coronavirus disease 2019 (COVID-19) cases on board the Diamond Princess cruise ship, Yokohama, Japan, 2020', *Eurosurveillance*, 25(10). Available at: https://doi.org/10.2807/1560-7917.es.2020.25.10.2000180.

Mlcochova, P. *et al.* (2021) 'SARS-CoV-2 B.1.617.2 Delta variant replication and immune evasion', *Nature*, 599(7883), pp. 114–119. Available at: https://doi.org/10.1038/s41586-021-03944-y.

Mohammad, T. *et al.* (2021) 'Genomic Variations in the Structural Proteins of SARS-CoV-2 and Their Deleterious Impact on Pathogenesis: A Comparative Genomics Approach', *Frontiers in Cellular and Infection Microbiology*, 11. Available at: https://doi.org/10.3389/fcimb.2021.765039.

Moon, C. (2020) 'Fighting COVID-19 exhausts T cells', *Nature Reviews Immunology*, 20(5), p. 277. Available at: https://doi.org/10.1038/s41577-020-0304-7.

Moriyama, S. *et al.* (2023) 'Structural delineation and computational design of SARS-CoV-2-neutralizing antibodies against Omicron subvariants', *Nature Communications*, 14(1). Available at: https://doi.org/10.1038/s41467-023-39890-8.

Mou, K. *et al.* (2021) 'Emerging mutations in envelope protein of SARS-CoV-2 and their effect on thermodynamic properties', *Informatics in Medicine Unlocked*, 25, p. 100675. Available at: https://doi.org/10.1016/j.imu.2021.100675.

Muus, C. *et al.* (2021) 'Single-cell meta-analysis of SARS-CoV-2 entry genes across tissues and demographics', *Nature Medicine*, 27(3), pp. 546–559. Available at: https://doi.org/10.1038/s41591-020-01227-z.

Nextclade --- clades.nextstrain.org (no date). Available at: https://clades.nextstrain.org (Accessed: 12 January 2025).

Ning, S., Pagano, J.S. and Barber, G.N. (2011) 'IRF7: activation, regulation, modification and function', *Genes & Immunity*, 12(6), pp. 399–414. Available at: https://doi.org/10.1038/gene.2011.21.

O'Connell, P. and Aldhamen, Y.A. (2020) 'Systemic innate and adaptive immune responses to SARS-CoV-2 as it relates to other coronaviruses', *Human Vaccines & Immunotherapeutics*, 16(12), pp. 2980–2991. Available at: https://doi.org/10.1080/21645515.2020.1802974.

Oostra, M. *et al.* (2008) 'Topology and Membrane Anchoring of the Coronavirus Replication Complex: Not All Hydrophobic Domains of nsp3 and nsp6 Are Membrane Spanning', *Journal of Virology*, 82(24), pp. 12392–12405. Available at: https://doi.org/10.1128/jvi.01219-08.

Ortiz-Prado, E. *et al.* (2020) 'Clinical, molecular, and epidemiological characterization of the SARS-CoV-2 virus and the Coronavirus Disease 2019 (COVID-19), a comprehensive literature review', *Diagnostic Microbiology and Infectious Disease*, 98(1), p. 115094. Available at: https://doi.org/10.1016/j.diagmicrobio.2020.115094.

Otter, J.A. *et al.* (2016) 'Transmission of SARS and MERS coronaviruses and influenza virus in healthcare settings: the possible role of dry surface contamination', *Journal of Hospital Infection*, 92(3), pp. 235–250. Available at: https://doi.org/10.1016/j.jhin.2015.08.027.

Ou, X. *et al.* (2020) 'Characterization of spike glycoprotein of SARS-CoV-2 on virus entry and its immune cross-reactivity with SARS-CoV', *Nature Communications*, 11(1). Available at: https://doi.org/10.1038/s41467-020-15562-9.

Padoan, A. *et al.* (2020) 'IgA-Ab response to spike glycoprotein of SARS-CoV-2 in patients with COVID-19: A longitudinal study', *Clinica Chimica Acta*, 507, pp. 164–166. Available at: https://doi.org/10.1016/j.cca.2020.04.026.

Pardi, N. *et al.* (2018) 'mRNA vaccines — a new era in vaccinology', *Nature Reviews Drug Discovery*, 17(4), pp. 261–279. Available at: https://doi.org/10.1038/nrd.2017.243.

Pardi, N., Hogan, M.J. and Weissman, D. (2020) 'Recent advances in mRNA vaccine technology', *Current Opinion in Immunology*, 65, pp. 14–20. Available at: https://doi.org/10.1016/j.coi.2020.01.008.

Park, M.D. (2020) 'Macrophages: a Trojan horse in COVID-19?', *Nature Reviews Immunology*, 20(6), p. 351. Available at: https://doi.org/10.1038/s41577-020-0317-2.

Park, S.B. *et al.* (2023) 'SARS-CoV-2 omicron variants harbor spike protein mutations responsible for their attenuated fusogenic phenotype', *Communications Biology*, 6(1). Available at: https://doi.org/10.1038/s42003-023-04923-x.

Park, Y.-J. *et al.* (2022) 'Imprinted antibody responses against SARS-CoV-2 Omicron sublineages', *Science*, 378(6620), pp. 619–627. Available at: https://doi.org/10.1126/science.adc9127.

Peacock, T.P. *et al.* (2021) 'The furin cleavage site in the SARS-CoV-2 spike protein is required for transmission in ferrets', *Nature Microbiology*, 6(7), pp. 899–909. Available at: https://doi.org/10.1038/s41564-021-00908-w.

Peiris, J. *et al.* (2003) 'Coronavirus as a possible cause of severe acute respiratory syndrome', *The Lancet*, 361(9366), pp. 1319–1325. Available at: https://doi.org/10.1016/S0140-6736(03)13077-2.

Peiris, J.S.M. *et al.* (2003) 'Clinical progression and viral load in a community outbreak of coronavirus-associated SARS pneumonia: a prospective study', *The Lancet*, 361(9371), pp. 1767–1772. Available at: https://doi.org/10.1016/s0140-6736(03)13412-5.

Peng, Q. *et al.* (2020) 'Structural and Biochemical Characterization of the nsp12-nsp7-nsp8 Core Polymerase Complex from SARS-CoV-2', *Cell Reports*, 31(11), p. 107774. Available at: https://doi.org/10.1016/j.celrep.2020.107774.

Petit, C.M. *et al.* (2005) 'Genetic analysis of the SARS-coronavirus spike glycoprotein functional domains involved in cell-surface expression and cell-to-cell fusion', *Virology*, 341(2), pp. 215–230. Available at: https://doi.org/10.1016/j.virol.2005.06.046.

Piccoli, L. *et al.* (2020) 'Mapping Neutralizing and Immunodominant Sites on the SARS-CoV-2 Spike Receptor-Binding Domain by Structure-Guided High-Resolution Serology', *Cell*, 183(4), pp. 1024-1042.e21. Available at: https://doi.org/10.1016/j.cell.2020.09.037.

Pillon, M.C. *et al.* (2021) 'Cryo-EM structures of the SARS-CoV-2 endoribonuclease Nsp15 reveal insight into nuclease specificity and dynamics', *Nature Communications*, 12(1). Available at: https://doi.org/10.1038/s41467-020-20608-z.

Pioli, P.D. (2019) 'Plasma Cells, the Next Generation: Beyond Antibody Secretion', *Frontiers in Immunology*, 10. Available at: https://doi.org/10.3389/fimmu.2019.02768.

Pišlar, A. *et al.* (2020) 'The role of cysteine peptidases in coronavirus cell entry and replication: The therapeutic potential of cathepsin inhibitors', *PLOS Pathogens*. Edited by T.C. Hobman, 16(11), p. e1009013. Available at: https://doi.org/10.1371/journal.ppat.1009013.

Planas, D. *et al.* (2021) 'Reduced sensitivity of SARS-CoV-2 variant Delta to antibody neutralization', *Nature*, 596(7871), pp. 276–280. Available at: https://doi.org/10.1038/s41586-021-03777-9.

Puhach, O. *et al.* (2022) 'Infectious viral load in unvaccinated and vaccinated individuals infected with ancestral, Delta or Omicron SARS-CoV-2', *Nature Medicine*, 28(7), pp. 1491–1500. Available at: https://doi.org/10.1038/s41591-022-01816-0.

Pung, R. *et al.* (2021) 'Factors influencing SARS-CoV-2 transmission and outbreak control measures in densely populated settings', *Scientific Reports*, 11(1), p. 15297. Available at: https://doi.org/10.1038/s41598-021-94463-3.

Qu, P. *et al.* (2022) 'Evasion of Neutralizing Antibody Response by the SARS-CoV-2 BA.2.75 Variant'. Available at: https://doi.org/10.1101/2022.08.14.503921.

Quinti, I. *et al.* (2021) 'IgA Antibodies and IgA Deficiency in SARS-CoV-2 Infection', *Frontiers in Cellular and Infection Microbiology*, 11. Available at: https://doi.org/10.3389/fcimb.2021.655896.

Rahimi, A., Mirzazadeh, A. and Tavakolpour, S. (2021) 'Genetics and genomics of SARS-CoV-2: A review of the literature with the special focus on genetic diversity and SARS-CoV-2 genome detection', *Genomics*, 113(1), pp. 1221–1232. Available at: https://doi.org/10.1016/j.ygeno.2020.09.059.

Rai, S. *et al.* (2012) 'Evaluation of the Antimicrobial Properties of Copper Surfaces in an Outpatient Infectious Disease Practice', *Infection Control & Hospital Epidemiology*, 33(2), pp. 200–201. Available at: https://doi.org/10.1086/663701.

Rashid, F. *et al.* (2022) 'Roles and functions of SARS-CoV-2 proteins in host immune evasion', *Frontiers in Immunology*, 13. Available at: https://doi.org/10.3389/fimmu.2022.940756.

Redondo, N. *et al.* (2021) 'SARS-CoV-2 Accessory Proteins in Viral Pathogenesis: Knowns and Unknowns', *Frontiers in Immunology*, 12. Available at: https://doi.org/10.3389/fimmu.2021.708264.

Reeve, L. *et al.* (2023) 'High attack rate in a large care home outbreak of SARS-CoV-2 BA.2.86, East of England, August 2023', *Eurosurveillance*, 28(39). Available at: https://doi.org/10.2807/1560-7917.es.2023.28.39.2300489.

Ren, W. *et al.* (2023) 'Evolution of Immune Evasion and Host Range Expansion by the SARS-CoV-2 B.1.1.529 (Omicron) Variant', *mBio*. Edited by X.-J. Meng, 14(2). Available at: https://doi.org/10.1128/mbio.00416-23.

Rhee, C. *et al.* (2020) 'Duration of Severe Acute Respiratory Syndrome Coronavirus 2 (SARS-CoV-2) Infectivity: When Is It Safe to Discontinue Isolation?', *Clinical Infectious Diseases*, 72(8), pp. 1467–1474. Available at: https://doi.org/10.1093/cid/ciaa1249.

Richard, A.S. *et al.* (2017) 'AXL-dependent infection of human fetal endothelial cells distinguishes Zika virus from other pathogenic flaviviruses', *Proceedings of the National Academy of Sciences*, 114(8), pp. 2024–2029. Available at: https://doi.org/10.1073/pnas.1620558114.

Rizvi, A. *et al.* (2023) 'Gastrointestinal and Hepatobiliary Symptoms and Disorders with Long (Chronic) COVID Infection', *Gastroenterology Clinics of North America*, 52(1), pp. 139–156. Available at: https://doi.org/10.1016/j.gtc.2022.09.002.

Robinot, R. *et al.* (2021) 'SARS-CoV-2 infection induces the dedifferentiation of multiciliated cells and impairs mucociliary clearance', *Nature Communications*, 12(1). Available at: https://doi.org/10.1038/s41467-021-24521-x.

Robson, F. *et al.* (2020) 'Coronavirus RNA Proofreading: Molecular Basis and Therapeutic Targeting', *Molecular Cell*, 79(5), pp. 710–727. Available at: https://doi.org/10.1016/j.molcel.2020.07.027.

Roe, M.K. *et al.* (2021) 'Targeting novel structural and functional features of coronavirus protease nsp5 (3CLpro, Mpro) in the age of COVID-19', *Journal of General Virology*, 102(3). Available at: https://doi.org/10.1099/jgv.0.001558.

Romano, M. *et al.* (2020) 'A Structural View of SARS-CoV-2 RNA Replication Machinery: RNA Synthesis, Proofreading and Final Capping', *Cells*, 9(5), p. 1267. Available at: https://doi.org/10.3390/cells9051267.

Romeo, A. *et al.* (2022) 'Potential Use of Tea Tree Oil as a Disinfectant Agent against Coronaviruses: A Combined Experimental and Simulation Study', *Molecules*, 27(12), p. 3786. Available at: https://doi.org/10.3390/molecules27123786.

Rosa, S.S. *et al.* (2021) 'mRNA vaccines manufacturing: Challenges and bottlenecks', *Vaccine*, 39(16), pp. 2190–2200. Available at: https://doi.org/10.1016/j.vaccine.2021.03.038.

Roy, A. V *et al.* (2024) 'Quercetin inhibits SARS-CoV-2 infection and prevents syncytium formation by cells co-expressing the viral spike protein and human ACE2', *Virology Journal*, 21(1). Available at: https://doi.org/10.1186/s12985-024-02299-w.

Russell, C.J. (2021) 'Hemagglutinin Stability and Its Impact on Influenza A Virus Infectivity, Pathogenicity, and Transmissibility in Avians, Mice, Swine, Seals, Ferrets, and Humans', *Viruses*, 13(5), p. 746. Available at: https://doi.org/10.3390/v13050746.

Sa Ribero, M. *et al.* (2020) 'Interplay between SARS-CoV-2 and the type I interferon response', *PLOS Pathogens*. Edited by K. Stapleford, 16(7), p. e1008737. Available at: https://doi.org/10.1371/journal.ppat.1008737.

Sah, P. *et al.* (2021) 'Asymptomatic SARS-CoV-2 infection: A systematic review and meta-analysis', *Proceedings of the National Academy of Sciences*, 118(34). Available at: https://doi.org/10.1073/pnas.2109229118.

Šali, A. and Blundell, T.L. (1993) 'Comparative Protein Modelling by Satisfaction of Spatial Restraints', *Journal of Molecular Biology*, 234(3), pp. 779–815. Available at: https://doi.org/10.1006/jmbi.1993.1626.

Santopolo, S., Riccio, A. and Santoro, M.G. (2021) 'The biogenesis of SARS-CoV-2 spike glycoprotein: multiple targets for host-directed antiviral therapy', *Biochemical and Biophysical Research Communications*, 538, pp. 80–87. Available at: https://doi.org/10.1016/j.bbrc.2020.10.080.

Santoro, L. *et al.* (2023) 'Role of Endothelium in Cardiovascular Sequelae of Long COVID', *Biomedicines*, 11(8), p. 2239. Available at: https://doi.org/10.3390/biomedicines11082239.

Saris, A. *et al.* (2021) 'Distinct cellular immune profiles in the airways and blood of critically ill patients with COVID-19', *Thorax*, 76(10), pp. 1010–1019. Available at: https://doi.org/10.1136/thoraxjnl-2020-216256.

Sars-CoV-2 circulating variants (no date). Available at: https://viralzone.expasy.org/9556 (Accessed: 18 January 2025).

SARS-CoV-2 variants of concern as of 20 December 2024 --- ecdc.europa.eu (no date). Available at: https://www.ecdc.europa.eu/en/covid-19/variants-concern (Accessed: 12 January 2025).

Satarker, S. and Nampoothiri, M. (2020) 'Structural Proteins in Severe Acute Respiratory Syndrome Coronavirus-2', *Archives of Medical Research*, 51(6), pp. 482–491. Available at: https://doi.org/10.1016/j.arcmed.2020.05.012.

Saunders, N. *et al.* (2023) 'TMPRSS2 is a functional receptor for human coronavirus HKU1', *Nature*, 624(7990), pp. 207–214. Available at: https://doi.org/10.1038/s41586-023-06761-7.

Scepankova, H. *et al.* (2021) 'Conventional and emergent technologies for honey processing: A perspective on microbiological safety, bioactivity, and quality', *Comprehensive Reviews in Food Science and Food Safety*, 20(6), pp. 5393–5420. Available at: https://doi.org/10.1111/1541-4337.12848.

Schneider, W.M., Chevillotte, M.D. and Rice, C.M. (2014) 'Interferon-Stimulated Genes: A Complex Web of Host Defenses', *Annual Review of Immunology*, 32(1), pp. 513–545. Available at: https://doi.org/10.1146/annurev-immunol-032713-120231.

Schreiber, G. (2020) 'The Role of Type I Interferons in the Pathogenesis and Treatment of COVID-19', *Frontiers in Immunology*, 11. Available at: https://doi.org/10.3389/fimmu.2020.595739.

Schultze, J.L. and Aschenbrenner, A.C. (2021) 'COVID-19 and the human innate immune system', *Cell*, 184(7), pp. 1671–1692. Available at: https://doi.org/10.1016/j.cell.2021.02.029.

Scialo, F. *et al.* (2020) 'ACE2: The Major Cell Entry Receptor for SARS-CoV-2', *Lung*, 198(6), pp. 867–877. Available at: https://doi.org/10.1007/s00408-020-00408-4.

Shang, J. *et al.* (2020) 'Structural basis of receptor recognition by SARS-CoV-2', *Nature*, 581(7807), pp. 221–224. Available at: https://doi.org/10.1038/s41586-020-2179-y.

Shekunov, E. V *et al.* (2023) 'Cyclic lipopeptides as membrane fusion inhibitors against SARS-CoV-2: New tricks for old dogs', *Antiviral Research*, 212, p. 105575. Available at: https://doi.org/10.1016/j.antiviral.2023.105575.

Shrestha, L.B. *et al.* (2022) 'Evolution of the SARS-CoV-2 omicron variants BA.1 to BA.5: Implications for immune escape and transmission', *Reviews in Medical Virology*, 32(5). Available at: https://doi.org/10.1002/rmv.2381.

Singh, K.K. *et al.* (2020) 'Decoding SARS-CoV-2 hijacking of host mitochondria in COVID-19 pathogenesis', *American Journal of Physiology-Cell Physiology*, 319(2), pp. C258–C267. Available at: https://doi.org/10.1152/ajpcell.00224.2020.

Sinha, A., Sangeet, S. and Roy, S. (2023) 'Evolution of Sequence and Structure of SARS-CoV-2 Spike Protein: A Dynamic Perspective', *ACS Omega*, 8(26), pp. 23283–23304. Available at: https://doi.org/10.1021/acsomega.3c00944.

Solanki, K. *et al.* (2022) 'Structural Analysis of Spike Proteins from SARS-CoV-2 Variants of Concern Highlighting Their Functional Alterations', *Future Virology*, 17(10), pp. 723–732. Available at: https://doi.org/10.2217/fvl-2022-0003.

Spinner, C.D. *et al.* (2020) 'Effect of Remdesivir vs Standard Care on Clinical Status at 11 Days in Patients With Moderate COVID-19: A Randomized Clinical Trial', *JAMA*, 324(11), p. 1048. Available at: https://doi.org/10.1001/jama.2020.16349.

Sposito, B. *et al.* (2021) 'The interferon landscape along the respiratory tract impacts the severity of COVID-19', *Cell*, 184(19), pp. 4953-4968.e16. Available at: https://doi.org/10.1016/j.cell.2021.08.016.

Stanford Coronavirus Antiviral & Resistance Database (CoVDB) --- covdb.stanford.edu (no date). Available at: https://covdb.stanford.edu/sierra/sars2/by-patterns (Accessed: 12 January 2025).

Stone, J.H. *et al.* (2020) 'Efficacy of Tocilizumab in Patients Hospitalized with Covid-19', *New England Journal of Medicine*, 383(24), pp. 2333–2344. Available at: https://doi.org/10.1056/nejmoa2028836.

Storti, B. *et al.* (2021) 'A spatial multi-scale fluorescence microscopy toolbox discloses entry checkpoints of SARS-CoV-2 variants in Vero E6 cells', *Computational and Structural Biotechnology Journal*, 19, pp. 6140–6156. Available at: https://doi.org/10.1016/j.csbj.2021.10.038.

Subramanian, G. *et al.* (2018) 'A new mechanism of interferon's antiviral action: Induction of autophagy, essential for paramyxovirus replication, is inhibited by the interferon stimulated gene, TDRD7', *PLOS Pathogens*. Edited by C.F. Basler, 14(1), p. e1006877. Available at: https://doi.org/10.1371/journal.ppat.1006877.

Sun, C. *et al.* (2022) 'Molecular characteristics, immune evasion, and impact of SARS-CoV-2 variants', *Signal Transduction and Targeted Therapy*, 7(1). Available at: https://doi.org/10.1038/s41392-022-01039-2.

Sun, H. *et al.* (2023) 'Structural basis for broad neutralization of human antibody against Omicron sublineages and evasion by XBB variant', *Journal of Virology*, 97(11). Available at: https://doi.org/10.1128/jvi.01137-23.

Surya, W., Li, Y. and Torres, J. (2018) 'Structural model of the SARS coronavirus E channel in LMPG micelles', *Biochimica et Biophysica Acta (BBA) - Biomembranes*, 1860(6), pp. 1309–1317. Available at: https://doi.org/10.1016/j.bbamem.2018.02.017.

Suthar, M.S. *et al.* (2020) 'Rapid Generation of Neutralizing Antibody Responses in COVID-19 Patients', *Cell Reports Medicine*, 1(3), p. 100040. Available at: https://doi.org/10.1016/j.xcrm.2020.100040.

Taefehshokr, N. *et al.* (2020) 'Covid-19: Perspectives on Innate Immune Evasion', *Frontiers in Immunology*, 11. Available at: https://doi.org/10.3389/fimmu.2020.580641.

Tamura, T. *et al.* (2024) 'Virological characteristics of the SARS-CoV-2 BA.2.86 variant', *Cell Host & Microbe*, 32(2), pp. 170-180.e12. Available at: https://doi.org/10.1016/j.chom.2024.01.001.

Tang, S. *et al.* (2020) 'Aerosol transmission of SARS-CoV-2? Evidence, prevention and control', *Environment International*, 144, p. 106039. Available at: https://doi.org/10.1016/j.envint.2020.106039.

Tarke, A. *et al.* (2021) 'Comprehensive analysis of T cell immunodominance and immunoprevalence of SARS-CoV-2 epitopes in COVID-19 cases', *Cell Reports Medicine*, 2(2), p. 100204. Available at: https://doi.org/10.1016/j.xcrm.2021.100204.

Tay, M.Z. *et al.* (2020) 'The trinity of COVID-19: immunity, inflammation and intervention', *Nature Reviews Immunology*, 20(6), pp. 363–374. Available at: https://doi.org/10.1038/s41577-020-0311-8.

Tegally, H. *et al.* (2021) 'Detection of a SARS-CoV-2 variant of concern in South Africa', *Nature*, 592(7854), pp. 438–443. Available at: https://doi.org/10.1038/s41586-021-03402-9.

Temsah, M.-H. *et al.* (2022) 'SARS-CoV-2 Omicron Variant: Exploring Healthcare Workers' Awareness and Perception of Vaccine Effectiveness: A National Survey During the First Week of WHO Variant Alert', *Frontiers in Public Health*, 10. Available at: https://doi.org/10.3389/fpubh.2022.878159.

The Human Protein Atlas --- proteinatlas.org (no date). Available at: https://www.proteinatlas.org/ (Accessed: 12 January 2025).

Thomas, S. (2021) 'Mapping the Nonstructural Transmembrane Proteins of Severe Acute Respiratory Syndrome Coronavirus 2', *Journal of Computational Biology*, 28(9), pp. 909–921. Available at: https://doi.org/10.1089/cmb.2020.0627.

Tirelli, C. *et al.* (2023) 'Exploring the Role of Immune System and Inflammatory Cytokines in SARS-CoV-2 Induced Lung Disease: A Narrative Review', *Biology*, 12(2), p. 177. Available at: https://doi.org/10.3390/biology12020177.

Tracking SARS-CoV-2 variants --- who.int (no date). Available at: https://www.who.int/activities/tracking-SARS-CoV-2-variants/ (Accessed: 12 January 2025).

Update on Omicron --- who.int (no date). Available at: https://www.who.int/news/item/28-11-2021-update-on-omicron (Accessed: 12 January 2025).

Uraki, R. *et al.* (2023) 'Characterization of a SARS-CoV-2 EG.5.1 clinical isolate in vitro and in vivo', *Cell Reports*, 42(12), p. 113580. Available at: https://doi.org/10.1016/j.celrep.2023.113580.

VanBlargan, L.A. *et al.* (2022) 'An infectious SARS-CoV-2 B.1.1.529 Omicron virus escapes neutralization by therapeutic monoclonal antibodies', *Nature Medicine*, 28(3), pp. 490–495. Available at: https://doi.org/10.1038/s41591-021-01678-y.

te Velthuis, A.J.W. and Fodor, E. (2016) 'Influenza virus RNA polymerase: insights into the mechanisms of viral RNA synthesis', *Nature Reviews Microbiology*, 14(8), pp. 479–493. Available at: https://doi.org/10.1038/nrmicro.2016.87.

Viana, R. *et al.* (2022) 'Rapid epidemic expansion of the SARS-CoV-2 Omicron variant in southern Africa', *Nature*, 603(7902), pp. 679–686. Available at: https://doi.org/10.1038/s41586-022-04411-y.

Viswanathan, T. *et al.* (2020) 'Structural basis of RNA cap modification by SARS-CoV-2', *Nature Communications*, 11(1). Available at: https://doi.org/10.1038/s41467-020-17496-8.

V'kovski, P. *et al.* (2020) 'Coronavirus biology and replication: implications for SARS-CoV-2', *Nature Reviews Microbiology*, 19(3), pp. 155–170. Available at: https://doi.org/10.1038/s41579-020-00468-6.

Wagner, A. *et al.* (2021) 'Neutralising SARS-CoV-2 RBD-specific antibodies persist for at least six months independently of symptoms in adults', *Communications Medicine*, 1(1). Available at: https://doi.org/10.1038/s43856-021-00012-4.

Walls, A.C. *et al.* (2016) 'Glycan shield and epitope masking of a coronavirus spike protein observed by cryo-electron microscopy', *Nature Structural & Molecular Biology*, 23(10), pp. 899–905. Available at: https://doi.org/10.1038/nsmb.3293.

Wan, Y. *et al.* (2020) 'Receptor Recognition by the Novel Coronavirus from Wuhan: an Analysis Based on Decade-Long Structural Studies of SARS Coronavirus', *Journal of Virology*. Edited by T. Gallagher, 94(7). Available at: https://doi.org/10.1128/jvi.00127-20.

Wang, C. *et al.* (2020) 'A human monoclonal antibody blocking SARS-CoV-2 infection', *Nature Communications*, 11(1). Available at: https://doi.org/10.1038/s41467-020-16256-y.

Wang, K. *et al.* (2020) 'CD147-spike protein is a novel route for SARS-CoV-2 infection to host cells', *Signal Transduction and Targeted Therapy*, 5(1), p. 283. Available at: https://doi.org/10.1038/s41392-020-00426-x.

Wang, Q. *et al.* (2020) 'Structural Basis for RNA Replication by the SARS-CoV-2 Polymerase', *Cell*, 182(2), pp. 417-428.e13. Available at: https://doi.org/10.1016/j.cell.2020.05.034.

Wang, Q. *et al.* (2023) 'Alarming antibody evasion properties of rising SARS-CoV-2 BQ and XBB subvariants', *Cell*, 186(2), pp. 279-286.e8. Available at: https://doi.org/10.1016/j.cell.2022.12.018.

Wang, S. *et al.* (2021) 'AXL is a candidate receptor for SARS-CoV-2 that promotes infection of pulmonary and bronchial epithelial cells', *Cell Research*, 31(2), pp. 126–140. Available at: https://doi.org/10.1038/s41422-020-00460-y.

Wang, Y. *et al.* (2020) 'A comprehensive investigation of the mRNA and protein level of ACE2, the putative receptor of SARS-CoV-2, in human tissues and blood cells', *International Journal of Medical Sciences*, 17(11), pp. 1522–1531. Available at: https://doi.org/10.7150/ijms.46695.

Wathelet, M.G. *et al.* (2007) 'Severe Acute Respiratory Syndrome Coronavirus Evades Antiviral Signaling: Role of nsp1 and Rational Design of an Attenuated Strain', *Journal of Virology*, 81(21), pp. 11620–11633. Available at: https://doi.org/10.1128/jvi.00702-07.

Weinreich, D.M. *et al.* (2021) 'REGN-COV2, a Neutralizing Antibody Cocktail, in Outpatients with Covid-19', *New England Journal of Medicine*, 384(3), pp. 238–251. Available at: https://doi.org/10.1056/nejmoa2035002.

WHO – COVID19 Vaccine Tracker --- https://covid19.trackvaccines.org (no date). Available at: https://covid19.trackvaccines.org/agency/who/ (Accessed: 12 January 2025).

WHO Director-General's opening remarks at the media briefing on COVID-19 - 11 March 2020 (no date). Available at: https://www.who.int/director-general/speeches/detail/who-director-general-s-opening-remarks-at-the-media-briefing-on-covid-19---11-march-2020 (Accessed: 18 January 2025).

Wibmer, C.K. *et al.* (2021) 'SARS-CoV-2 501Y.V2 escapes neutralization by South African COVID-19 donor plasma', *Nature Medicine*, 27(4), pp. 622–625. Available at: https://doi.org/10.1038/s41591-021-01285-x.

Wiersinga, W.J. *et al.* (2020) 'Pathophysiology, Transmission, Diagnosis, and Treatment of Coronavirus Disease 2019 (COVID-19): A Review', *JAMA*, 324(8), p. 782. Available at: https://doi.org/10.1001/jama.2020.12839.

Willett, B.J. *et al.* (2022) 'SARS-CoV-2 Omicron is an immune escape variant with an altered cell entry pathway', *Nature Microbiology*, 7(8), pp. 1161–1179. Available at: https://doi.org/10.1038/s41564-022-01143-7.

Williams, T.L. *et al.* (2021) 'Differential expression in humans of the viral entry receptor ACE2 compared with the short deltaACE2 isoform lacking SARS-CoV-2 binding sites', *Scientific Reports*, 11(1). Available at: https://doi.org/10.1038/s41598-021-03731-9.

Wölfel, R. *et al.* (2020) 'Virological assessment of hospitalized patients with COVID-2019', *Nature*, 581(7809), pp. 465–469. Available at: https://doi.org/10.1038/s41586-020-2196-x.

World Health Organization (WHO) --- who.int (no date). Available at: https://www.who.int (Accessed: 12 January 2025).

World Health Statistics 2020 (no date). Available at: https://iris.who.int/bitstream/handle/10665/332070/9789240005105-eng.pdf (Accessed: 12 January 2025).

World health statistics 2021 (no date). Available at: https://iris.who.int/bitstream/handle/10665/342703/9789240027053-eng.pdf?sequence=1 (Accessed: 12 January 2025).

Wrapp, D. *et al.* (2020) 'Cryo-EM structure of the 2019-nCoV spike in the prefusion conformation', *Science*, 367(6483), pp. 1260–1263. Available at: https://doi.org/10.1126/science.abb2507.

Wu, D. *et al.* (2020) 'The SARS-CoV-2 outbreak: What we know', *International Journal of Infectious Diseases*, 94, pp. 44–48. Available at: https://doi.org/10.1016/j.ijid.2020.03.004.

Xiao, F. *et al.* (2020) 'Evidence for Gastrointestinal Infection of SARS-CoV-2', *Gastroenterology*, 158(6), pp. 1831-1833.e3. Available at: https://doi.org/10.1053/j.gastro.2020.02.055.

Yan, R. *et al.* (2020) 'Structural basis for the recognition of SARS-CoV-2 by full-length human ACE2', *Science*, 367(6485), pp. 1444–1448. Available at: https://doi.org/10.1126/science.abb2762.

Yan, R. *et al.* (2021) 'Structural basis for the different states of the spike protein of SARS-CoV-2 in complex with ACE2', *Cell Research*, 31(6), pp. 717–719. Available at: https://doi.org/10.1038/s41422-021-00490-0.

Yang, S. *et al.* (2024) 'Fast evolution of SARS-CoV-2 BA.2.86 to JN.1 under heavy immune pressure', *The Lancet Infectious Diseases*, 24(2), pp. e70–e72. Available at: https://doi.org/10.1016/S1473-3099(23)00744-2.

Yao, Z. *et al.* (2024) 'Molecular insights into the adaptive evolution of SARS-CoV-2 spike protein', *Journal of Infection*, 88(3), p. 106121. Available at: https://doi.org/10.1016/j.jinf.2024.106121.

Young, B.E. *et al.* (2020) 'Effects of a major deletion in the SARS-CoV-2 genome on the severity of infection and the inflammatory response: an observational cohort study', *The Lancet*, 396(10251), pp. 603–611. Available at: https://doi.org/10.1016/S0140-6736(20)31757-8.

Yu, I.T.S. *et al.* (2004) 'Evidence of Airborne Transmission of the Severe Acute Respiratory Syndrome Virus', *New England Journal of Medicine*, 350(17), pp. 1731–1739. Available at: https://doi.org/10.1056/nejmoa032867.

Yu, J. *et al.* (2022) 'Neutralization of the SARS-CoV-2 Omicron BA.1 and BA.2 Variants', *New England Journal of Medicine*, 386(16), pp. 1579–1580. Available at: https://doi.org/10.1056/NEJMc2201849.

Yu, X. *et al.* (2022) 'Reduced sensitivity of SARS-CoV-2 Omicron variant to antibody neutralization elicited by booster vaccination', *Cell Discovery*, 8(1). Available at: https://doi.org/10.1038/s41421-022-00375-5.

Yurkovetskiy, L. *et al.* (2020) 'Structural and Functional Analysis of the D614G SARS-CoV-2 Spike Protein Variant', *Cell*, 183(3), pp. 739-751.e8. Available at: https://doi.org/10.1016/j.cell.2020.09.032.

Zahradník, J. *et al.* (2021) 'SARS-CoV-2 variant prediction and antiviral drug design are enabled by RBD in vitro evolution', *Nature Microbiology*, 6(9), pp. 1188–1198. Available at: https://doi.org/10.1038/s41564-021-00954-4.

Zawilska, J.B. and Kuczyńska, K. (2022) 'Psychiatric and neurological complications of long COVID', *Journal of Psychiatric Research*, 156, pp. 349–360. Available at: https://doi.org/10.1016/j.jpsychires.2022.10.045.

Zhang, L. *et al.* (2024) 'SARS-CoV-2 BA.2.86 enters lung cells and evades neutralizing antibodies with high efficiency', *Cell*, 187(3), pp. 596-608.e17. Available at: https://doi.org/10.1016/j.cell.2023.12.025.

Zhang, Z. *et al.* (2022) 'Structure of SARS-CoV-2 membrane protein essential for virus assembly', *Nature Communications*, 13(1). Available at: https://doi.org/10.1038/s41467-022-32019-3.

Zhao, S. *et al.* (2024) 'Long COVID is associated with severe cognitive slowing: a multicentre cross-sectional study', *eClinicalMedicine*, 68, p. 102434. Available at: https://doi.org/10.1016/j.eclinm.2024.102434.

Zheng, M. *et al.* (2020) 'Functional exhaustion of antiviral lymphocytes in COVID-19 patients', *Cellular & Molecular Immunology*, 17(5), pp. 533–535. Available at: https://doi.org/10.1038/s41423-020-0402-2.

Zhou, P. *et al.* (2020) 'A pneumonia outbreak associated with a new coronavirus of probable bat origin', *Nature*, 579(7798), pp. 270–273. Available at: https://doi.org/10.1038/s41586-020-2012-7.

Zhou, S. *et al.* (2023) 'SARS-CoV-2 E protein: Pathogenesis and potential therapeutic development', *Biomedicine & Pharmacotherapy*, 159, p. 114242. Available at: https://doi.org/10.1016/j.biopha.2023.114242.

Zhou, W. *et al.* (2021) 'Impact of mutations in SARS-COV-2 spike on viral infectivity and antigenicity', *Briefings in Bioinformatics*, 23(1). Available at: https://doi.org/10.1093/bib/bbab375.

Zhu, C. *et al.* (2021) 'Molecular biology of the SARs-CoV-2 spike protein: A review of current knowledge', *Journal of Medical Virology*, 93(10), pp. 5729–5741. Available at: https://doi.org/10.1002/jmv.27132.

Zhu, N., Zhang, D., Wang, W., Li, X., Yang, B., Song, J., Zhao, X., Huang, B., Shi, W., Lu, R., Niu, P., Zhan, F., Ma, X., Wang, D., Xu, W., Wu, G., Gao, George F, *et al.* (2020) 'A Novel Coronavirus from Patients with Pneumonia in China, 2019', *New England Journal of Medicine*, 382(8), pp. 727–733. Available at: https://doi.org/10.1056/nejmoa2001017.

Zhu, N., Zhang, D., Wang, W., Li, X., Yang, B., Song, J., Zhao, X., Huang, B., Shi, W., Lu, R., Niu, P., Zhan, F., Ma, X., Wang, D., Xu, W., Wu, G., Gao, George F., *et al.* (2020) 'A Novel Coronavirus from Patients with Pneumonia in China, 2019', *New England Journal of Medicine*, 382(8), pp. 727–733. Available at: https://doi.org/10.1056/nejmoa2001017.

Zou, L. *et al.* (2020) 'SARS-CoV-2 Viral Load in Upper Respiratory Specimens of Infected Patients', *New England Journal of Medicine*, 382(12), pp. 1177–1179. Available at: https://doi.org/10.1056/nejmc2001737.

Züst, R. *et al.* (2011) 'Ribose 2'-O-methylation provides a molecular signature for the distinction of self and non-self mRNA dependent on the RNA sensor Mda5', *Nature Immunology*, 12(2), pp. 137–143. Available at: https://doi.org/10.1038/ni.1979.



The PhD Fellowship was co-financed with funds from the National Operational Programme for Research and Innovation 2014-2020, by FSE REACT-EU funds

Action IV.4 "PhD Courses and Research contracts on innovation topics" and Action IV.5 "PhD Courses on Green related topics".